Andean Geology 48 (3): 359-402. September, 2021
doi: 10.5027/andgeoV48n3-3158

Andean Geology
www.andeangeology.cl

Geochemistry of Cenozoic plutonic rocks in the extra-Andean southern Patagonia as evidence for a magmatic arc migration process

***Alejandro Sánchez V.[1, 2, 3], Michel de Saint-Blanquat[2], Francisco Hervé[1, 4], Mireille Polvé[2], Diego Morata[1, 5], Phillipe de Parseval[2], Mathieu Benoit[2]**

[1] *Departamento de Geología, Facultad de Ciencias Físicas y Matemáticas, Universidad de Chile. Plaza Ercilla 803, Santiago, Chile. alejandro.sanchez.v@usach.cl; fherve@ing.uchile.cl; dmorata@ing.uchile.cl*

[2] *Géosciences Environnement Toulouse, Université de Toulouse, CNRS, IRD, UPS, CNES, 31400 Toulouse, France. michel.desaintblanquat@get.omp.eu; mathieu.benoit@get.omp.eu; polvem@gmail.com; philippe.deparseval@get.omp.eu*

[3] *Present address: Departamento de Ingeniería en Minas, Universidad de Santiago de Chile, Libertador Bernardo O'Higgins #3363, Santiago, Chile.*

[4] *Carrera de Geología, Universidad Andrés Bello, Sazié 2119, Santiago.*

[5] *Centro de Excelencia en Geotermia de los Andes (CEGA, ANID-Fondap), Universidad de Chile, Plaza Ercilla 803, Santiago, Chile.*

** Corresponding authors: alejandro.sanchez.v@usach.cl*

ABSTRACT. In this work, we present the results of a petrographic and geochemical study that involves seven Cenozoic plutons located in a NS trending belt in western Patagonia, south of the present Chile Triple-Junction and to the east of the present magmatic arc. Four plutons were studied in the northern end, and three in the southern part of the belt. The petrographic and geochemical characteristics (major and trace element contents, εNd_t, $^{87}Sr/^{86}Sr$ initial ratios), of these plutons are different enough to propose a further classification for them: Only the Monte Balmaceda intrusive complex in the southern end of the belt is alkaline (*sensu stricto*). The Río de Las Nieves and San Lorenzo plutons in the northern area, and the Torres del Paine intrusive complex, in the southern area have "intra-plate transitional" calc-alkaline affinity. Paso de Las Llaves and Cerro Negro del Ghío plutons in the northern area, and Cerro Donoso pluton in the southern area show "arc transitional" calc-alkaline character. The "transitional" character, together with the pluton's location, and their regional geological context, can be explained by a Mio-Pliocene eastward arc migration coeval with the beginning of the Chile Rise subduction. A slab flattening hypothesis is favoured to explain the arc-migration, which together with the different length and time of arrival of the Chile Rise segments to the subduction zone, contributed to the heterogeneous geochemistry of the studied plutons.

Keywords: Plutonism, Cenozoic, Patagonia, Geochemistry, Back-arc.

RESUMEN: Geoquímica de rocas plutónicas en la Patagonia extra-andina, como evidencia de procesos de migración de arco magmático. En este trabajo se presentan resultados de un estudio petrográfico y geoquímico de siete plutones cenozoicos, que son parte de una franja de orientación N-S, ubicada en el trasarco actual de la Patagonia occidental, al sur del punto triple. Se estudiaron cuatro plutones en el sector norte y tres en el extremo sur de la franja. Las características petrográficas y geoquímicas (elementos mayores y trazas, εNd_t, y razones iniciales de $^{87}Sr/^{86}Sr$) de esos plutones son lo suficientemente variadas como para proponer una subclasificación de ellos. Sólo el complejo intrusivo Monte Balmaceda, en el extremo sur, es alcalino (*sensu stricto*). Los plutones Río de Las Nieves y San Lorenzo, en el área norte, y el complejo intrusivo Torres del Paine, en el área sur, son calcoalcalinos "transicionales de intraplaca". Los plutones Paso de Las Llaves y Cerro Negro del Ghío, en el área norte, y el plutón Cerro Donoso, en el área sur, son calcoalcalinos "transicionales de arco magmático". El carácter "transicional" de los plutones, junto con su ubicación geográfica y contexto geológico regional, puede explicarse mediante una migración del arco magmático hacia el este, durante el Mioceno-Plioceno, coincidente con el comienzo de la subducción de la Dorsal Chile. La hipótesis de un aplanamiento del ángulo de subducción de la placa subductada es preferida para explicar la migración del arco hacia el este, la que además de la geometría y tiempos de llegada de los segmentos de la dorsal a la zona de subducción, contribuyeron a la heterogeneidad geoquímica de los plutones.

Palabras clave: Plutonismo, Cenozoico, Patagonia, Geoquímica, Trasarco.

1. Introduction

Igneous rocks are widely distributed in southern Patagonia, from the latitude of the Chile Triple Junction to the south, in the form of several magmatic units. Among these rocks, the South Patagonian batholith (SPB) records episodic Jurassic to Neogene arc magmatism (*e.g.*, Weaver *et al.*, 1990; Bruce *et al.*, 1991, Hervé *et al.*, 2007), while effusive rocks (plateau lavas and volcanic fields), distributed throughout the Patagonian back-arc region (Fig. 1), have been emplaced since the Paleocene (see reviews in D'Orazio *et al.*, 2004; Guivel *et al.*, 2006). Arc and back-arc magmatism have been the focus of several studies aimed to decipher the genesis, magmatic evolution, and/or emplacements of the magmas in a continental crust environment, as well as to determine the extent to which subduction of active ridges under Patagonia has been involved in these processes since the Eocene, especially in the back-arc domain (*e.g.,* Charrier *et al.*, 1979; Cande and Leslie, 1986; Stern *et al.*, 1990; Ramos and

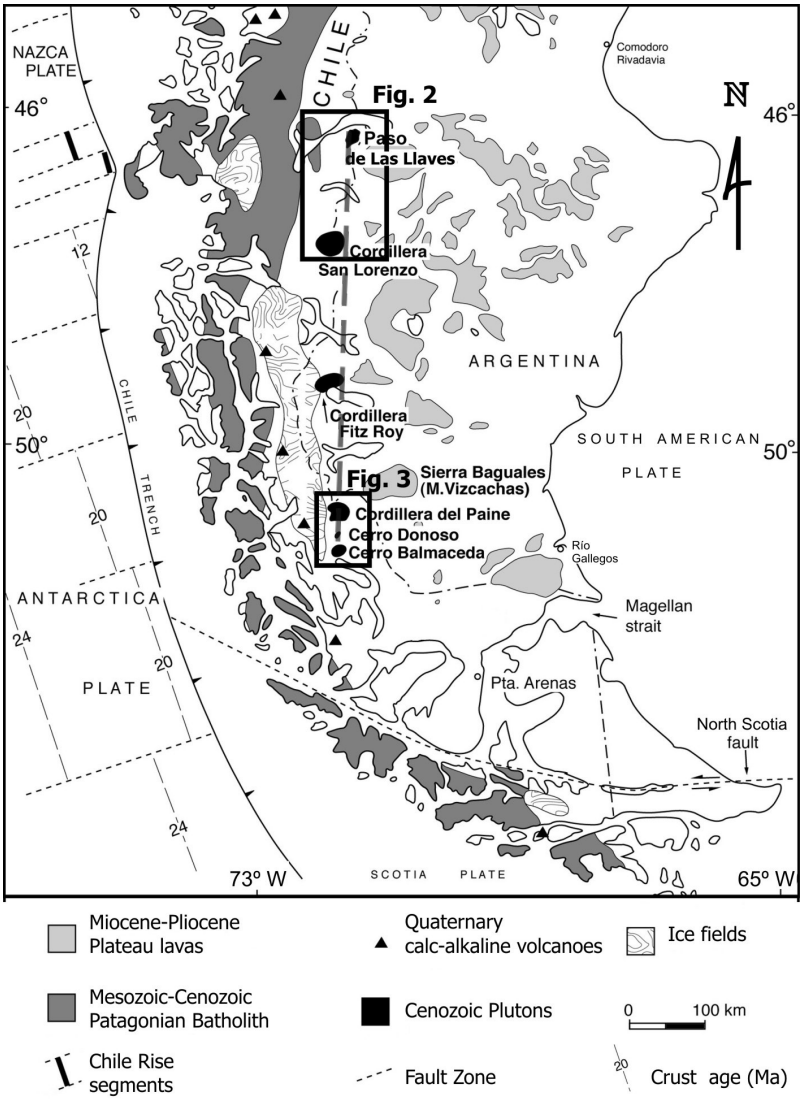

FIG. 1. Regional map of south Patagonia illustrating the main magmatic units. The segmented line shows the extra-Andean plutons location, between the South Patagonian batholith to the west and the plateau lavas to the east. Northern and southern areas location are shown as figures 2 and 3 boxes. Map after Michael (1984).

Kay, 1992; Gorring *et al.*, 1997, 2003; D'Orazio *et al.*, 2001, 2005; Espinoza *et al.*, 2005, 2010; Guivel *et al.*, 2006). Using geochemistry and geochronology as main tools, some of the plateau lavas have been linked genetically to a slab window beneath Patagonia, which opened due to the subduction of the Chile Rise active spreading center. Some hypotheses suggest a slab tear -instead of a slab window- previous to the opening of the slab window to explain some of the magmatism, while others suggest a transitional geochemical character from arc to back-arc setting (reviews in D'Orazio *et al.*, 2004; Guivel *et al.*, 2006; Espinoza *et al.*, 2010).

Between the SPB and the plateaus lavas, in the extra-Andean region, a belt of plutons crops out with a north-south trend, firstly recognized by Michael (1983) (Fig. 1). Even though, several studies have been carried out in these plutons to decipher the nature of the magmatism that generates them, most of them have been focused on single plutons or restricted areas (*e.g.,* Nullo *et al.*, 1978; Michael, 1984, 1991; Welkner, 1999; Michel *et al.*, 2008; Ramírez de Arellano *et al.*, 2008, 2012a; Leuthold *et al.*, 2012, 2013). As for the plateau lavas, the ridge collision and its subsequent subduction beneath the South American Plate has also been proposed as a trigger process for the plutonism of this belt (Michael, 1984), because the age of the Torres del Paine laccolith -one of these plutons-coincides roughly with the timing of the Chile Rise collision. This interpretation has been made assuming that this whole plutonic suite shares common characteristics, a reasoning that could easily lead to erroneous conclusions. Furthermore, this belt has not been studied in detail and, as already indicated by Sánchez *et al.* (2009) or Ramírez de Arellano *et al.* (2012b), these plutons do not exhibit a homogeneous geochemical character. Thus, a more detailed and integrative work was conducted on them with the main aim to elucidate the geochemical features along the plutonic suite and to find possible patterns to enlighten the nature of this heterogeneity.

In this work we present new field relationships, petrographic and geochemical (major, trace elements and Sr-Nd isotope ratios) data for 7 plutons of the intrusive bodies mentioned above, 4 at the northern end of the belt and 3 in the southern part (Fig. 1). The geochemical data show varying patterns, which evidence a more complex origin for this belt than previously thought, with a range in alkalinity from calc-alkaline (*s.s.*) to alkaline (*s.s.*). We propose a subdivision of the transitional character based on petrography and geochemical data of the studied and reviewed plutons. Finally, we use these data to explore possible geological scenarios during the Miocene that could explain this wide geochemical range observed in the plutonism, considering previously proposed hypotheses for single plutons and the role of the Chile Rise subduction. The arc migration hypothesis believed to be a main process at the mid-Miocene (following Gorring *et al.*, 1997 and Espinoza *et al.*, 2010), where arc magmatism shifted eastward, involves several factors with a variable degree of importance, such as crust/sub-lithospheric mantle/astenospheric mantle melt interaction (Espinoza *et al.*, 2010). In this sense, the melting, assimilation, storage and homogenization (MASH) zone hypothesis (Hildreth and Moorbath, 1988) allows us to consider all these variables to support geochemical diversity, supposing that this MASH zone was generated in the extra-Andean domain by arc migration and evolved in different ways according to the particular tectonic scenarios at the time and location of the studied plutons.

The plutons included in this work are divided in two areas accord to its geographic location and tectonic particularities (Fig. 1): the northern area includes the Miocene Paso de Las Llaves, Cerro Negro del Ghío, and San Lorenzo plutons and the Pliocene Río de Las Nieves, and alkaline plutons in Meseta del Lago Buenos Aires (Fig. 2). In the southern area Torres del Paine and Monte Balmaceda intrusive complexes, the Paine External Gabbros and the Cerro Donoso pluton are considered (Fig. 3).

2. Geological Setting

All along the southwestern Patagonia margin, from the Chile Triple Junction (*ca.* 46° 30' S) to the south, metasedimentary rocks crop out. They consist predominantly of polydeformed metaturbidites originally deposited in a passive continental margin (Faúndez *et al.*, 2002) between late Devonian and late Permian (Hervé *et al.*, 2003). They are unconformably covered by Upper Jurassic-early Cretaceous silicic volcanic rocks associated to rift processes pre Gondwana break-up (Feraud *et al.*, 1999; Pankhurst *et al.*, 2000). These rocks are widely distributed in south Patagonia and are locally known by various formation names, for example, Ibáñez, El Quemado, Tobífera and Lemaire in northern,

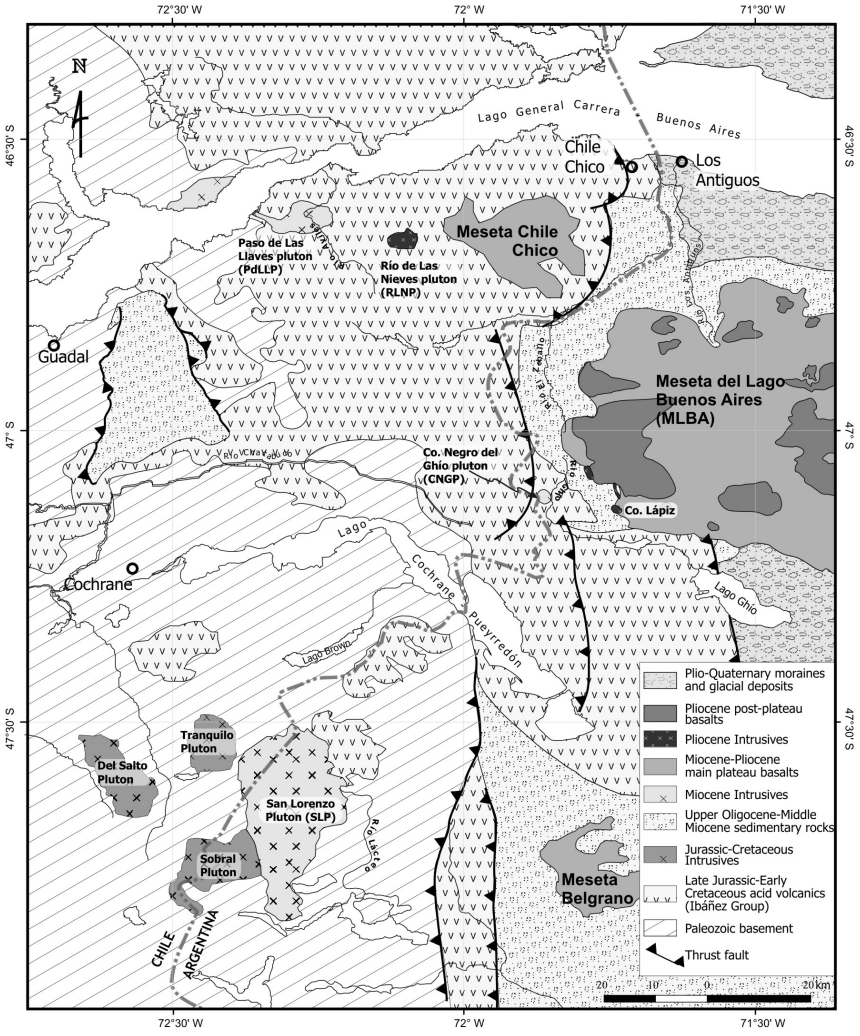

FIG. 2. Geologic map of the northern area, showing the location of Paso de Las Llaves, Cerro Negro del Ghío, Río de Las Nieves and San Lorenzo plutons. Geology simplified after Welkner (1999), Welkner *et al.* (2002), Giacosa and Franchi (2001), Lagabrielle *et al.* (2007), Espinoza *et al.* (2008), Scalabrino *et al.* (2010), Espinoza *et al.* (2010), Boutonnet *et al.* (2010).

central, and southern Patagonia, and Tierra del Fuego (Argentina), respectively. In the north of the studied area (El Quemado and Ibáñez formations, hereafter Ibáñez Group), they consist of Upper Jurassic subaerial rhyolites (Suárez and De la Cruz, 2000; Pankhurst *et al.*, 2000), whereas in the south they are considered to have been deposited in a submarine environment prior to and contemporaneous with the opening of the Rocas Verdes Marginal Basin (Dalziel *et al.*, 1974; Bruhn *et al.*, 1978; Allen, 1982; Wilson, 1991; Stern and de Wit, 2003; Calderón *et al.*, 2007a). The Magallanes (Austral, in Argentina) foreland basin overlies the Rocas Verdes basin, initially developed as a sag basin (Late Jurassic-Early Cretaceous Zapata Formation) which evolved to a foreland basin since the mid-Cretaceous (Biddle *et al.*, 1986). This basin has continental facies in the north and east, and deep marine facies southward and close to the main cordillera (Biddle *et al.*, 1986; Macellari *et al.*, 1989; Wilson, 1991). In the north, this basin was not connected to an open sea; therefore, Cretaceous sedimentary deposits are scarce, whilst in the Paleogene there were volcano-sedimentary successions within restricted sub-basins (see review in Giacosa and Franchi, 2001).

The major magmatic units in the southern Patagonia are shown simplified in figure 1, summarized into

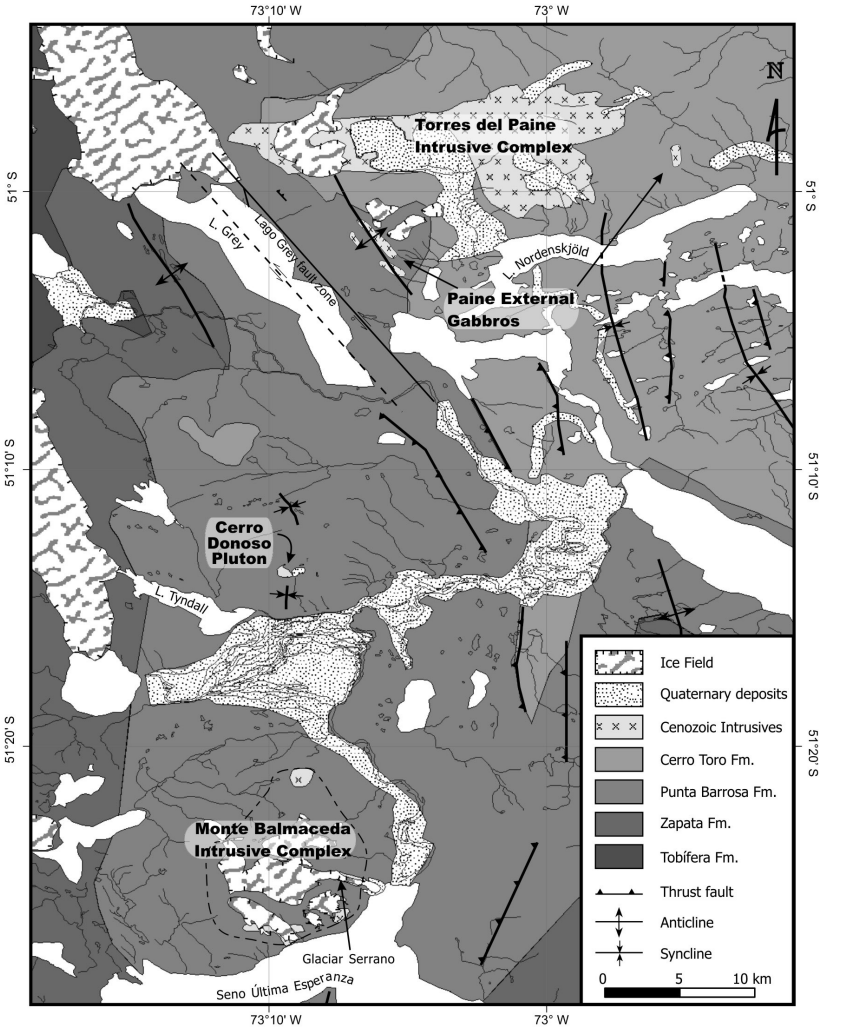

FIG. 3. Geological map of the southern area, showing the location of Torres del Paine intrusive complex, the Paine External Gabbros, Cerro Donoso pluton and Monte Balmaceda intrusive complex. Geology after Stewart *et al.* (1971), Muñoz (1981), Soffia (1988), Wilson (1991), Sernageomin (2002), Fildani *et al.* (2003), Fault zones from Altenberger *et al.* (2003).

two plutonic and two volcanic units. The main plutonic unit comprises the Mesozoic-Cenozoic South Patagonian batholith (SPB), which intrudes the metasedimentary basement (Stewart *et al.*, 1971; Weaver *et al.*, 1990; Bruce *et al.*, 1991; Hervé *et al.*, 2007). The Neogene plutons in the batholith are considered to be formed from mantle-derived magmas, with scarce crustal assimilation (Hervé *et al.*, 2007; Fanning *et al.*, 2009). The other plutonic unit is the focus of this paper. It was firstly considered as an approximate N-S trending belt of Cenozoic plutons, satellites to the SPB, located in the extra-Andean zone (Michael, 1984), they intrude volcanic rocks of the Ibáñez Group or the metasedimentary basement (northern area), or sedimentary rocks of the Magallanes (Austral) foreland basin (southern area) (Figs. 1, 2 and 3). They are mostly granitoids, and further geological data is presented in section 4. The Fitz Roy pluton (Chalten plutonic complex) is an exception, as this complex has a range of lithologies from ultramafic to granitic rocks (Ramírez de Arellano *et al.*, 2008) with typical calc-alkaline geochemical features (Michael, 1983; Kosmal and Spikermann, 2002; Ramírez de Arellano, 2011). The latter author proposed that subduction-derived fluids triggered the magma-genesis of this complex. It has a K-Ar age of

18 Ma (Nullo *et al.*, 1978), and an emplacement time span between 16.95 and 16.35 Ma has been determined for the suite (Ramírez de Arellano *et al.*, 2012a).

The Cenozoic, mainly Miocene-Pleistocene, basaltic plateau lavas are located predominantly in the Argentinean pampa, in a back-arc position. Other minor but key mid-Miocene extrusive units are the Chile Chico rhyolites (Espinoza *et al.*, 2005), and Cerro Zeballos lavas (Espinoza *et al.*, 2010), which outcrop in the northern area and are used for comparison. Lastly, the active volcanic arc is located in the cordilleran axis (Fig. 1), conformed by at least six Holocene volcanic centers of the Andean Austral Volcanic Zone (49-54ºS) (Stern *et al.*, 1984; Stern and Kilian, 1996). Geochemical characteristic of these magmatic units are summarized in figure 4.

The tectonic scenario in south Patagonia has *grosso modo* two elements important to this work. First, the Magallanes Fold and Thrust Belt (review in Suárez *et al.*, 2000), which thrusts principally Magallanes foreland basin rocks, but also the Jurassic rhyolites. And second, the collision of segments of an active spreading center (Chile Rise) with the South American Plate first at 55º S at *ca.* 15 Ma, which generated a tectonic triple junction (Cande and Leslie, 1986) that migrated northward to its present position (~46º30' S) (see Breitsprecher and Thorkelson, 2009).

3. Methods

Field work was performed in the Aysén (Chile) and Santa Cruz (Argentina) regions northern area, during November and December, 2007. Paso de Las Llaves, Cerro Negro del Ghío, and plutons in Meseta del Lago Buenos Aires were sampled then. The samples of San Lorenzo and Río de Las Nieves plutons were collected in earlier campaigns by D. Morata. The southern area at Última Esperanza (Chile) region was studied in December 2004, and January and February 2007. Torres del Paine, Balmaceda intrusive complexes and Cerro Donoso pluton were sampled then.

Rock samples for geochemical and isotopic analyses consisted of 1-3 kg of material, which were crushed and split to 200 g, and then pulverised in an agate mill. The mineral chemistry analyses were conducted using a Cameca SX50 electronic microprobe at the Laboratoire des Mécanismes et Transfert en Géologie (LMTG), Toulouse (France), now Géosciences Environnement Toulouse (GET). Analytical conditions were 15 kV voltage and 20 nA current. The results for the northern and southern areas are listed on tables 1 and 2, respectively.

Major elements analyses were conducted for samples from different facies of the Paso de Las Llaves, Cerro Negro del Ghío, and San Lorenzo plutons, in the northern area; and at the Monte Balmaceda

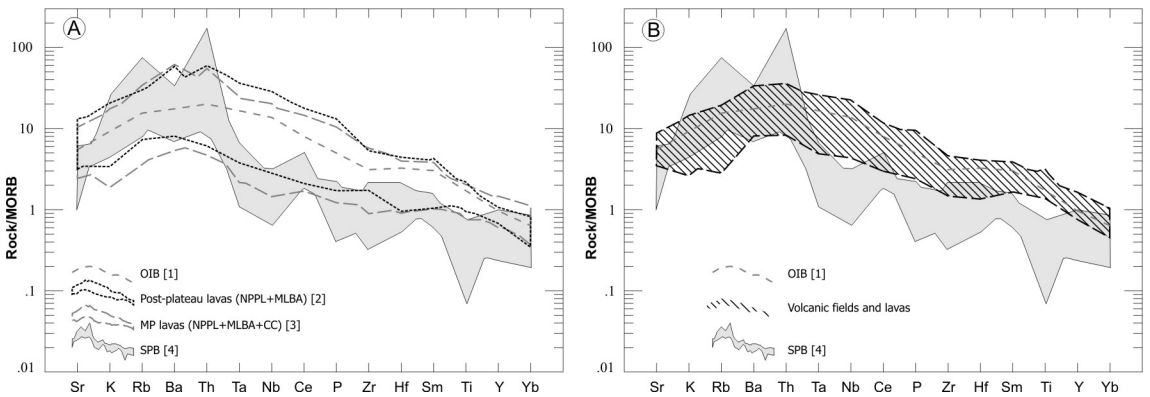

FIG. 4. MORB normalized spider diagrams (Pearce, 1983) from previous works on magmatic units in Patagonia. **A.** Northern area, main plateau lavas and post-plateau lavas. **1. OIB**: Ocean Island Basalt average (Sun and McDonough, 1989); **2.** Post-plateau Lavas includes **NPPL**: North Patagonian Plateau Lavas, Central, Belgrano, and Muerte plateaus (Gorring and Kay, 2001) and **MLBA**: Meseta del Lago Buenos Aires (Guivel *et al*., 2006); **3. MP**: Main Plateau lavas, includes the **NPPL**: Central, Belgrano, Noreste, and Muerte plateaus (Gorring and Kay, 2001); **CC**: Meseta Chile Chico (Espinoza *et al*., 2005), and MLBA (Guivel *et al*., 2006); **4. SPB**: Neogene South Patagonian batholith (Hervé *et al*., 2007). **B.** Southern area lavas from volcanic fields: Glencross Area (D'Orazio *et al*., 2001) and Camusú-Aike (D'Orazio *et al*., 2005).

TABLE 1. SELECTED FELDSPAR MICROANALYSES FROM PASO DE LAS LLAVES AND CERRO NEGRO DEL GHÍO PLUTONS.

Unit	Paso de Las Llaves tonalite							Paso de Las Llaves diorite					Cerro Negro del Ghío diorite						
Sample	07LL2				07LL25			07LL20					07SM13						
Label	I2	I3	D1	D4	C3	G-4	G-5	D2	D1	D3	A1	A2	K3	A1	A3	I5	I1	I-L1-1	I-L1-17
cristal loc	rim	core	core	rim	core	core	rim	core	interm	rim	core	interm	mass	core	rim	core	rim	rim	core
SiO_2 wt%	54.39	47.39	54.98	62.46	49	49.12	57.52	51.79	44.44	54.1	44.38	45.04	67.31	52.04	61.82	53.71	61.31	58.47	56.24
TiO_2	0	0	0.12	0.04	0.12	0.12	0	0	0	0	0	0	0	0	0	0	0	0	0
Al_2O_3	28.4	33.01	28.08	22.83	31.76	31.45	26.07	29.06	33.65	27.58	34.07	33.96	21.16	29.67	23.5	28.48	23.75	25.63	26.55
Fe_2O_3	0.36	0.56	0.35	0.36	0.44	0.53	0.33	0.32	0.37	0.36	0.34	0.3	0	0.47	0.17	0.38	0.12	0.23	0.38
MgO	0	0	0	0	0	0	0	0	0	0	0	0	0	0	0	0	0	0	0
CaO	11.11	16.84	10.73	4.98	15.2	14.87	8.55	12.18	18	10.5	18.6	18.06	1.75	13.02	5.3	11.49	5.65	8.03	9.55
SrO	-	-	-	-	-	-	-	-	-	-	-	-	-	-	-	-	-	-	-
BaO	-	-	0	0	0.03	0	0	-	-	-	-	-	-	-	-	-	-	-	-
Na_2O	5.14	2.05	5.21	8.52	2.77	2.99	6.62	4.15	1.04	5.16	0.94	1.12	10.56	4	7.95	4.82	8.02	6.94	5.81
K_2O	0.24	0.06	0.29	0.4	0.1	0.07	0.29	0.16	0.01	0.29	0	0.02	0.1	0.13	0.74	0.26	0.73	0.4	0.32
Rb_2O	-	-	-	-	-	-	-	-	-	-	-	-	-	-	-	-	-	-	-
Total	99.64	99.91	99.78	99.59	99.42	99.15	99.36	97.66	97.51	97.99	98.33	98.49	100.88	99.33	99.49	99.13	99.58	99.69	98.85
Si	2.466	2.181	2.486	2.782	2.255	2.265	2.596	2.402	2.102	2.49	2.086	2.108	2.923	2.379	2.759	2.451	2.739	2.627	2.558
Ti	0	0	0.004	0.001	0.004	0.004	0	0	0	0	0	0	0	0	0	0	0	0	0
Al/Al IV	1.518	1.79	1.497	1.198	1.722	1.709	1.387	1.588	1.877	1.496	1.887	1.874	1.083	1.599	1.236	1.531	1.251	1.357	1.423
Al VI	0	0	0	0	0	0	0	0	0	0	0	0	0	0	0	0	0	0	0
Fe^{3+}	0.012	0.019	0.012	0.012	0.015	0.018	0.011	0.011	0.013	0.013	0.012	0.01	0	0.016	0.006	0.013	0.004	0.008	0.013
Mg	0	0	0	0	0	0	0	0	0	0	0	0	0	0	0	0	0	0	0
Ca	0.54	0.83	0.52	0.238	0.749	0.735	0.413	0.605	0.913	0.518	0.937	0.906	0.081	0.638	0.254	0.562	0.271	0.386	0.465
Sr	-	-	-	-	-	-	-	-	-	-	-	-	-	-	-	-	-	-	-
Ba	-	-	0	0	0.001	0	0	-	-	-	-	-	-	-	-	-	-	-	-
Na	0.452	0.183	0.457	0.736	0.247	0.267	0.579	0.373	0.096	0.46	0.085	0.102	0.889	0.355	0.688	0.426	0.695	0.604	0.512
K	0.014	0.004	0.017	0.023	0.006	0.004	0.016	0.01	0.001	0.017	0	0.001	0.005	0.008	0.042	0.015	0.042	0.023	0.019
Rb	-	-	-	-	-	-	-	-	-	-	-	-	-	-	-	-	-	-	-
Cation Sum	5.002	5.007	4.993	4.991	4.999	5.003	5.003	4.99	5.001	4.994	5.007	5.001	4.983	4.994	4.985	4.998	5.002	5.004	4.99
Ab	44.936	17.971	45.971	73.87	24.663	26.538	57.395	37.765	9.481	46.258	8.354	10.066	91.115	35.478	69.948	42.502	68.988	59.627	51.415
An	53.676	81.663	52.319	23.857	74.679	73.027	40.975	61.264	90.47	52.043	91.646	89.832	8.336	63.771	25.778	56.011	26.871	38.132	46.718
Or	1.389	0.366	1.707	2.272	0.604	0.435	1.63	0.971	0.05	1.698	0	0.102	0.549	0.75	4.274	1.487	4.141	2.241	1.866
Celsian	0	0	0.003	0	0.055	0	0	0	0	0	0	0	0	0	0	0	0	0	0

Cation per formula unit based on 8O.

TABLE 2. SELECTED FELDSPAR MICROANALYSES FROM DONOSO GRANITE (07DN7) AND BALMACEDA LEUCOGRANITES (07BA4, 07BA7A).

Unit	Cerro Donoso Pluton granite							Monte Balmaceda leucogranites									
Sample	07DN7							07BA4					07BA7a				
Label	C1-L1_1	C1-L1_13	C10-L1_1	C10-L1_11	C4-2	C4-3	C9-8	C2-3	C2-4	C2-7	C2-8	C4-14	C2-4	C2-3	C2-6	C2-7	C2-8
cristal loc	core	rim	rim	core	rim	core	core	core	exol.	rim/int	core	core	Or	Ab		pert.	
SiO_2 wt%	47.42	58.18	65.3	50.92	61.26	56.35	64.15	66.52	65.17	66.23	65.25	64.52	64.2	65.98	66.76	65.25	62.45
TiO_2	0.13	0.04	0	0.01	0.02	0	0	0	0.05	0.21	0	0.15	0	0	0	0.09	0
Al_2O_3	34.12	26.76	22.01	31.25	24.27	27.12	19.32	18.81	22.29	20.65	18.94	18.11	18.12	21.06	19.23	18.8	19.34
Fe_2O_3	0.28	0.18	0.09	0.29	0.04	0.15	0.14	0.13	0.14	0.06	0.11	0	0.01	0.06	0.11	0.33	0.09
MgO	0	0	0	0	0	0	0	0	0	0	0	0	0	0	0	0	0
CaO	17.37	8.83	3.67	14.09	5.91	9.3	0.02	0.33	0.81	1.87	0.02	0	0	2.27	0.09	0.26	0.07
SrO	-	-	-	-	-	-	-	-	-	-	-	-	-	-	-	-	-
BaO	0	0	0	0.01	0	0	0.22	0.07	0	0	0	0	0.01	0	0.04	0.04	0
Na_2O	1.69	6.26	9.98	3.59	8.54	5.93	0.61	5.63	9.47	10.79	3.17	0.67	0.26	11.08	7.39	3.29	0.35
K_2O	0.03	0.61	0.28	0.05	0.32	0.27	15.21	8.64	2.4	0.33	12.01	15.88	16.61	0.27	6.5	11.99	15.91
Rb_2O	-	-	-	-	-	-	-	-	-	-	-	-	-	-	-	-	-
Total	101.05	100.88	101.34	100.21	100.36	99.12	99.65	100.13	100.34	100.13	99.52	99.34	99.21	100.72	100.13	100.06	98.21
Si	2.156	2.588	2.848	2.314	2.718	2.551	2.966	2.993	2.872	2.911	2.985	3	2.999	2.891	2.983	2.976	2.943
Ti	0.005	0.001	0	0	0.001	0	0	0	0.002	0.007	0	0.005	0	0	0	0.003	0
Al/Al IV	1.829	1.403	1.131	1.674	1.269	1.447	1.053	0.997	1.157	1.069	1.021	0.993	0.997	1.087	1.013	1.011	1.074
Al VI	0	0	0	0	0	0	0	0	0	0	0	0	0	0	0	0	0
Fe^{3+}	0.01	0.006	0.003	0.01	0.001	0.005	0.005	0.004	0.005	0.002	0.004	0	0	0.002	0.004	0.011	0.003
Mg	0	0	0	0	0	0	0	0	0	0	0	0	0	0	0	0	0
Ca	0.846	0.421	0.172	0.686	0.281	0.451	0.001	0.016	0.038	0.088	0.001	0	0	0.106	0.005	0.013	0.004
Sr	-	-	-	-	-	-	-	-	-	-	-	-	-	-		-	-
Ba	0	0	0	0	0	0	0.004	0.001	0	0	0	0	0	0	0.001	0.001	0
Na	0.149	0.54	0.844	0.317	0.735	0.521	0.054	0.492	0.809	0.919	0.282	0.06	0.023	0.941	0.64	0.291	0.032
K	0.002	0.035	0.016	0.003	0.018	0.016	0.897	0.496	0.135	0.018	0.701	0.942	0.989	0.015	0.37	0.697	0.956
Rb	-	-	-	-	-	-	-	-	-	-	-	-	-	-	-	-	-
Cation sum	4.996	4.994	5.014	5.004	5.023	4.991	4.98	5	5.018	5.015	4.994	5	5.009	5.043	5.015	5.004	5.013
Ab	14.97	54.229	81.85	31.484	71.093	52.742	5.682	48.937	82.412	89.656	28.621	6.005	2.29	88.555	63.03	29.062	3.261
An	84.849	42.268	16.644	68.215	27.18	45.683	0.096	1.579	3.877	8.567	0.112	0	0	10.019	0.447	1.261	0.356
Or	0.181	3.503	1.506	0.278	1.727	1.575	93.812	49.368	13.71	1.777	71.267	93.995	97.683	1.425	36.453	69.605	96.383

Cation per formula unit based on 8O

intrusive complex and Cerro Donoso pluton in the southern area. The analyses used the ICP-AES plasma 400 of the Departamento de Geología, Universidad de Chile and RGM-1 and QLO-1 were employed as standards. Procedures are in Calderón *et al.* (2007b). The results for the northern and southern areas are listed on tables 3 and 4, respectively.

Trace elements measurements were performed in samples from the same plutons mentioned above, and in samples from different facies from the Torres del Paine Intrusive Complex in the southern area. All the trace elements analyses were carried out using a quadrupole ICP-MS 7500 ce. from Agilent Technologies. The analytical drift was controlled and calibrated by an internal Re-In standard at the LMTG (now GET). Procedures are described in Aries *et al*. (2000). GS-N, AC-E and GA were used as standards. The results for the northern and southern areas are listed on tables 3 and 4, respectively.

We used the traditional major element classification of Irvine and Baragar, (1971) and the alumina saturation index (A/CNK-A/NK) diagram with $A/CNK=Al_2O_3/(CaO+Na_2O+K_2O)$ (mol.%) and $A/NK=Al_2O_3/(Na_2O+K_2O)$ (mol.%) (Shand, 1943); but also some trace elements diagrams were used in order to dismiss possible alteration (*s.l.*) effects on major elements content. To control the alkaline character, the Nb/Y ratio and Co-Th diagrams were employed. The former is considered an alkaline indicator (Pearce and Cann, 1973; Winchester and Floyd, 1977), while the latter may be indicative of a transport mechanism in subduction settings, similar to K (Hastie *et al.*, 2007). The REE (Rare Earth Elements) diagrams used are normalized to chondrites and so is $Eu/Eu^*=Eu_N/sqr(Sm_N*Gd_N)$ (Nakamura, 1974). In order to discriminate arc signatures, MORB normalized (Pearce, 1983) spider diagrams were used. In the latter diagrams, data from previous works on magmatic units are plotted for comparison.

The Nd and Sr isotopic measurement listed on tables 5 and 6 were made on whole rocks powders from the same samples used for the trace elements measurements, with an upgraded MAT 261 thermal ionization mass spectrometer at the LMTG, Toulouse (GET). La Jolla and NBS 987 reference material were used as standards for Nd and Sr ratios, respectively.

To compare the results, all the new data are plotted in similar diagrams together with data from the SPB (representing arc signature) and from the plateau lavas (Fig. 4).

4. Field realationships and petrography

Based in our field studies and in results of previous work, as indicated in the text, the field relationships for the different plutons, are indicated below. Additionally, some key data in each pluton, namely previous geochronology, are presented according to their geographic location from north to south.

4.1. Paso de Las Llaves Pluton

This pluton has a near elliptical shape with an E-W long axis of *ca*. 12 km. There are two main outcrop areas, one in the coast of the General Carrera-Buenos Aires lake (Paso de Las Llaves area), and the other in the valley of the Río Avilés (Fig. 2), both heavily covered by forest. In the Paso de Las Llaves area, biotite-amphibole tonalite to granodiorite facies predominate. In the contact areas, the pluton hosts mostly gneissic xenoliths up to 20 cm in length with preferred vertical disposition (Fig. 5A). Near the southwestern side of the pluton, the tonalites intrude pyroxene dioritic facies. In the tonalites, plagioclase is the main component, usually with a calcium rich core (An_{50-80}) with a poikilitic texture and a zoned sodium-rich rim (commonly around An_{25}) (Table 1), whereas K-feldspar-quartz inter-growth, pyroxene, apatite, titanite and zircon appear as minor phases. The diorites have porphyritic texture and, in general terms, they have similar mineralogy than the tonalites, but with higher content of pyroxene, and lesser content of amphibole and biotite. The plagioclase is calcic-rich (An_{60-90}) with zoned border. In addition, a porphyritic granitic facies is present in the north-east margin of the pluton, with quartz, plagioclase, mica and garnet phenocrysts (sample 07LL3). Otherwise, Vargas and Hervé (1995) have described miarolitic cavities within granodioritic facies in the Paso de Las Llaves area, ascribing these facies to a shallow emplacement level (<5 km).

In the Río Avilés area, the scarce outcrops are mainly of the granitic facies, with lobate contacts with the diorites (Fig. 5B) that suggest their synchronous emplacement. This unit is called Granito Avilés and its granitic rocks are biotite-rich, have relict pyroxenes in association with biotite and, close to the diorites, are amphibole rich. The diorites exhibit similar petrographic characteristics to those observed in Paso de Las Llaves area.

TABLE 3. CHEMICAL COMPOSITION OF PLUTON SAMPLES FROM THE NORTHERN AREA.

Sample	07LL2	07LL3	07LL4	07LL5	07LL6	07LL7	07LL9	07LL11	07LL12	07LL14	07LL15	07LL10	0 7LL25	07LL17	07LL18	07LL19	07LL20	07LL22	07LL23	07SM1	07SM6	07SM8	07SM13	COY0230	COY0231	COY0232	COY0233	COY0234	COY0235	CH4131	07SM3	07SM4	07SM2
Lat. °S	46,6274	46,6279	46,6282	46,6288	46,6292	46,6296	46,63033	46,63000	46,62950	46,62789	46,62779	46,63092	46,62977	46,62977	46,6165	46,61783	46,61594	46,60019	46,60019	47,11214	47,11268	47,11404	47,08499	-	-	-	-	-	-	-	47,12116	47,12006	47,08269
Lon. °W	72,3549	72,3590	72,3597	72,3601	72,3604	72,3605	72,36069	72,36061	72,36047	72,3594	72,35779	72,36006	72,36327	72,36327	72,26566	72,2692	72,26772	72,22856	72,22856	71,85268	71,85264	71,85735	71,8839	-	-	-	-	-	-	-	71,73196	71,73846	71,72465
Unit	TLLPa	Gt-graniteb	TLLP	dike	dike	TLLP	TLLP	diorite Las Llaves	TLLP	Ibáñez Fm.	TLLP	TLLP	TLLP	GAc	GA	GA	diorite Avilés	dike	dike	CNGPd	CNGP	CNGP	CNGP	SLPe	SLP	SLP	SLP	SLP-dike?	SLP	RLNPf	Co. Lápiz	Co. Lápiz	Mifeldi
Rock type	tonalite	granite	tonalite	rhyolite	basalt	tonalite	tonalite	diorite	tonalite	rhyolite	tonalite	tonalite	tonalite	granite	granite	granite	diorite	riolita	basalt	qtz-diorite	qtz-diorite	qtz-diorite	qtz-diorite	monzogranite	monzogranite	monzogranite	monzogranite	andesite	monzogranite	granite	alkali granite	alkali granite	porphyritic syenite
Major elements (wt%)																																	
SiO_2	51.43	72.12	50.55	71.35	47.27	53.40	49.64	49.93	52.48	70.21	49.78	50.08	50.03	66.70	60.00	62.81	46.65	74.46	43.34	58.13	58.90	59.27	59.56	74.47	75.55	74.35	73.38	59.34	73.49	62.18	72.15	67.63	63.12
TiO_2	1.28	0.28	1.59	0.36	1.40	0.79	1.35	1.36	1.29	0.16	1.60	1.32	1.45	0.52	0.81	0.69	1.14	0.14	0.95	0.73	0.76	0.74	0.72	0.11	0.12	0.18	0.20	1.19	0.18	0.91	0.06	0.17	0.66
Al_2O_3	18.70	14.70	18.50	14.80	16.02	21.68	20.00	18.30	17.40	15.50	15.00	18.50	18.30	15.20	16.70	16.00	18.90	14.40	15.10	17.40	17.00	17.00	17.70	13.60	13.00	13.50	13.50	15.70	14.00	16.30	14.50	15.30	16.80
Fe_2O_3	3.38	0.38	3.91	1.52	2.57	2.96	3.59	3.19	1.94	0.47	4.99	3.92	3.36	1.56	2.48	2.45	4.74	0.87	2.50	3.64	3.24	3.28	2.46	0.87	0.79	0.78	0.49	3.12	0.66	2.53	2.11	3.47	3.24
FeO	5.36	2.20	5.52	0.72	5.20	3.60	4.52	5.60	6.12	1.88	5.20	5.16	6.08	2.00	3.28	2.44	6.24	0.24	5.64	2.12	2.48	2.20	1.96	0.60	0.64	0.80	1.48	3.52	1.12	2.48	0.04	0.08	1.84
MnO	0.16	0.05	0.17	0.03	0.13	0.11	0.13	0.15	0.16	0.04	0.19	0.15	0.16	0.07	0.14	0.07	0.17	0.03	0.28	0.15	0.16	0.16	0.17	0.03	0.05	0.04	0.05	0.09	0.05	0.10	0.05	0.07	0.10
MgO	4.08	0.52	3.85	0.34	4.75	2.78	4.80	4.95	5.13	0.76	7.38	4.93	4.73	1.60	2.74	2.35	6.44	0.14	9.81	1.61	1.67	1.61	1.58	0.15	0.15	0.22	0.21	3.08	0.27	2.00	0.03	0.07	0.75
CaO	8.37	2.54	8.90	0.93	9.05	8.56	9.50	9.41	8.67	1.35	8.96	8.94	8.61	3.56	5.35	4.13	10.42	0.71	8.25	5.90	6.25	5.83	5.20	0.70	0.72	0.80	0.85	5.04	0.90	3.78	0.30	0.82	2.30
Na_2O	3.28	2.46	3.32	3.87	3.42	4.00	4.15	3.53	2.86	2.08	3.38	3.47	3.72	3.57	3.65	3.48	2.89	4.03	1.96	4.38	4.44	4.42	4.93	3.94	3.79	4.46	4.02	3.32	4.25	4.11	5.25	5.36	5.26
K_2O	1.61	3.59	1.90	4.28	1.40	0.91	0.93	1.92	1.84	6.20	1.64	1.28	2.01	3.87	3.33	4.10	1.31	2.51	2.13	3.07	2.90	2.98	2.48	4.39	4.22	4.08	4.48	2.96	4.13	3.57	4.53	5.18	4.41
P_2O_5	0.51	0.10	0.45	0.15	0.65	0.21	0.20	0.50	0.45	0.07	0.47	0.41	0.52	0.22	0.32	0.24	0.32	0.06	0.30	0.32	0.32	0.32	0.29	0.04	0.04	0.05	0.07	0.39	0.07	0.29	0.04	0.05	0.30
LOI	1.41	0.86	0.95	1.57	8.05	0.71	1.00	1.01	1.30	1.04	1.11	1.58	0.90	0.71	0.82	1.05	0.66	2.13	8.66	2.06	1.72	1.88	1.73	0.62	0.50	0.54	0.88	1.84	0.44	1.47	0.62	1.30	0.80
Total	99.57	99.80	99.61	99.92	99.91	99.71	99.81	99.85	99.64	99.76	99.70	99.74	99.87	99.58	99.62	99.81	99.88	99.72	98.92	99.51	99.84	99.69	98.78	99.52	99.57	99.80	99.61	99.59	99.56	99.72	99.68	99.50	99.58
Trace elements (ppm)																																	
Sc	21.00	9.50	-	6.60	21.00	-	-	26.00	-	-	-	25.00	24.50	-	14.70	12.50	31.00	-	-	-	8.60	-	7.80	-	6.00	-	-	16.70	4.90	10.50	-	-	-
V	211.00	23.00	-	31.30	204.00	-	-	265.00	-	-	-	268.00	274.00	-	124.60	110.00	284.00	-	-	-	141.00	-	109.00	-	5.20	-	-	130.00	7.30	82.00	-	-	-
Cr	7.80	5.90	-	7.50	124.00	-	-	29.20	-	-	-	13.10	16.20	-	30.40	52.00	164.00	-	-	-	4.60	-	8.90	-	4.30	-	-	68.00	4.30	7.70	-	-	-
Co	20.10	2.75	-	2.42	22.70	-	-	24.50	-	-	-	18.00	24.50	-	12.70	10.90	32.10	-	-	-	8.29	-	7.40	-	0.78	-	-	18.20	1.30	8.90	-	-	-
Ni	16.10	11.00	-	8.30	85.00	-	-	27.00	-	-	-	19.90	27.00	-	18.70	19.30	57.40	-	-	-	10.20	-	6.80	-	5.10	-	-	81.00	6.70	7.40	-	-	-
Cu	35.00	22.00	-	13.61	185.00	-	-	264.00	-	-	-	196.00	29.70	-	21.80	15.10	45.00	-	-	-	26.00	-	133.00	-	155.00	-	-	33.40	37.30	84.90	-	-	-
Zn	113.00	60.20	-	47.70	147.80	-	-	118.00	-	-	-	100.00	121.20	-	91.80	69.00	96.00	-	-	-	79.00	-	91.00	-	70.00	-	-	113.00	68.00	86.00	-	-	-
Ga	18.90	16.90	-	16.20	20.30	-	-	19.80	-	-	-	20.30	19.99	-	17.20	18.10	17.20	-	-	-	22.90	-	22.20	-	19.10	-	-	20.50	18.10	18.10	-	-	-
Ge	1.25	1.70	-	1.57	1.60	-	-	1.40	-	-	-	1.36	1.43	-	1.40	1.50	1.60	-	-	-	1.70	-	1.80	-	1.79	-	-	1.49	1.44	1.50	-	-	-
As	3.30	3.40	-	1.90	2.87	-	-	3.15	-	-	-	2.00	1.90	-	2.80	2.20	11.00	-	-	-	3.20	-	6.40	-	2.40	-	-	4.30	1.60	12.90	-	-	-
Rb	59.90	169.00	-	117.80	28.10	-	-	63.00	-	-	-	38.20	55.00	-	123.00	177.00	44.10	-	-	-	105.00	-	71.00	-	199.00	-	-	77.00	154.00	127.00	-	-	-
Sr	828.00	69.40	-	202.00	1,057.00	-	-	820.00	-	-	-	808.00	787.00	-	579.00	488.00	601.00	-	-	-	1,210.00	-	949.00	-	53.00	-	-	509.00	100.00	434.00	-	-	-
Y	18.06	25.00	-	19.80	16.80	-	-	22.60	-	-	-	19.80	24.20	-	21.00	18.60	22.40	-	-	-	21.50	-	23.20	-	25.60	-	-	25.00	21.20	25.50	-	-	-
Zr	168.00	136.00	-	259.00	194.00	-	-	148.00	-	-	-	109.00	161.00	-	299.00	291.00	70.50	-	-	-	183.00	-	180.30	-	122.70	-	-	294.00	159.80	327.00	-	-	-
Nb	10.60	8.60	-	15.40	23.00	-	-	12.70	-	-	-	10.75	18.39	-	17.29	15.90	2.90	-	-	-	15.30	-	11.00	-	24.10	-	-	22.20	27.00	21.20	-	-	-
Mo	2.40	1.80	-	0.58	1.60	-	-	2.90	-	-	-	2.10	3.60	-	2.70	71.00	0.70	-	-	-	0.72	-	0.80	-	1.20	-	-	1.50	1.90	1.50	-	-	-
Rh	0.05	l.d	-	0.02	0.04	-	-	0.07	-	-	-	0.04	0.04	-	0.04	0.02	0.06	-	-	-	0.07	-	0.03	-	0.06	-	-	0.04	0.03	0.04	-	-	-
Ag	0.58	0.44	-	0.59	0.52	-	-	0.46	-	-	-	0.45	0.50	-	0.66	0.59	0.30	-	-	-	0.79	-	0.42	-	0.47	-	-	0.83	0.44	0.90	-	-	-
Cd	0.29	0.10	-	0.17	0.20	-	-	0.18	-	-	-	0.15	0.26	-	0.21	0.27	0.22	-	-	-	0.13	-	l.d	-	0.13	-	-	0.20	0.11	0.31	-	-	-
Sn	2.50	6.70	-	5.80	1.23	-	-	2.16	-	-	-	2.00	4.76	-	2.03	3.14	1.40	-	-	-	3.93	-	0.95	-	6.00	-	-	3.20	3.50	2.10	-	-	-
Sb	0.80	7.00	-	0.37	1.10	-	-	1.23	-	-	-	1.18	1.10	-	0.76	0.45	2.87	-	-	-	0.50	-	0.21	-	0.65	-	-	2.90	0.46	1.43	-	-	-
Cs	3.07	5.90	-	4.29	4.10	-	-	3.67	-	-	-	3.29	2.77	-	7.18	6.20	4.68	-	-	-	2.53	-	6.70	-	4.00	-	-	2.16	3.94	2.72	-	-	-

table 3 continued.

Sample	07LL2	07LL3	07LL4	07LL5	07LL6	07LL7	07LL9	07LL11	07LL12	07LL14	07LL15	07LL10	0 7LL25	07LL17	07LL18	07LL19	07LL20	07LL22	07LL23	07SM1	07SM6	07SM8	07SM13	COY0230	COY0231	COY0232	COY0233	COY0234	COY0235	CH4131	07SM3	07SM4	07SM2
Lat. °S	46,6274	46,6279	46,6282	46,6288	46,6292	46,6296	46,63033	46,63000	46,62950	46,62789	46,62779	46,63092	46,62977	46,62977	46,6165	46,61783	46,61594	46,60019	46,60019	47,11214	47,11268	47,11404	47,08499	-	-	-	-	-	-	-	47,12116	47,12006	47,08269
Lon. °W	72,3549	72,3590	72,3597	72,3601	72,3604	72,3605	72,36069	72,36061	72,36047	72,3594	72,35779	72,36006	72,36327	72,36327	72,26566	72,2692	72,26772	72,22856	72,22856	71,85268	71,85264	71,85735	71,8839	-	-	-	-	-	-	-	71,73196	71,73846	71,72465
Unit	TLLPa	Gt-graniteb	TLLP	dike	dike	TLLP	TLLP	diorite Las Llaves	TLLP	Ibáñez Fm.	TLLP	TLLP	TLLP	GAc	GA	GA	diorite Avilés	dike	dike	CNGPd	CNGP	CNGP	CNGP	SLPe	SLP	SLP	SLP	SLP-dike?	SLP	RLNPf	Co. Lápiz	Co. Lápiz	Mifeldi
Rock type	tonalite	granite	tonalite	rhyolite	basalt	tonalite	tonalite	diorite	tonalite	rhyolite	tonalite	tonalite	tonalite	granite	granite	granite	diorite	riolita	basalt	qtz-diorite	qtz-diorite	qtz-diorite	qtz-diorite	monzogranite	monzogranite	monzogranite	monzogranite	andesite	monzogranite	granite	alkali granite	alkali granite	porphyritic syenite
Ba	438.00	464.00	-	862.00	442.30	-	-	492.00	-	-	-	428.00	540.00	-	875.00	768.00	251.00	-	-	-	680.00	-	796.00	-	152.00	-	-	539.00	430.00	663.00	-	-	-
La	35.40	49.10	-	28.50	49.70	-	-	40.60	-	-	-	34.20	43.40	-	48.70	42.40	22.80	-	-	-	51.10	-	44.80	-	44.40	-	-	47.60	53.40	56.10	-	-	-
Ce	47.70	75.10	-	33.80	73.20	-	-	60.90	-	-	-	45.80	63.60	-	72.00	62.20	25.60	-	-	-	74.50	-	66.00	-	50.10	-	-	72.70	73.30	84.00	-	-	-
Pr	6.14	8.49	-	3.92	8.91	-	-	7.70	-	-	-	6.00	7.90	-	8.40	7.40	3.80	-	-	-	9.00	-	8.20	-	5.44	-	-	8.68	7.40	9.90	-	-	-
Nd	25.80	30.80	-	14.50	34.00	-	-	32.30	-	-	-	25.70	32.30	-	31.40	27.20	16.40	-	-	-	34.00	-	32.40	-	19.53	-	-	33.80	23.80	37.40	-	-	-
Sm	5.60	5.90	-	3.50	6.70	-	-	6.42	-	-	-	5.70	6.90	-	6.00	5.40	4.30	-	-	-	6.60	-	6.10	-	4.30	-	-	6.80	4.15	6.60	-	-	-
Eu	1.81	1.06	-	0.84	1.89	-	-	1.96	-	-	-	1.66	2.03	-	1.60	1.33	1.42	-	-	-	1.86	-	1.90	-	0.26	-	-	1.71	0.45	1.54	-	-	-
Gd	5.40	6.00	-	3.48	5.80	-	-	6.70	-	-	-	5.60	6.70	-	5.90	5.07	4.60	-	-	-	6.30	-	5.70	-	4.54	-	-	6.80	4.30	6.44	-	-	-
Tb	0.65	0.81	-	0.52	0.68	-	-	0.86	-	-	-	0.76	0.88	-	0.75	0.66	0.65	-	-	-	0.71	-	0.72	-	0.74	-	-	0.90	0.62	0.84	-	-	-
Dy	3.80	5.00	-	3.20	3.80	-	-	5.10	-	-	-	4.28	5.21	-	4.40	3.65	4.10	-	-	-	4.33	-	4.40	-	4.50	-	-	5.20	3.70	5.10	-	-	-
Ho	0.72	0.94	-	0.67	0.69	-	-	0.91	-	-	-	0.81	0.96	-	0.86	0.67	0.88	-	-	-	0.81	-	0.85	-	0.91	-	-	0.95	0.76	0.95	-	-	-
Er	2.22	2.99	-	2.07	1.87	-	-	2.75	-	-	-	2.34	2.90	-	2.40	2.10	2.60	-	-	-	2.34	-	2.70	-	2.80	-	-	2.58	2.34	2.90	-	-	-
Tm	0.29	0.41	-	0.32	0.24	-	-	0.36	-	-	-	0.28	0.40	-	0.37	0.28	0.38	-	-	-	0.34	-	0.40	-	0.42	-	-	0.37	0.36	0.43	-	-	-
Yb	1.90	2.80	-	2.21	1.50	-	-	2.40	-	-	-	2.00	2.60	-	2.40	1.84	2.60	-	-	-	2.20	-	2.60	-	3.00	-	-	2.40	2.57	2.94	-	-	-
Lu	0.27	0.43	-	0.35	0.23	-	-	0.36	-	-	-	0.27	0.42	-	0.40	0.32	0.38	-	-	-	0.38	-	0.42	-	0.45	-	-	0.37	0.38	0.45	-	-	-
Hf	4.33	4.40	-	7.09	4.60	-	-	3.70	-	-	-	3.20	4.58	-	8.20	7.50	2.00	-	-	-	4.90	-	4.03	-	5.00	-	-	7.50	4.80	8.50	-	-	-
Ta	0.71	0.77	-	1.28	1.25	-	-	0.75	-	-	-	0.64	1.17	-	1.27	1.18	0.21	-	-	-	0.89	-	0.61	-	2.60	-	-	1.44	2.60	1.52	-	-	-
W	1.12	1.60	-	0.81	0.46	-	-	0.95	-	-	-	0.53	0.80	-	1.90	1.27	0.42	-	-	-	1.10	-	0.57	-	3.46	-	-	1.34	2.20	3.10	-	-	-
Tl	0.20	0.60	-	0.44	0.10	-	-	l.d.	-	-	-	0.13	l.d	-	0.37	0.50	0.11	-	-	-	0.39	-	0.51	-	0.73	-	-	0.28	0.39	0.46	-	-	-
Pb	11.36	25.10	-	7.70	9.23	-	-	9.40	-	-	-	6.40	10.90	-	27.50	13.20	11.20	-	-	-	6.70	-	6.10	-	14.30	-	-	18.00	13.90	12.70	-	-	-
Bi	1.24	1.43	-	0.80	1.72	-	-	0.06	-	-	-	1.56	0.24	-	0.33	0.19	1.19	-	-	-	2.10	-	1.83	-	0.62	-	-	1.39	1.29	2.91	-	-	-
Th	8.40	15.18	-	26.50	4.86	-	-	6.90	-	-	-	4.40	7.74	-	15.20	17.50	2.50	-	-	-	11.70	-	7.70	-	22.20	-	-	10.50	20.40	18.50	-	-	-
U	1.76	2.90	-	5.40	1.12	-	-	1.84	-	-	-	1.02	2.04	-	4.30	4.70	0.63	-	-	-	2.70	-	2.03	-	5.90	-	-	2.57	4.00	3.90	-	-	-

a. TLLP: Tonalite in Paso de Las Llaves area.

b. Gt-granite: Porphyritic garnet bearing granite.

c. GA: Avilés Granite.

d. CNGP: Cerro Negro del Ghío pluton.

e. SLP: San Lorenzo pluton.

f. RLNP: Río de Las Nieves pluton.

l.d. Under detection limit.

TABLE 4. CHEMICAL COMPOSITION OF PLUTON SAMPLES FROM THE SOUTHERN AREA.

sample	07DN4	07DN5	07DN7	07DN9	07DN6	07DN11	07DN2	07BA3	07BA4	07BA6	07BA8	07BA22	07BA25	07BA26	07BA27	TP6	TP7A	TP7B	TP8	TP9	TP11	TP12	TP14	TP16
Lat. ºS	51,229	51,228	51,228	51,228	51,229	51,225	51,234	51,349	51,349	51,354	51,346	51,417	51,411	51,412	51,412	50,981	50,977	50,977	50,977	50,978	50,975	50,968	50,973	50,976
Lon. ºW	73,157	73,159	73,159	73,156	73,161	73,140	73,136	73,153	73,153	73,150	73,145	73,109	73,112	73,109	73,110	73,048	73,050	73,050	73,051	73,053	73,048	73,040	73,034	73,038
Unit	CDPa	CDP	CDP	CDP	CDP	dyke	dyke	BMCb	BMC	BLGc	BLG	dyke	BMC	BLG	BLG	PMCd	PGe	PMC	PG	PMC	PG	PG	PG	PG
rock type	granite	granite	granite	granite	qtz diorite	rhyol.	basalt	diorite	diorite	Leucogte	Leucogte	pink dke.	gabbro	granite	granite	diorite	felsic intrusion	mafic enclave	granite	diorite	granite	granite	granite	miarolitic gte.
Major elements (wt%)																								
SiO_2	57.3	66.1	65.7	62.4	55.87	69.5	45.7	52	53.4	74.9	78.43	75.69	48.7	75.3	75	-	-	-	-	-	-	-	-	-
TiO_2	0.77	0.4	0.44	0.53	0.71	0.15	2.63	2.27	1.85	0.21	0.16	0.2	3.1	0.18	0.16	-	-	-	-	-	-	-	-	-
Al_2O_3	18.3	17	16.9	17	16	15.9	17.8	16.7	17	13.2	12	11.7	15.5	12	12.5	-	-	-	-	-	-	-	-	-
Fe_2O_3	1.15	0.79	0.76	2.12	1.58	1	2.19	1.89	2	1.32	0.34	0.85	2.24	1.52	1.04	-	-	-	-	-	-	-	-	-
FeO	5.12	2.2	2.6	2.8	5.84	1.4	8.4	7.08	6.12	0.12	0.08	1.76	8.76	0.6	1	-	-	-	-	-	-	-	-	-
MnO	0.13	0.06	0.06	0.09	0.22	0.09	0.15	0.14	0.13	0.03	0.01	0.05	0.15	0.03	0.03	-	-	-	-	-	-	-	-	-
MgO	3.14	1.53	1.69	2.19	5.67	0.31	5.14	2.8	2	0.06	0.05	0.05	3.48	0.04	0.06	-	-	-	-	-	-	-	-	-
CaO	6.04	3.23	3.43	4.94	6.84	1.57	10.14	4.59	4.16	0.16	0.19	0.11	8.62	0.12	0.17	-	-	-	-	-	-	-	-	-
Na_2O	3.49	3.51	3.4	3.47	2.79	3.57	2.66	4.85	5.15	3.64	3.35	3.4	4.26	4.13	4.55	-	-	-	-	-	-	-	-	-
K_2O	2.51	3.3	3.27	2.55	2.02	3.18	0.1	3.14	3.99	5.3	4.56	4.45	1.88	4.68	4.94	-	-	-	-	-	-	-	-	-
P_2O_5	0.4	0.2	0.22	0.32	0.41	0.11	0.48	0.79	0.71	0.05	0.03	0.02	0.52	0.03	0.03	-	-	-	-	-	-	-	-	-
LOI	1.33	1.5	1.33	1.25	1.92	2.76	4.33	3.67	3.16	0.85	0.46	1.41	2.35	0.88	0.4	-	-	-	-	-	-	-	-	-
Total	99.68	99.82	99.8	99.66	99.87	99.54	99.72	99.92	99.67	99.84	99.66	99.69	99.56	99.51	99.88	-	-	-	-	-	-	-	-	-
Trace elements (ppm)																								
Sc	41	40	34	33.9	24.3	32	43	34.2	33	25	2.8	3.6	42	26	25	71	66	63	72	70	58	66	64	68
Ti	-	-	-	-	-	-	-	-	-	-	-	-	-	-	-	7,378	1,732	11,886	1,972	6,017	1,565	2,360	1,772	397
V	125	126.4	62.9	74	172	13.5	205	102	58.25	12.6	5	2.9	220	13.1	10.567	106	33.1	189	34.7	142	28.8	41	36.6	21.2
Cr	36	34.7	24.9	25.2	215	2.46	177	8.8	7.87	2.2	3.4	3.82	20.4	14.53	1.753	14.2	4.5	112	4.2	11.7	3.3	6.3	6.6	3.6
Co	15.1	15.1	5.9	9	23.7	3.9	42	32	24.606	1.045	0.98	47	27.4	43.1	6.762	14.0	2	35.7	5.3	20.4	2.8	9.3	3.19	0.64
Ni	31	16.5	9.8	22	71.4	15.7	57	15.8	14.005	4.6	2.39	6.7	17.4	4.5	6.692	23.5	14.1	115	13.9	18.0	15.9	13.3	12.6	16.1
Cu	19.8	6.2	41.3	9.5	63	12.7	37	2.84	4.763	2.064	59.4	9.7	31.5	1.6	8.069	168	67	246	30.6	59	108	43	41.6	41
Zn	73	73.6	36.4	51	115	65.3	104.3	132	113	35	26.8	147	139	107	89	149	74	222	96	150	86	116	128	60
Ga	38.4	37.5	37.9	38.6	19.7	38.9	20.1	23.6	24.8	19.4	25.5	38.3	30.4	31.1	30.475	22.3	18.7	22.6	21.9	21.5	19.0	21.6	19.5	17.4
Ge	7.1	6.71	6.8	7.6	2	6	4.2	9.8	10.1	7	1.63	1.5	4.7	12.1	10.513	1.4	1.17	1.6	1.6	1.6	1.45	1.51	1.5	1.53
As	2.35	2	2.1	4	3.7	1.5	3.8	47	39	3.3	2.55	1.8	7	1.45	7.06	-	-	-	-	-	-	-	-	-
Se	1.9	l.d	1.5	0	-	2.4	1.4	4	3.1	1.2	-	-	2.2	3.2	l.d	-	-	-	-	-	-	-	-	-
Rb	92	90.6	154	88.8	122.8	119.8	0.89	191.3	179	222	404	141.7	41.5	130	131	96	122	195	171	124	173	155	170	202
Sr	669	658	689	793	636	231	635	493	445	37.9	22	8	528	9.1	7.28	570	207	741	307	814	273	312	240	17.3
Y	19.6	19.3	11.47	15.12	28	8.13	18.6	35.6	40.1	35.14	46.7	44.3	25.3	47.4	41.7	25.6	10.8	25.5	21.8	23.6	25.2	22.1	19.3	28.7
Zr	150	153	137	147	124	82	97	333	365	116	192	462	206	368	354	262	175	212	208	200	179	212	188	92
Nb	9.2	8.69	8	7.8	9.72	14.1	19.2	53.1	55.4	17.1	24.8	65.9	41.6	67.6	54.3	32.2	19.6	36.6	22.2	15.4	22.2	25.9	23.4	23.3
Mo	1.015	0.553	1.33	2.2	9.9	3.3	2	1.6	4.2	4.5	1.98	2.56	2.7	1.7	2.7	-	-	-	-	-	-	-	-	-
Rh	0.031	0.015	0.013	0.022	l.d	0.02	0.018	0.023	0.012	0.009	l.d	0.02	0.023	0.009	0.023	-	-	-	-	-	-	-	-	-
Ag	0.59	0.7	0.718	0.52	0.5	0.58	0.58	0.77	0.84	0.47	0.52	0.93	0.736	0.9	0.702	-	-	-	-	-	-	-	-	-
Cd	l.d	0.061	l.d.	l.d	0.13	0.05	0.06	0.22	0.4	l.d	0.13	0.32	0.25	0.18	0.24	l.d.	l.d.	l.d.	l.d.	l.d.	l.d.	0.21	0.24	l.d.
Sn	2.2	1.32	1.25	1.6	4.7	3.13	1.46	35.422	26	6.7	4.15	8.3	4.8	9.165	7.24	24.0	2.6	6.0	2.14	9.6	14.8	3.7	3.1	3.0

table 4 continued.

sample	07DN4	07DN5	07DN7	07DN9	07DN6	07DN11	07DN2	07BA3	07BA4	07BA6	07BA8	07BA22	07BA25	07BA26	07BA27	TP6	TP7A	TP7B	TP8	TP9	TP11	TP12	TP14	TP16
Lat. ºS	51,229	51,228	51,228	51,228	51,229	51,225	51,234	51,349	51,349	51,354	51,346	51,417	51,411	51,412	51,412	50,981	50,977	50,977	50,977	50,978	50,975	50,968	50,973	50,976
Lon. ºW	73,157	73,159	73,159	73,156	73,161	73,140	73,136	73,153	73,153	73,150	73,145	73,109	73,112	73,109	73,110	73,048	73,050	73,050	73,051	73,053	73,048	73,040	73,034	73,038
Unit	CDPa	CDP	CDP	CDP	CDP	dyke	dyke	BMCb	BMC	BLGc	BLG	dyke	BMC	BLG	BLG	PMCd	PGe	PMC	PG	PMC	PG	PG	PG	PG
rock type	granite	granite	granite	granite	qtz diorite	rhyol.	basalt	diorite	diorite	Leucogte	Leucogte	pink dke.	gabbro	granite	granite	diorite	felsic intrusion	mafic enclave	granite	diorite	granite	granite	granite	miarolitic gte.
Sb	0.82	0.459	0.45	1.01	0.37	1.7	0.44	3.97	3.92	1.35	0.41	0.8	0.49	0.68	0.551	0.95	0.86	1.12	1.24	1.95	1.06	0.60	1.32	1.14
Cs	3.88	3.9	5.3	2.99	8.1	3.35	0.63	23.49	10.8	11.948	5.8	0.833	2.49	1.22	1.91	4.8	2.87	12.6	4.1	5.3	3.17	5.9	8.6	6.0
Ba	562	562	638	640	461	687	89.6	254	411	88.2	40.2	22.8	206.4	18.3	18.95	656	462	764	632	534	549	562	441	23.2
La	33.2	33.1	36.6	40.1	45.5	28.4	20.2	49.4	51.2	35.7	45.7	62.8	33.3	69.7	56.2	44	35.1	53	65	40.8	46.6	50	41.1	36.5
Ce	59	57.7	59.7	69.3	67.9	46.6	33.2	90.5	95	67.4	64	98	55.8	122	98.6	80	55	88	94	78	80	79	66	53
Pr	7	6.8	6.36	7.7	8.9	5.23	4.4	10.8	11.479	6.45	6.3	10.8	7.14	13.5	10.78	9.2	5.5	9.7	9.6	9.2	8.4	7.9	6.6	5.5
Nd	26.8	27	22	28.5	35.5	17.9	20.1	41.8	45.4	21.2	19.4	38.9	30.54	47.8	38	36	19.4	37.4	34.0	35.7	30.2	26.9	22.1	19.8
Sm	5.42	5.246	3.8	4.98	7.3	3.2	4.9	9.4	9.75	4.7	4.1	8.4	7.1	10.1	8.2	7.3	3.5	7.2	5.8	6.6	5.6	5.0	4.1	4.4
Eu	1.45	1.55	1.06	1.41	1.8	0.95	1.91	2.4	2.783	0.324	0.14	0.48	2.19	0.49	0.42	1.63	0.77	1.79	1.02	1.56	0.86	0.84	0.70	0.13
Gd	5.1	5	3.37	4.2	6.9	2.8	5.4	9.2	10	5.2	5.1	9.5	7.5	10.4	8.6	5.5	2.51	5.4	3.7	4.4	4.1	3.6	2.9	3.7
Tb	0.66	0.68	0.41	0.57	0.95	0.32	0.73	1.239	1.39	0.92	1	1.43	1.05	1.6	1.39	0.85	0.36	0.81	0.60	0.70	0.66	0.59	0.48	0.69
Dy	3.71	3.7	2.24	3	5.6	1.57	4.3	7.5	8.1	6.2	7.7	8.6	5.7	9.5	8.6	5.1	1.90	4.6	3.6	4.1	4.0	3.6	3.09	4.5
Ho	0.74	0.74	0.41	0.61	1.04	0.28	0.73	1.37	1.57	1.29	1.64	1.73	1.03	1.76	1.63	1.02	0.37	0.90	0.73	0.84	0.83	0.75	0.65	0.94
Er	2.285	2.2	1.24	1.69	3.17	0.93	2	3.84	4.19	4	5.6	4.9	2.7	5.185	4.7	2.8	1.04	2.5	2.06	2.3	2.4	2.21	1.9	2.9
Tm	0.28	0.294	0.17	0.23	0.45	0.107	0.25	0.5	0.61	0.58	0.85	0.64	0.32	0.72	0.63	0.40	0.148	0.35	0.31	0.33	0.37	0.31	0.28	0.45
Yb	2.05	2	1.3	1.45	2.9	0.78	1.5	3.4	3.83	3.7	5.9	4.5	2.1	4.4	3.9	2.5	1.02	2.17	2.06	2.2	2.4	2.1	1.97	2.9
Lu	0.29	0.33	0.21	0.25	0.47	0.13	0.22	0.46	0.53	0.52	0.77	0.63	0.3	0.58	0.53	0.37	0.16	0.31	0.31	0.32	0.37	0.32	0.33	0.43
Hf	4.17	4.16	3.69	4.1	3.7	2.8	2.71	8.2	8.3	4.18	6.9	12.5	5.3	10.7	9.9	6.7	4.5	4.8	5.6	5.2	5.0	5.6	5.05	3.5
Ta	0.97	0.99	1.03	0.96	0.7	1.54	1.72	4.45	4.7	2.75	3.65	4.65	3	5.36	4.52	2.00	0.99	1.92	1.85	1.02	2.16	2.01	1.79	2.77
W	5.13	6	0.8	0.25	1.38	15.6	47.6	87	47.1	5.56	11.7	270	1.1	291	40.06	-	-	-	-	-	-	-	-	-
Tl	0.52	0.6	1.16	0.54	0.58	0.93	0.006	1.64	1.52	0.96	0.84	0.31	0.35	0.7	0.51	0.40	0.48	0.82	0.61	0.54	0.59	0.59	0.72	0.79
Pb	10.4	10.7	9.9	11.08	6.1	20.8	2.41	51.1	26.5	15.2	8.9	10.9	5.74	6.5	9.9	12.0	14.9	6.4	16.8	8.8	13.5	17.4	16.6	19.2
Bi	0.15	5.2	5.2	4.2	1.8	0.377	7.3	3.6	4	4.6	2.46	0.22	3.3	5	0.29	0.23	l.d	4.9	2.55	0.17	8.2	8.4	0.13	0
Th	8.77	8.9	13.5	12.4	7.35	11.2	1.7	13.3	12.17	36.1	44	12.95	3.76	18	14.7	12.1	20.1	7.5	27.8	12.4	20.9	20.7	21.5	30.1
U	1.26	1.29	3.7	1.45	1.9	3.93	0.49	3.6	3.36	8.5	9.6	3.65	1.37	4.1	4.4	3.2	2.53	2.31	3.9	2.52	3.3	2.7	1.79	5.3

a. CDP: Cerro Donoso pluton.

b. BMC: Monte Balmaceda Mafic Complex.

c. BLG: Monte Balmaceda Leucogranites.

d. PMC: Torres del Paine Mafic Complex.

e. PG: Torres del Paine granites.

l.d. Under detection limit.

TABLE 5. WHOLE ROCK Sr AND Nd ISOTOPIC DATA OF PLUTON SAMPLES FROM THE NORTHERN AREA.

Sample	Unit	Age (Ma)	Sm (ppm)	Nd (ppm)	$^{147}Sm/^{144}Nd$	$^{143}Nd/^{144}Nd$	$(^{143}Nd/^{144}Nd)t$	eps (Nd)	Rb (ppm)	Sr (ppm)	$^{87}Rb/^{86}Sr$	$^{87}Sr/^{86}Sr$	$(^{87}Sr/^{86}Sr)t$
07LL2	TLLPa	9	5.6	25.8	0.1312	0.512688	0.512680	1.1	59.9	828	0.2092	0.704778	0.704751
07LL3	Gt-graniteb	9	5.9	30.8	0.1158	0.512362	0.512354	-5.3	169	69.4	7.0548	0.721085	0.720083
07LL5	dike	9	3.5	14.5	0.1459	0.512633	0.512623	0	117.8	202	1.6869	0.705277	0.705037
07LL6	dike	9	6.7	34	0.1191	0.512722	0.512715	1.7	28.1	1,057	0.0769	0.704596	0.704586
07LL10	TLLP	9	5.7	25.7	0.1341	0.512703	0.512695	1.3	38.2	808	0.1367	0.704629	0.704611
07LL11	diorite Las Llaves	9	6.42	32.3	0.1202	0.512702	0.512695	1.3	63	820	0.2222	0.704512	0.704483
07LL25	TLLP	9	6.9	32.3	0.1292	0.512752	0.512744	2.3	55	787	0.2021	0.704527	0.704501
07LL18	GAc	8	6	31.4	0.1155	0.512669	0.512663	0.7	123	579	0.6144	0.704637	0.704564
07LL19	GA	8	5.4	27.2	0.1200	0.512708	0.512701	1.4	177	488	1.0491	0.704648	0.704523
07LL20	diorite Avilés	8	4.3	16.4	0.1585	0.512730	0.512721	1.8	44.1	601	0.2122	0.704322	0.704297
07SM6	CNGPd	15	6.6	34	0.1174	0.512779	0.512768	2.9	105	1,210	0.2510	0.703851	0.703798
07SM13	CNGP	15	6.1	32.4	0.1138	0.512754	0.512743	2.4	71	949	0.2164	0.704152	0.704107
CH4131	RLNPe	3	6.6	37.4	0.1067	0.512701	0.512699	1.3	127	434	0.8464	0.704662	0.704624
COY0231	SLPf	6	4.3	19.53	0.1331	0.512561	0.512555	-1.4	199	53	10.8617	0.706159	0.705166
COY0234	SLPg	6	6.8	33.8	0.1216	0.512651	0.512646	0.3	77	509	0.4376	0.705089	0.705049
COY0235	SLP	6	4.15	23.8	0.1054	0.512609	0.512605	-0.5	154	100	4.4546	0.705490	0.705083

a. TLLP: Tonalite in Paso de Las Llaves area.

b. Porphyritic garnet bearing granite.

c. GA: Avilés Granite.

d. CNGP: Cerro Negro del Ghío pluton.

e. RLNP: Río de Las Nieves pluton.

f. SLP: San Lorenzo pluton (granites).

g. SLP: San Lorenzo pluton (andesite).

TABLE 6. WHOLE ROCK Sr AND Nd ISOTOPIC DATA OF PLUTON SAMPLES FROM THE SOUTHERN AREA.

Sample	Unit	Age (Ma)	Sm (ppm)	Nd (ppm)	$^{147}Sm/^{144}Nd$	$^{143}Nd/^{144}Nd$	$(^{143}Nd/^{144}Nd)t$	eps (Nd)	Rb (ppm)	Sr (ppm)	$^{87}Rb/^{86}Sr$	$^{87}Sr/^{86}Sr$	$(^{87}Sr/^{86}Sr)t$
07BA25	BMCa	15	7.1	30.54	0.1406	0.512892	0.512878	5.1	41.5	528	0.2273	0.703304	0.703254
07BA3	BMC	15	9.4	41.8	0.1360	0.512886	0.512872	5.0	191.3	493	1.1222	0.703511	0.703265
07BA4	BMC	15	9.75	45.4	0.1298	0.512891	0.512878	5.1	179	445	1.1633	0.703574	0.703319
07BA6	BLGb	15	4.7	21.2	0.1340	0.512737	0.512723	2.1	222	37.9	16.9499	0.709278	0.705557
07BA8	BLG	15	4.1	19.4	0.1278	0.512765	0.512752	2.6	404	22	53.1989	0.720833	0.709153
07BA22	BLG	15	8.4	38.9	0.1306	0.512854	0.512841	4.3	141.7	8	51.3382	0.725927	0.714655
07BA26	BLG	15	10.1	47.8	0.1278	0.512866	0.512853	4.6	130	9.1	41.3782	0.719066	0.709981
07BA27	BLG	15	8.2	38	0.1305	0.512854	0.512841	4.3	131	7.28	52.1313	0.721179	0.709733
07DN2	basaltic dike	27	4.9	20.1	0.1474	0.512929	0.512903	5.8	0.89	635	0.0041	0.704406	0.704404
07DN4	CDPc	27	5.42	26.8	0.1223	0.512606	0.512584	-0.4	92	669	0.3978	0.705092	0.704938
07DN5	CDP	27	5.246	27	0.1175	0.512638	0.512617	0.3	90.6	658	0.3983	0.704868	0.704713
07DN6	CDP	27	7.3	35.5	0.1243	0.512636	0.512614	0.2	122.8	636	0.5585	0.704901	0.704684
07DN7	CDP	27	3.8	22	0.1044	0.512633	0.512614	0.2	154	689	0.6465	0.704857	0.704606
07DN9	CDP	27	4.98	28.5	0.1056	0.512629	0.512610	0.1	88.8	793	0.3239	0.704910	0.704784
07DN11	rhyolitic dike	27	3.2	17.9	0.1081	0.512557	0.512538	-1.3	119.8	231	1.5002	0.705739	0.705157
TP6	PMCd	13	7.3	36.0	0.1230	0.512680	0.512670	0.9	96.1	570.5	0.4871	0.704480	0.704393
TP7A	PGe	13	3.5	19.4	-	-	-	-	121.6	206.9	-	-	-
TP7B	PMC	13	7.2	37.4	0.1159	0.512767	0.512757	2.6	195.2	741.3	0.7618	0.704488	0.704352
TP8	PG	13	5.8	34.0	0.1038	0.512581	0.512572	-1.0	171.2	306.9	1.6136	0.704893	0.704604
TP9	PMC	13	6.6	35.7	0.1122	0.512706	0.512697	1.5	124.5	814.2	0.4421	0.704019	0.703940
TP11	PG	13	5.6	30.2	0.1129	0.512576	0.512567	-1.1	172.7	273.3	1.8281	0.704933	0.704606
TP12	PG	13	5.0	26.9	0.1113	0.512616	0.512607	-0.3	155.0	312.3	1.4355	0.705025	0.704768
TP13	PG	13	-	-	0.0000	0.512606	-	-	-	-	-	0.707890	-
TP14	PG	13	4.1	22.1	0.1113	0.512623	0.512614	-0.2	169.8	240	2.0463	0.705179	0.704813
TP16	PG	13	4.4	19.8	0.1342	0.512594	0.512583	-0.8	202.2	17.3	33.8965	0.710579	0.704514

italics represent anomalous values

a. BMC: Monte Balmaceda Mafic Complex.

b. BLG: Monte Balmaceda Leucogranites.

c. CDP: Cerro Donoso pluton.

d. PMC: Torres del Paine Mafic Complex.

e. PG: Torres del Paine granites.

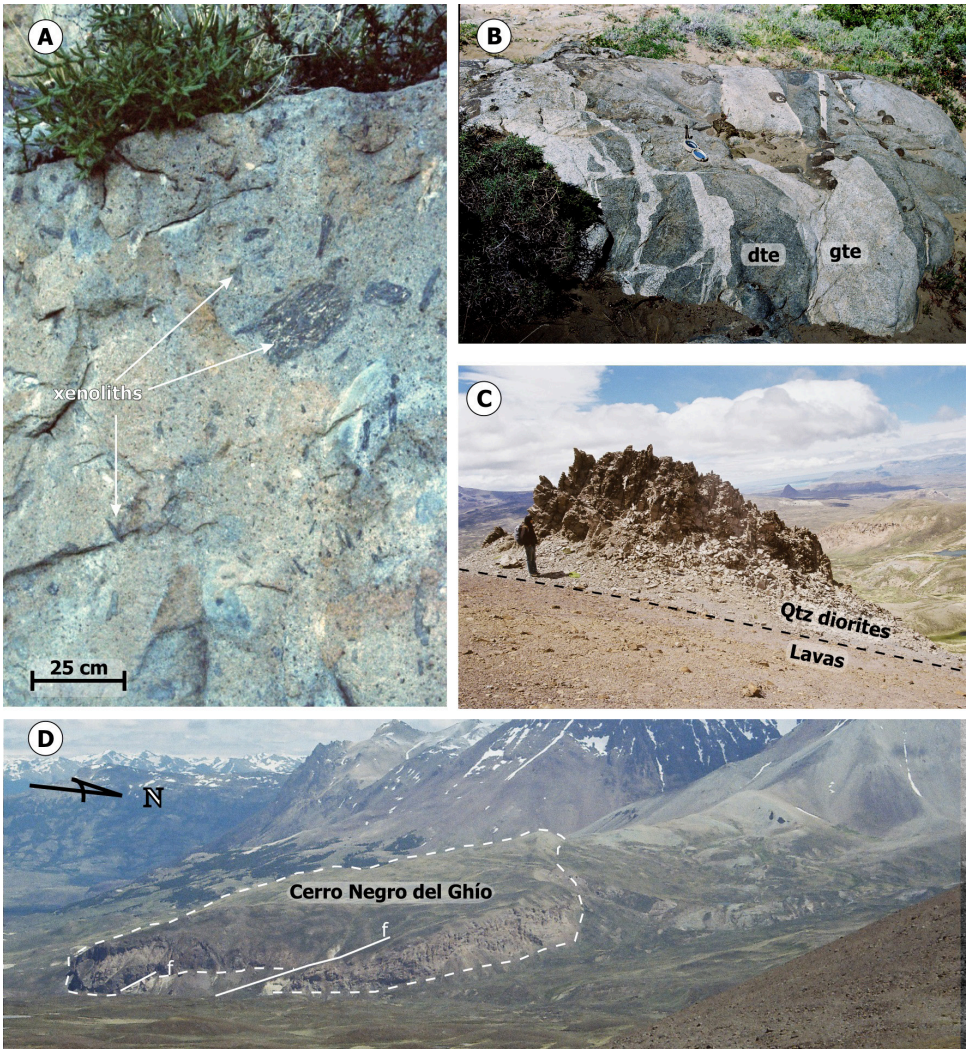

FIG. 5. Field photographs from northern area. **A.** Schist xenoliths close to a vertical contact of the Paso de Las Llaves pluton. **B.** Granite (gte) intrusion in diorite (dte) with lobate contacts. Río Avilés area, Paso de Las Llaves pluton. **C.** Hill top northward of Cerro Negro del Ghío pluton, where quartz-diorite intrude lavas from the Ibáñez Group. The sample 07SM13 is from this area. **D.** Cerro Negro del Ghío pluton. The sill like disposition can be appreciated as well as a distinct whitish facies in the southeast border of the intrusive.

Previous radiometric data, with different geochronological methods, indicate an age range from 8.9 to 11.1 Ma (Petford and Turner, 1996; Pankhurst *et al.*, 1999; Suárez and De la Cruz, 2001). Pankhurst *et al.* (1999) referred to this pluton as a satellite body of the South Patagonian batholith.

4.2. Cerro Negro del Ghío Pluton

The main outcrop of this pluton is nearly round in shape, approximately 1.8 km in diameter, with a horizontal tabular disposition (Fig. 5D). Another outcrop area appears as a smaller (<1 km in diameter) isolated body on the top of a hill a few kilometers northward (Fig. 5C). The contact relationships can be observed at the bottom of the main outcrop and in the northern margin of the smaller outcrop (Fig. 5C) where quartz diorites intrude host lavas. The eastern and northern margins of the largest outcrop are cut by normal faults.

This pluton consists mainly of porphyritic quartz-diorites with large plagioclase (An_{45-57}, up to An_{63} cores;

Table 1) and hornblende phenocrysts, minor phases are pyroxene and biotite. In the groundmass an intergrowth of quartz with Na-rich plagioclase (Ab_{84-91}) predominates. Other phases are pyroxene, hornblende and opaque minerals, and glass is also present locally. Mafic enclaves are rare and they have sharp contacts with the quartz-diorite. A second major facies of the pluton is observed in the core of the outcrop where a more whitish facies seems to have been intruded into the main quartz-diorite (Fig. 5D).

The Cerro Negro del Ghío pluton has a K-Ar hornblende age of 15.8±0.6 Ma (Ramos, 2002), and two bulk rock K-Ar determinations yielding 15.8±0.7 and 18±1.2 Ma (Ramos, 2002).

4.3. San Lorenzo Pluton

This intrusive is part of a plutonic complex composed by the Sobral (*ca.* 143 Ma), Tranquilo (*ca.* 84 Ma), Del Salto (*ca.* 84 Ma) and San Lorenzo (6.2±0.12 Ma; ($^{40}Ar/^{39}Ar$ in biotite; Welkner, 1999, 2000)) plutons. Del Salto pluton is the only one of the complex with alkaline mineralogy (Welkner *et al.*, 2002). The San Lorenzo pluton intrudes the Jurassic Sobral pluton (Welkner, 1999, 2000) (Fig. 2), where biotite syenogranite is the predominant facies. In addition, monzonites and hornblende and biotite granodiorite horizontally layered enclaves are common in monzogranite facies (Welkner, 1999). In this work, we studied monzogranite samples with similar characteristics to those mentioned by Welkner (1999), but we also found that they have abundant granophyric textures (*e.g.,* mirmekites), and an andesitic facies with unexposed contact relation with the other facies, probably corresponding to a dike (sample COY0234).

4.4. Río de Las Nieves Pluton

This pluton has a near elliptical outcrop shape, with a *ca.* 6 km long axis and a *ca*. 3.5 km short axis (Fig. 2). Difficult access has precluded detailed descriptions of this unit and its field relations. Nonetheless, Morata *et al.* (2002) described it as a biotite quartz-monzonite. In this work we studied a biotite and hornblende monzo-granite with perthite phases and oscillatory-zoned plagioclase as major mineral phases and Fe-Ti oxides, apatite and zircon as minor mineral phases. A K-Ar age determination in biotite gave 3.2±0.4 Ma (Morata *et al*., 2002).

4.5. Alkaline plutons in the Meseta del Lago Buenos Aires

There are 3 intrusions, the Pico Rojo syeno-diorite of circular shape (Espinoza *et al.*, 2008), the Mifeldi pluton, a laccolith-shaped microsyenite, and the Cerro Lápiz volcanic neck, composed by micro-granites. They are all alkaline felsic rocks (Espinoza *et al.*, 2008) that crop out in the west border of the Meseta del Lago Buenos Aires basaltic plateau (Fig. 2). Both, Mifeldi and Cerro Lápiz, have an intrusive relationship with the lavas. The Pico Rojo contact with the lavas is not exposed (Espinoza *et al.*, 2008). These plutons have ages which range between 3.98±0.1 (K-Ar in whole rock), and 3.29±0.22 ($^{40}Ar/^{39}Ar$ in groundmass) (Brown *et al*., 2004; Espinoza *et al.*, 2008).

4.6. Torres del Paine intrusive complex

This complex has a nearly elliptical shape covering an area of 150 km^2 (Michael, 1984), with a maximum E-W elongation of 16 km (Fig. 3). It is laccolith-shaped and has an exposed maximum vertical elevation of over 2,500 m (Michel *et al.*, 2008). Country rocks show variable degrees of deformation at the roof and eastern edge of the complex, and a contact metamorphic aureole that obliterates the ubiquitous slaty cleavage of the host rock. This complex is constituted by the basal Paine Mafic Complex (PMC) and by the Paine Granite (PG). The PMC restricted outcrops are overlain by the PG at a nearly constant altitude of 1,000 m a.s.l. (Michael, 1984).

The PMC consists of a *ca*. 400 m thick layer of mafic facies, mainly composed by gabbros, monzodiorites, quartz monzodiorites and large granite patches (Michael, 1991), but also gabbronorites (Leuthold *et al*., 2013). The gabbros are located at the lowest levels and they grade into quartz-monzodiorites near the PG contact in the upper 300 m of the PMC (Michael, 1991). Some of the gabbros have cumulate and/or layering textures. The mafic and intermediate rocks are often in sharp irregular contact and no smooth progression of composition is observed. The granite patches have engulfed contacts with the mafic rocks (Michael, 1991). The base of the PMC does not crop out, and there is no reported contact between this unit and the country rocks. Plagioclase crystals

in the gabbros are usually large (up to 4 mm) and are strongly and discontinuously zoned, having An_{70} cores and An_{15} rims, with a narrow transition between An_{55} and An_{25} (Michael, 1991).

The PG has a maximum vertical extent of about 2000 m (Michael, 1984). Some glacial valleys expose many contact zones with the country rocks, where aplitic spires into the host rocks are visible. In the upper part, stepping (staircase-shaped) contact is a frequent feature of the intrusion, and in some cases the aplitic spires are linked to steps. In the eastern part of the pluton, the bottom of the granite is not in contact with PMC rocks but directly with the country rocks, suggesting that the PMC has a smaller extension than the PG. The eastern termination of the pluton is underlain by a giant magmatic breccia (up to metric sized blocks), suggesting an eastward magma propagation during pluton construction. The PG can be subdivided into three units (Michel *et al*., 2008), from top to bottom: Unit I, II and III. Unit I is a silica-rich biotite granite, with abundant granophyric and miarolitic textures, and corresponds to the upper unit in contact with the roof country rocks. Unit II consists of reddish-weathering biotite-hornblende granite and is equivalent to the red granite of Michael (1984). Unit III is younger than Unit I (Michel *et al*., 2008). It is the most voluminous and consists in a grey-weathering biotite and hornblende granite, which corresponds to the white granite of Michael (1984). The base of this unit is in contact with the basal PMC. The plagioclase within the granite commonly shows a strong zonation from An_{50} cores to An_{15} rims and some crystals have discontinuously zoned calcic cores, up to An_{78} (Michael, 1991) with rare large crystals up to 3 mm in diameter with $An_{25\text{-}10}$ (Michael, 1984). On the basis of petrographicevidence, geochemistry and microprobe analyses, Michael (1983, 1984, 1991) considered the Paine Granite and the Paine Mafic Complex as co-magmatic and consangineous (*sic*) units.

Dating in the PG gave ages mostly between 12.5 and 13 Ma (Halpern, 1973; Sánchez *et al*., 2006; Michel *et al.,* 2008; Leuthold *et al*., 2012).

4.7. Paine External Gabbros

These rocks correspond to isolated outcrops in the neighbourhood of the Torres del Paine Intrusive Complex, in the form of sills and dikes.

Michael (1983) described olivine-two pyroxene gabbros and bronzite orthoclase gabbros, with geochemical analyses showing a calc-alkaline trend. Altenberger *et al.* (2003) found that some of these rocks are folded together with the country rocks, and thus pre-date the regional deformation and the Torres del Paine intrusive complex emplacement. These authors described the gabbros as composed by plagioclase, hornblende, clinopyroxene, biotite, apatite and opaque minerals; and with a geochemical alkaline composition (Altenberger *et al*., 2003, and references therein). A K-Ar age determination in biotite yielded 29.4±0.8 Ma (Altenberger *et al*., 2003). A U-Pb determination in zircons, in rocks from the same area studied by Altenberger *et al.* (2003), gave 16.9±0.2 Ma (Fosdick *et al*., 2011), but the gabbros studied by the later authors are undeformed.

Thus, these "external gabbros" represent at least two pulses of basic magmas at the Oligocene (deformed) and at the Miocene (undeformed).

4.8. Cerro Donoso Pluton

This pluton has an approximately circular shape, with a 750 m diameter in plan view, with vertical discordant contacts with the host rocks (Fig. 6A). Country rocks are smoothly plunging sandstones dominated turbidites from the Punta Barrosa Formation (Cretaceous) in which the Cerro Donoso pluton generated a contact metamorphic aureole tens of meters wide (Muñoz, 1981).

The main facies consists in a medium grained hornblende and biotite-bearing granodiorite. At lower levels, it also bears some mafic enclaves and quartz veins (Fig. 6B). In an internal area of the pluton there is a vertical fabric highlighted by the hornblende alignment (Fig. 6C). The pluton locally has a porphyritic texture with large (1-4 mm) plagioclase crystals set within a recrystallized quartz mass. A common feature of the plagioclases are re-absorption/re-crystallization textures (Fig. 7A). Some of them are strongly zoned (*e.g.,* from an An_{68} core to An_{16} rim) (Table 2), and/or with a sieve-like texture and sericitic alteration. Many plagioclase grains are around 0.5 mm in diameter and compositionally $An_{42\text{-}44}$, some have Na-rich rims. The orthoclase is perthitic and partially replaced by muscovite. The biotite is partially replaced by chlorite.

Within the pluton, a quartz diorite facies crops out as a sill (Fig. 6D), which is a hornblende and

biotite-rich facies, with large (>1 mm) and highly altered hornblende crystals, coexisting with small, fresh and euhedral ones. A particular characteristic of this facies is that some hornblende seems to form by replacement of older biotite. This appears to correlate with plagioclase growth, in which two step developments can be recognized: **1)** a relatively homogeneous core with sieve texture and **2)** zoned borders. These features may be indicative of strong compositional variations during the crystallization of the magma.

The vertical fabric revealed by the hornblende orientation, as well as by all vertical contacts of the main pluton, together with the circular outcrop shape, suggests that the granitic intrusion cooled while the magma was ascending by a cheminée conduit.

In the surroundings of the pluton outcrop area, there are several rhyolitic and andesitic-basalt dikes, most of them with a N-S to N10ºW strike. One of the rhyolitic dikes is faulted (Fig. 6E), so at least this dike pre-dates regional deformation, similarly to the

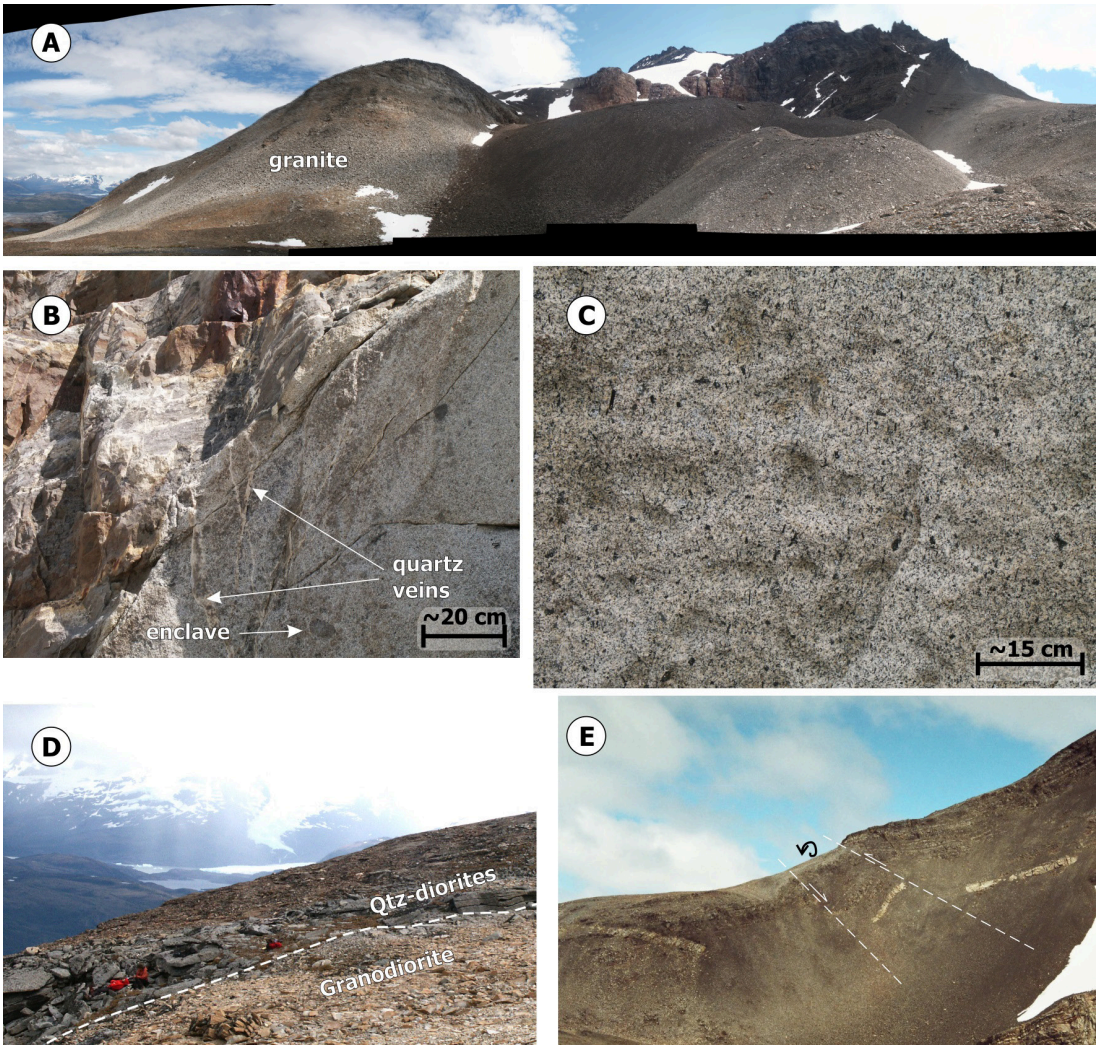

FIG. 6. Field photographs from cerro Donoso in the southern area. **A.** Cerro Donoso pluton, panoramic view to the east showing vertical contacts. **B.** Granodioritic facies in the lower levels of the outcrop (930-1,000 m a.s.l.), quartz-veins and mafic enclaves are frequent characteristics inside the granodiorite. **C.** Vertical fabric given by hornblende crystals orientation in the granodiorite, this facies area is near the "core" of the pluton. **D.** Quartz-diorite outcrop with sub-horizontal disposition, representing the only massive mafic facies found in this pluton. **E.** A faulted rhyolitic dike in the nearby area of the Cerro Donoso pluton. Dike is *ca.* 60 cm wide.

Paine External Gabbros. No dikes were found cutting the main pluton, which is undeformed. Therefore, the deformation events pre-date the main pluton intrusion.

4.9. Monte Balmaceda intrusive complex

This complex is composed of apparently disconnected bodies (Fig. 8A), but our mapping shows that all outcrops probably belong to the same intrusion. It has an N-S elongated outcrops area, which covers around 180 km^2 (Fig. 3). The 3-D shape is laccolithic, and the field relations are similar to those of Torres del Paine Intrusive Complex. Even though not all the outcrops could be examined, two main igneous facies for the intrusive complex have been recognized: a yellow alkali feldspar leucogranite (BLG), and a mafic

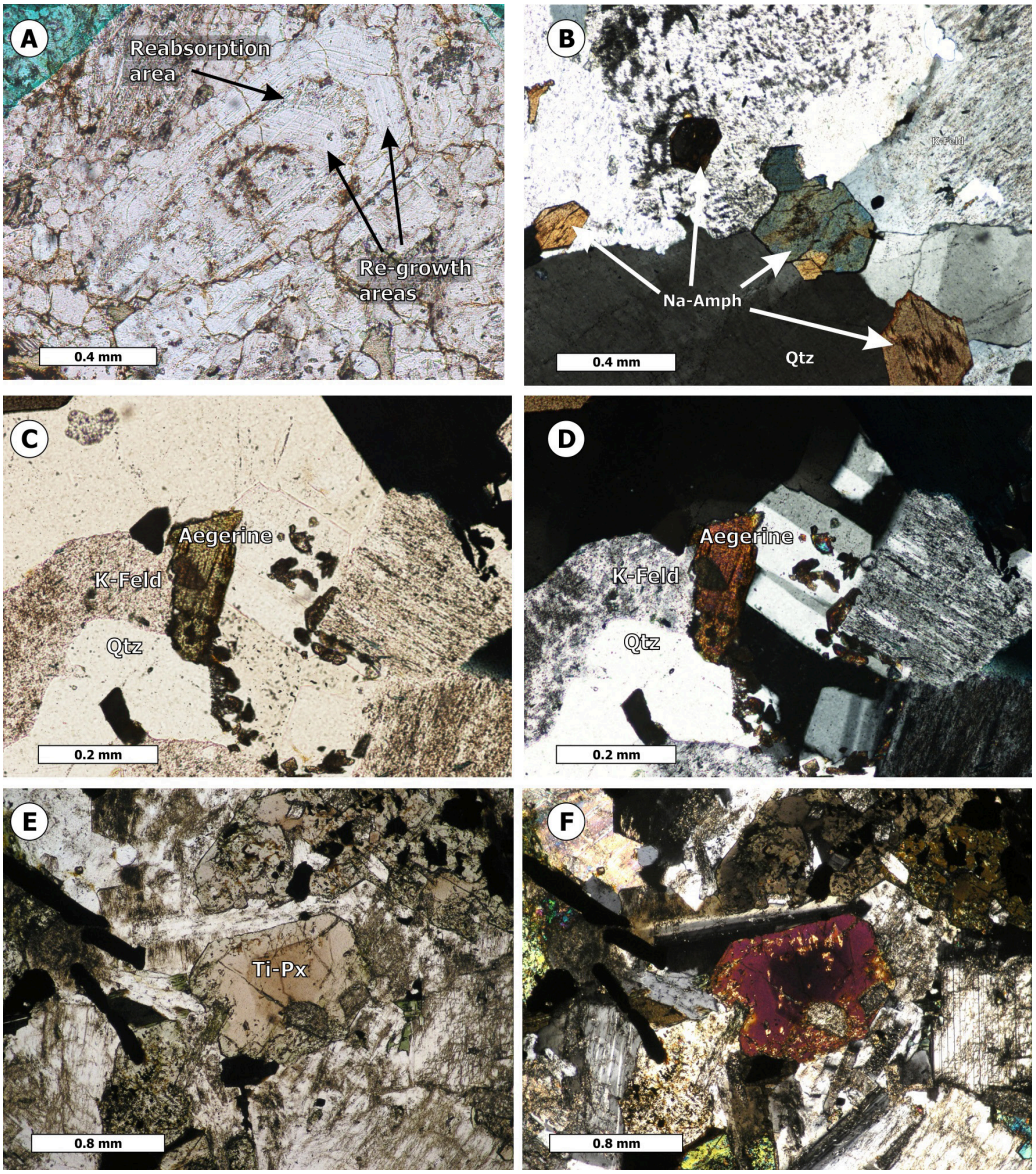

FIG. 7. Micro-photographs. **A.** Plagioclase with several growth stages, plane light, from the granite in Cerro Donoso pluton. **B.** Sodic amphiboles in the leucogranite facies, polarized light. **C.** Aegerine pyroxene in the leucogranites, plane light. **D.** Idem C, polarized light. **E.** Titanium-rich augite in the alkaline gabbro. **F.** Idem E, polarized light. B to F are from the Monte Balmaceda intrusive complex.

facies, including massive gabbro and granodiorite with monzonite patches in mafic enclave areas, here called Balmaceda Mafic Complex (BMC) because of their complex intrusive relations (Fig. 9A-E).

The Balmaceda leucogranites are found mainly on the northern slope of the mountain (over 700 m a.s.l.) in a near circular outcrop, having vertical intrusive contacts with the host rocks, which are horizontal to sub-horizontally layered hornfelsic shales (Fig. 8A, B). It consists mainly of yellow perthite or alkali feldspar-rich (Or_1-Ab_{89} to Or_{95}-Ab_5; Table 2) granites (syenogranites and alkali

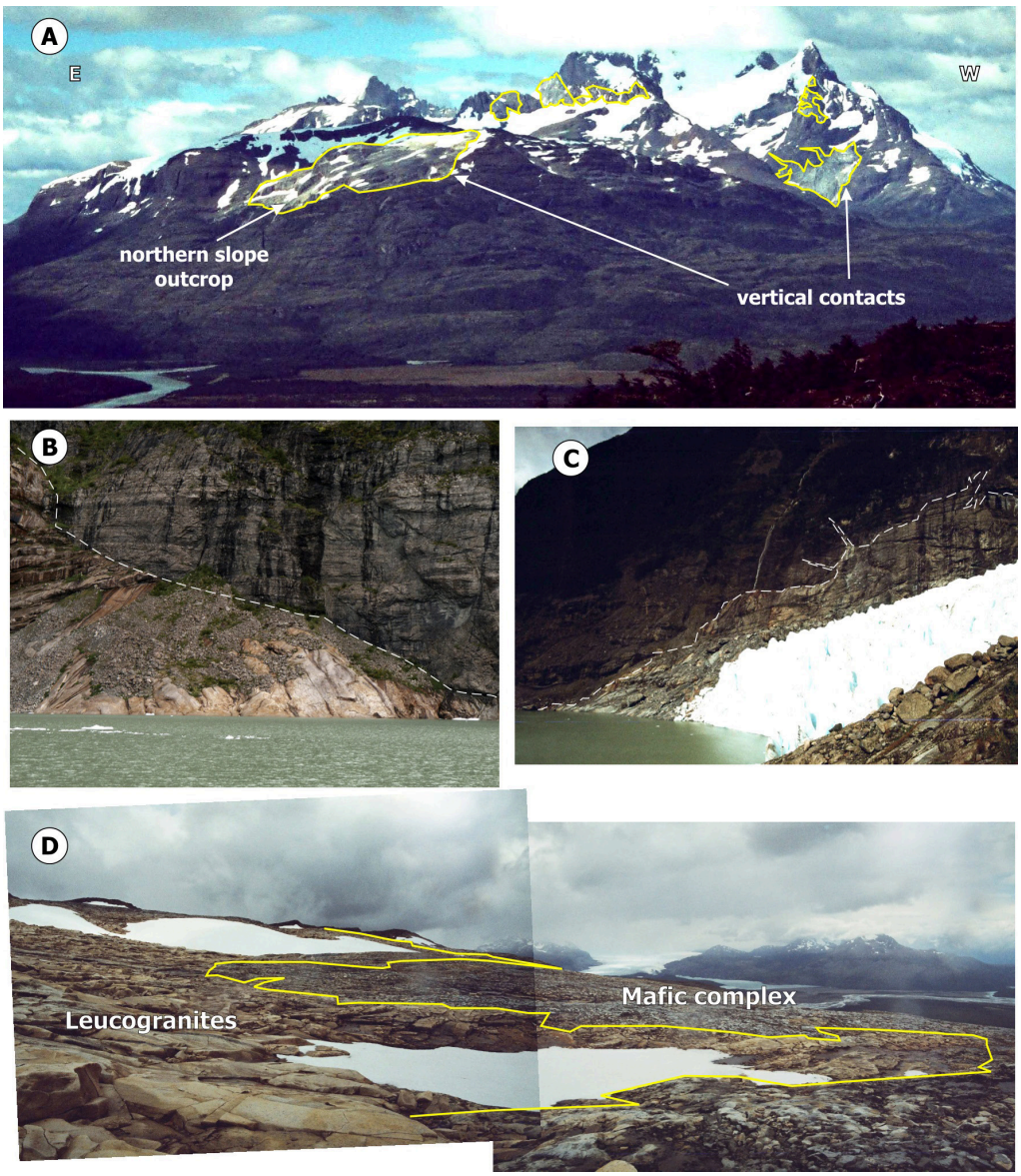

FIG. 8. Field photographs from the Monte Balmaceda intrusive complex, southern area. **A.** Panoramic view of the northern face of the Monte Balmaceda. Some of the disconnected outcrops of intrusive rocks are shown highlighted by yellow borders. **B.** Discordant intrusive contacts with sub-horizontal layered sedimentary rocks. **C.** Intrusive contact showing some "stepping", a common feature in the Glaciar Serrano area. **D.** Zig-zag contact between the Leucogranites and the Balmaceda Mafic Complex, the outcrop is in the Monte Balmaceda northern face. This pattern is caused by the subhorizontal contact between these units, with the mafic unit below the felsic one.

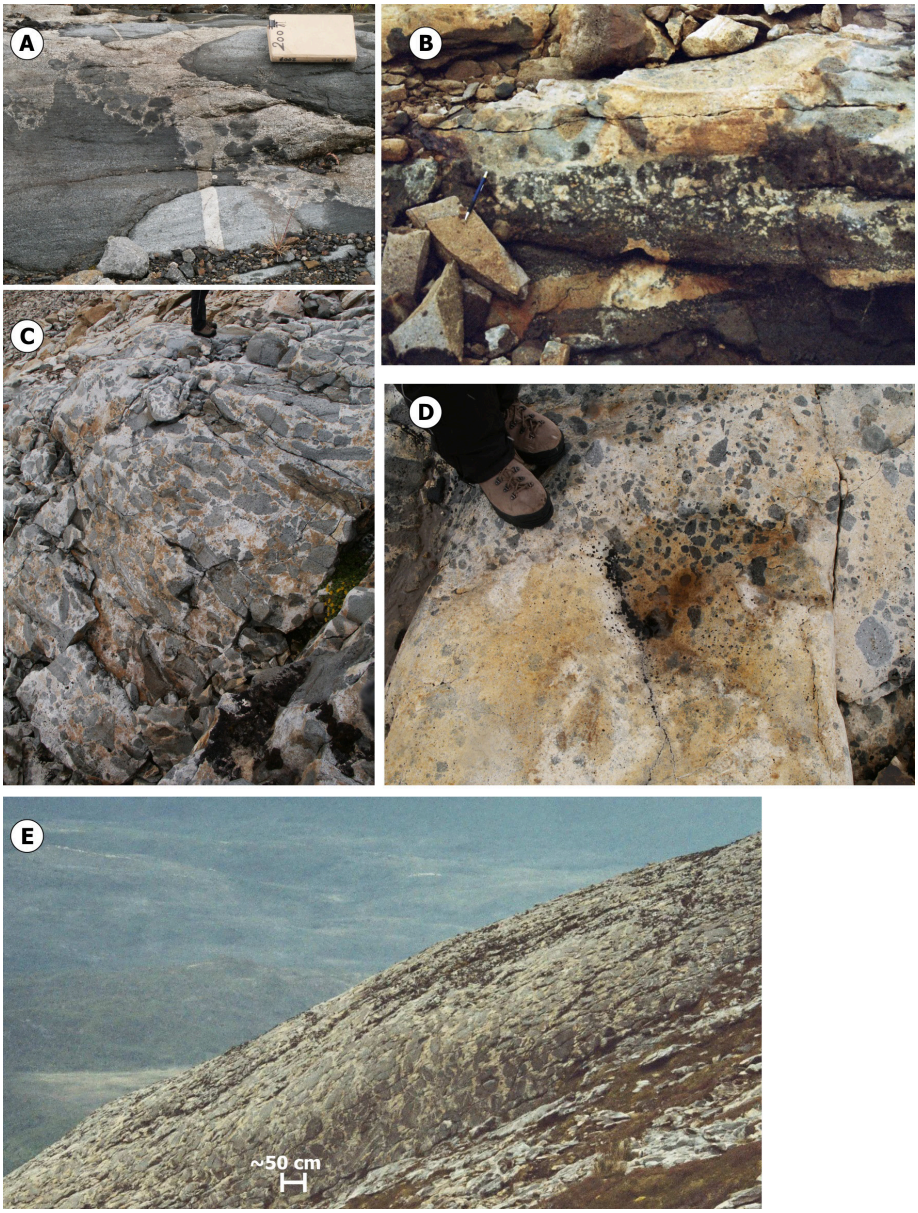

FIG. 9. Field photographs from the Balmaceda Mafic Complex, southern area. **A.** Granitic facies intrusion into the gabbro generated mafic enclaves. Glaciar Serrano area. **B.** Lobate contact between felsic and mafic intrusive rocks, suggesting that both facies coexisted as unconsolidated magmas. Monte Balmaceda northern slope outcrop. **C.** Mafic enclaves in the leucogranites with horizontal elongation. Northern slope outcrop at 950 m a.s.l. **D.** Detail of a contact zone between the Leucogranites and the Balmaceda Mafic Complex, where some enclaves of the mafic complex are hosted in the leucogranite. Magma mixing and mingling evidences. **E.** Rounded mafic enclaves with vertical elongation. It resembles a mafic unconsolidated magma brecciation by a felsic magma pervasive intrusion into the gabbro. Outcrop in the northern slope of Monte Balmaceda at *ca.* 750 m a.s.l.

feldspar granites) with coarse to fine grained textures. At higher altitude (at 1,045 m a.s.l.) it has centimetric (1 to *ca.*15 cm) miarolitic cavities, although, cavities larger than 5 cm are exceptional. Minor miarolitic cavities are also recognized in the BLG rocks in the Glaciar Serrano area, located only few m a.s.l. The mafic minerals are scarce in this facies, but in one sample sodic amphibole (riebeckite/arfvedsonite)

and aegerine (identified by optical properties), as well as epidote phases are present (Fig. 7B-D).

The Balmaceda Mafic Complex consists of gabbro/diorite that have complex intrusive relationships with the leucogranites. Patches of granodiorite and large areas of mafic enclaves within granodiorite crop out in the northern slope area (between 700 and *ca*. 1,000 m a.s.l.). Some characteristic features are the vertical enclave orientations in lower altitude, and sub-horizontal in higher altitude (Fig. 9C, D), evidencing a pseudostratigraphic pattern in the pluton. Mixing and mingling textures between the felsic and mafic facies are present, in which monzonite patches are common, containing alkali feldspar and labradorite/andesine plagioclase. The massive mafic facies comprise alkaline gabbros and quartz-diorites. The gabbros contain pink titaniferous augite (some of them might have aegerine rims) (Fig. 7E, F), biotite, oxidized amphibole and K-feldspar, apatite being a frequent accessory mineral. In the mingling facies the diorites do not contain pyroxene but are rich in biotite and oxidized amphiboles. Locally, the mafic enclaves host micro-enclaves of coarse grained leucogranite with a rim of chlorite and/or calcite. Intrusive relationships suggest that felsic and mafic facies coexisted as magmas, as there is evidence for the felsic facies intruding the mafic ones generating mafic engulfed enclaves (Fig. 9A).

Several dikes, mainly rhyolitic in composition, are present on the north slope of the mountain around the main outcrops and they have N0-10°W sub-vertical trends.

5. New geochemical data

5.1. Miocene northern area plutons

Paso de Las Llaves, Cerro Negro del Ghío, and San Lorenzo plutons are included in this section (Fig. 2).

5.1.1 Paso de Las Llaves Pluton

Based on silica content (Fig. 10A), this pluton can be divided into two groups: **1)** tonalites and diorites, with SiO_2=49.6-53.4 wt%; and **2)** Granito Avilés, with 60-66.7 wt% SiO_2. The basaltic and rhyolitic dikes have around 45 and 72 wt% SiO_2, respectively. In addition, the tonalites and diorites have an A/NK ratio (Shand, 1943) above 2, while Granito Aviles and the rhyolitic dikes have A/NK between 1.5 and 1.8. All these magmatic units are on and around the Irvine and Baragar (1971) alkaline-subalkaline limit, being clearly more alkaline than the SPB (Figs. 10A and 11A). A few mafic rocks from both areas have normative nepheline.

The pluton suite has steep patterns in Light Rare Earth Elements (LREE) and flat in the Heavy REE (HREE) (Fig. 12A). In the spider diagrams, a remarkable feature is the similar pattern of the whole suite with SPB (representing a magmatic arc signature) as the Nb-Ta anomalies and the enrichment in Large Ion Lithophile Elements (LILE) (Fig. 12B). Nevertheless, in this pluton it is possible to distinguish LILE and High Field Strength Elements (HFSE) enrichment in Granito Avilés (GA), with Zr and Hf content similar to OIB averages. The GA unit, therefore, shows a less marked Nb-Ta negative anomaly compared to the suite. Additionally, GA presents a slight negative anomaly in Ti, Sr and P just enough to be distinguishable from the tonalites and diorites, which have similar patterns to the SPB. The rhyolitic dike has a similar pattern with GA, but more pronounced negative anomalies for the above mentioned elements.

The Nd and Sr isotopic composition of the pluton suite (7 analysed samples) display εNd_t between +0.7 and +2.3, and $(^{87}Sr/^{86}Sr)_i$ ratio from 0.7040 to 0.7050, including the basaltic dike, while the rhyolitic dike has an εNd_t=0 and $(^{87}Sr/^{86}Sr)_i$>0.7050 (Table 5; Fig. 13A, B).

Otherwise, the porphyritic garnet bearing granite (07LL3, Paso de Las Llaves pluton) has up to 72.1 wt% SiO_2, an A/NK ratio between 1.5 and 1.8, and is clearly sub-alkaline (Figs. 10A and 11A). This granite can also be distinguished from the whole suite due to its remarkable negative Eu anomaly with Eu/Eu*=0.55 (Fig. 12A). In the spider diagram, it exhibits a similar pattern to Granito Avilés (Fig. 12B). Furthermore, this facies has εNd_t=-5.3 (Table 5, Fig. 13A) and reflects a magma source different to the rest of the unit, with a consequent difference in its geochemical character (alumina, alkalinity and the trace elements pattern as mentioned above) and in its mineralogy, especially the presence of garnet (Section 4.1).

5.1.2. Cerro Negro del Ghío Pluton

This pluton has a homogeneous composition, with SiO_2=58.1-59.6 wt%, and a A/NK ratio

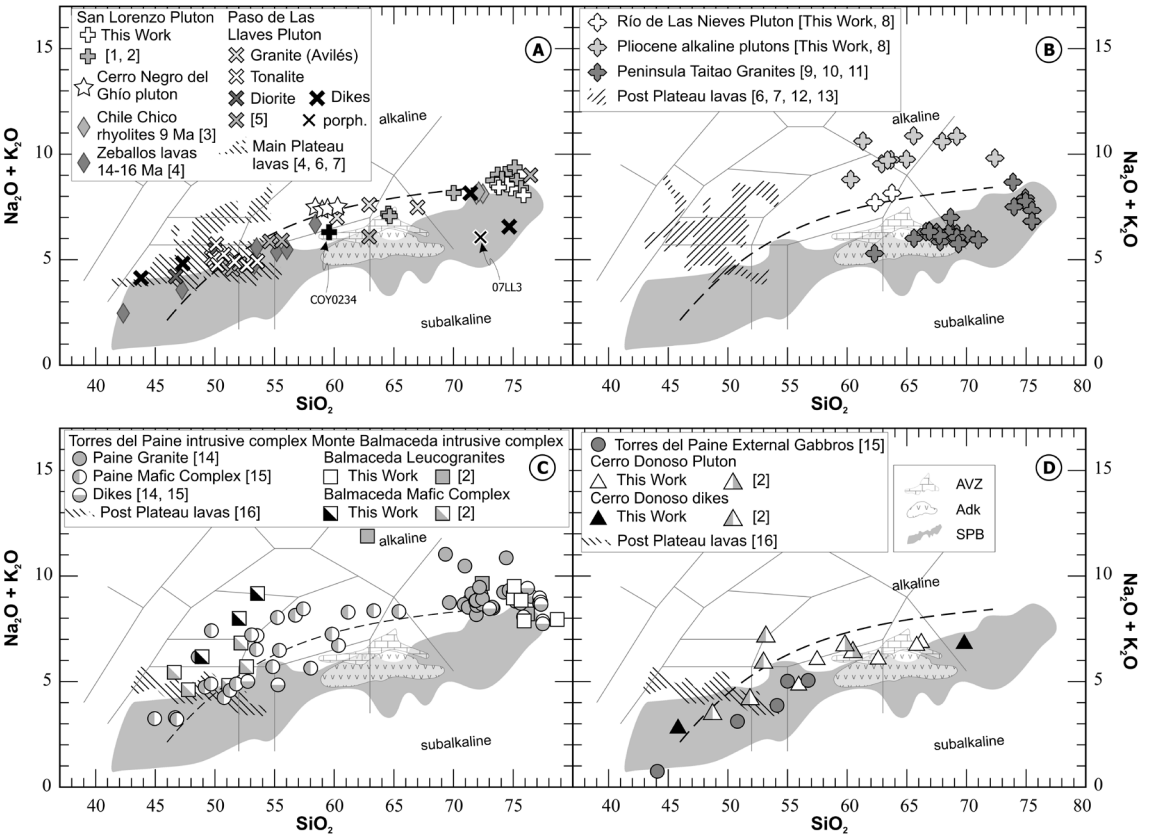

FIG. 10. TAS diagrams. **A.** Miocene pluton from the northern area. **B.** Pliocene plutons from the northern area. **C.** Miocene Torres del Paine and Monte Balmaceda intrusive complexes. **D.** Cerro Donoso pluton and Paine External Gabbros. Limit between the alkaline and subalalkaline areas (dashed line) is from Irvine and Baragar (1971). References: **1.** Welkner (1999); **2.** Michael (1983); **3.** Espinoza *et al.* (2005); **4.** Espinoza *et al.* (2010); **5.** Vargas and Hervé (1995); **6.** Gorring and Kay (2001); **7.** Guivel *et al.* (2006); **8.** Espinoza *et al.* (2008); **9.** Kaeding *et al.* (1990); **10.** Guivel *et al.* (1999); **11.** Anma *et al.* (2009); **12.** Baker *et al.* (1981); **13.** Gorring *et al.* (2003); **14.** Michael (1984); **15.** Michael (1991); **16.** Camusú Aike volcanic field (D'Orazio *et al.*, 2005), Las Vizcachas plateau (Muñoz, 1982) and Glenn Cross Area (D'Orazio *et al.*, 2001); SPB: South Patagonian batholith (Hervé *et al.*, 2007); **AVZ:** Austral Volcanic Zone (Stern and Killian, 1996); **Adk:** extra-andean adakites (Ramos *et al.*, 2004). Alkalies and SiO_2 content in wt%.

(Shand, 1943) between 1.5 and 1.8. In addition, all samples are located in the alkaline field of Irvine and Baragar (1971) on the TAS diagram (Fig. 10A).

Cerro Negro del Ghío pluton has a steep pattern in LREE (Fig. 12C), which is clearly more enriched compared to SPB, and a flat pattern in HREE, despite showing a slight upward concave pattern (Fig. 12C). In the spider diagram, its samples exhibit an intermediate pattern between the tonalites and Granito Avilés units from Paso de Las Llaves pluton, with a high LILE/HFSE ratio, a less pronounced Nb-Ta negative anomaly and slight negative Ti anomaly (Fig. 12D).

From the two sampled locations, this pluton shows homogeneous Nd and Sr isotopic composition with εNd_t=+2.6±0.3 and $(^{87}Sr/^{86}Sr)_i$<0.7050 (0.7039±0.2) (Table 5; Fig. 13A, B).

This pluton has been related to the volcanic units of the neighboring area (Espinoza *et al.,* 2010; Boutonnet *et al.*, 2010). Since the Cerro Negro del Ghío pluton and the Zeballos lavas (Espinoza, *et al.*, 2010) share many geochemical characteristics, including their isotopic signature (Figs. 10A, 11B and 13B), these magmatic units are interpreted to be genetically linked, the Cerro Negro del Ghío pluton being the plutonic equivalent of Zeballos lavas.

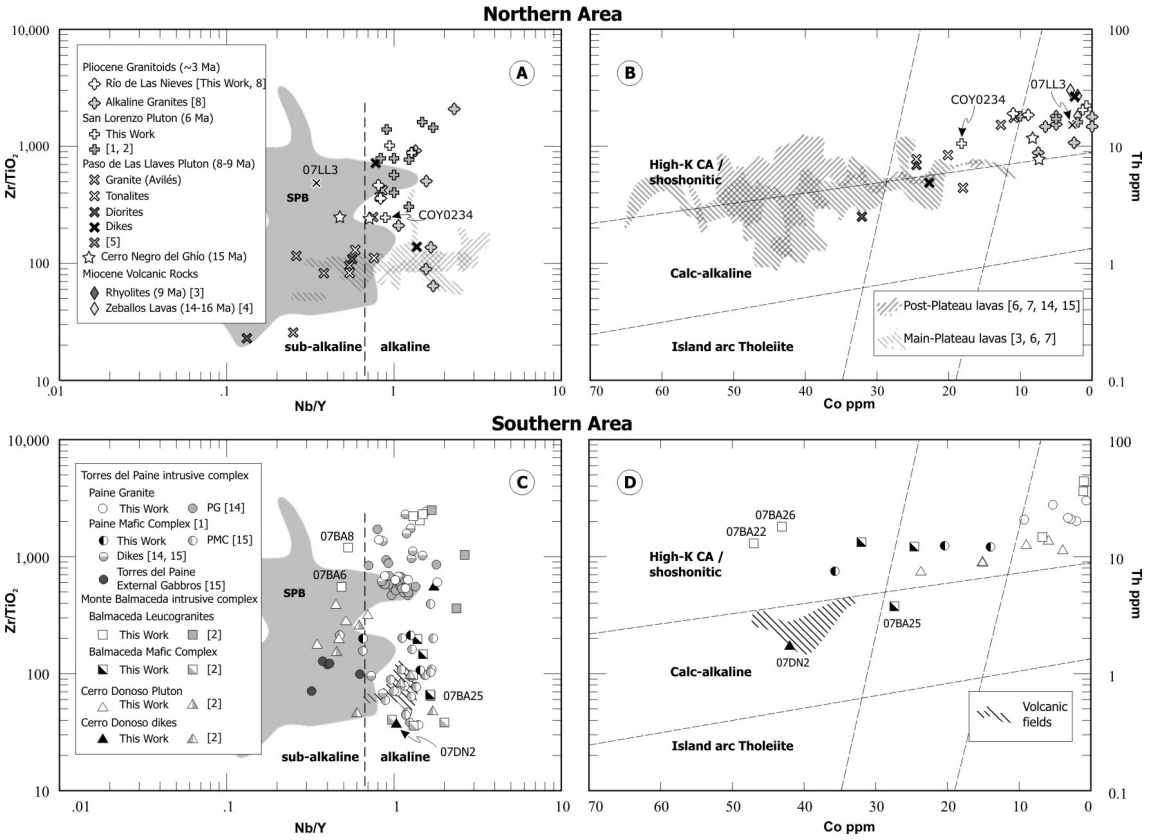

FIG. 11. Trace elements alkaline discrimination diagrams. **A.** Zr/TiO_2 *versus* Nb/Y diagram (Winchester and Floyd, 1977) northern area plutons. **B.** Th-Co diagram (Hastie *et al*., 2007) for the northern area plutons. **C.** Zr/TiO_2-Nb/Y diagram for plutons from the southern area. **D.** Th *versus* Co diagram for plutons from the southern area. Only two samples from the Balmaceda Leucogranites (07BA22 and 07BA26) have anomalous high Co content for a high silica granite, nevertheless the content in Th is coherent with their K content. On the contrary, sample 07BA25 has lower Co concentrations than less basic samples from the Balmaceda Mafic Complex, so the calc-alkaline plot of this sample may be an artifact. The shaded area in A and C represents the projection of the SPB (South Patagonian batholith) samples (from Hervé *et al*., 2007) and the dashed areas the Miocene-Pliocene plateau lavas and volcanic field samples from the Camusú Volcanic fields in D: the Aike volcanic field (D'Orazio *et al*., 2005), and the Glenn Cross Area (D'Orazio *et al*., 2001). The other references as in figure 10.

5.1.3. The San Lorenzo Pluton

This pluton has predominantly SiO_2>70 wt%. Only few samples have SiO_2<65 wt% (Fig. 10A) and among them is the andesitic one (COY0234) with a SiO_2 content of 59.3 wt%. The granite samples have A/NK between 1 and 1.3 (lowest values in the plutons sampled in the Northern Area). They are in the alkaline-calc-alkaline limit (Fig. 10A; Irvine and Baragar, 1971), but plot in the high-K calc-alkaline field of Peccerillo and Taylor (1976) (not shown) and in the Th-Co diagram (Fig. 11B), or even alkaline in the Zr/TiO_2-Nb/Y diagram (Fig.11A), while the intermediate samples have an A/NK ratio (Shand, 1943) between 1.5 and 1.8 and also fall in the high-K calc-alkaline fields (Table 3; Figs. 10A and 11B). Many samples have normative corundum reflecting a peraluminous character (Zen, 1988).

This pluton is enriched in LREE with respect to SPB and the HREE show a slight upward concave pattern (Fig. 12E). The granites have a negative Eu anomaly, which is very pronounced in some samples (Eu/Eu*=0.2-0.7). They have no -or very subtle-Nb-Ta anomaly, very pronounced Sr, P and Ti negatives anomalies, as well as high content in LIL and HFS elements (Fig. 12F). The intermediate rocks have less pronounced anomalies in Eu, Sr, P and Ti, or none at all.

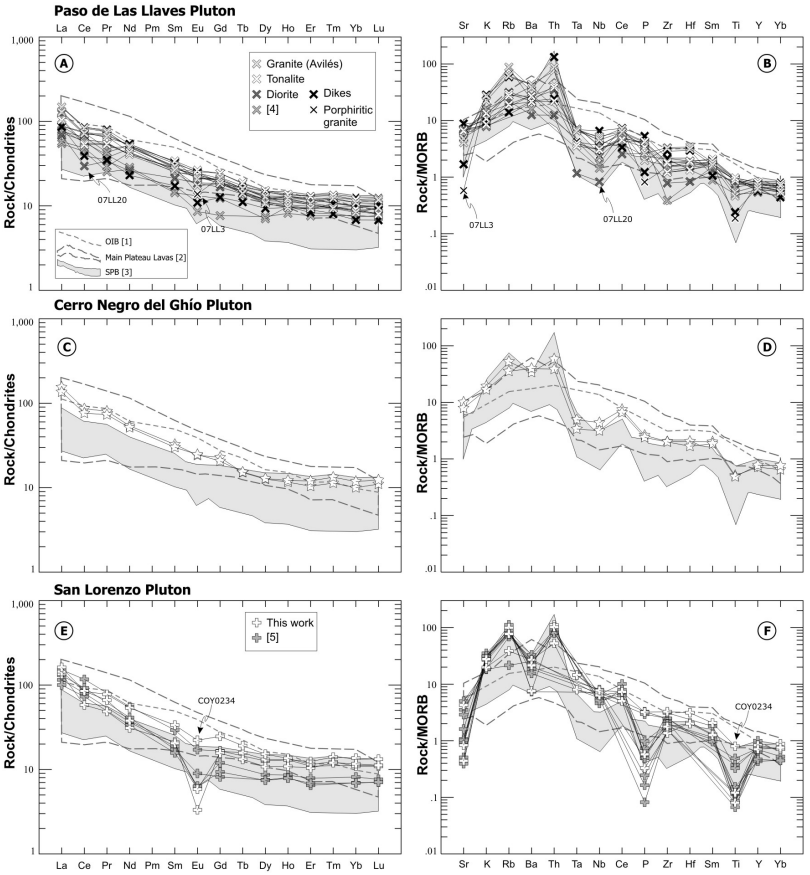

FIG. 12. Trace elements patterns for plutons from the northern area. REE diagrams are normalized to chondrite (Nakamura, 1974), and the spider diagrams to MORB (Pearce, 1983). **A.** REE pattern for Paso de Las Llaves pluton. **B.** Spider diagrams for Paso de Las Llaves pluton. **C.** REE pattern for Cerro Negro del Ghío pluton. **D.** Spider diagrams for Cerro Negro del Ghío pluton. **E.** REE pattern for San Lorenzo pluton. **F.** Spider diagrams for San Lorenzo pluton. **1. OIB:** Ocean Island Basalt average, (Sun and McDonough, 1989); **2.** Main Plateau lavas, includes the Meseta Central, Belgrano, Noreste, and Muerte (Gorring and Kay, 2001), Meseta Chile Chico (Espinoza *et al.*, 2005), and Meseta del Lago Buenos Aires (Guivel *et al.,* 2006); **3. SPB:** Neogene South Patagonian batholith (Hervé *et al.*, 2007); **4.** Samples from Vargas and Hervé (1995); **5.** Samples from Michael (1983) and Welkner (1999).

The two granite samples from the San Lorenzo pluton have εNd_t <0, while the andesite sample has εNd_t >0. The Sr_i ratio is similar for the 3 analysed samples, around 0.7051 (Table 5; Fig. 13A, B).

5.2. Pliocene northern area plutons

New data for a granite sample from the Río de Las Nieves pluton are presented together with new major elements data for the alkaline plutons in Meseta del Lago Buenos Aires (Table 3). These data are compared and complemented with previous published data (Espinoza *et al.*, 2008).

5.2.1. Río de Las Nieves

This pluton has between 62 and 64 wt% SiO_2 and plots on the alkaline/sub-alkaline limit of Irvine and Baragar (1971) (Fig. 10B). The REE show a pronounced steep pattern in LREE and a flat one in HREE, indeed it is very enriched in LREE with respect to the SPB (Fig. 14A). The LILE and HFSE are also enriched in this pluton, with a subtle Nb-Ta negative anomaly and high content on Th, Zr and Hf (Fig. 14B). The trace elements for this pluton follow an intermediate pattern between the alkaline Pliocene plutons (Espinoza *et al.*, 2008) and the SPB, very similar to the San Lorenzo pluton signatures (Figs. 12F and 14B).

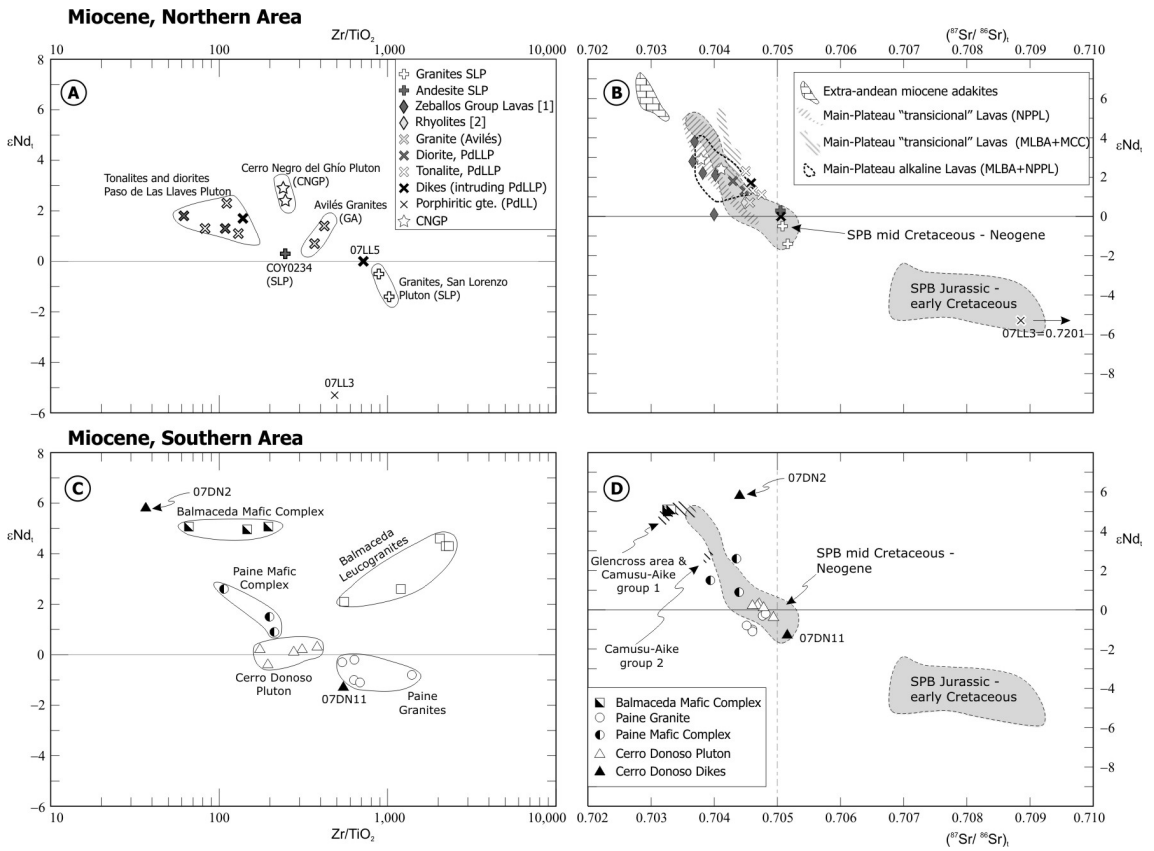

FIG. 13. Isotopic composition diagrams for Miocene plutons from the northern and southern areas. **A.** εNdt *versus* Zr/TiO_2 ratio for plutons from the northern area. **1.** Zeballos Group Lavas, Espinoza *et al.* (2010); **2.** Miocene rhyolites, Espinoza *et al.* (2005). **B.** εNdt *versus* $(^{87}Sr/^{86}Sr)i$ ratio for plutons from the northern area, with bulk Earth divisions at present time. Data plotted for comparison: Extra-andean adakites (Ramos *et al*., 2004); Miocene "transitional" and alkaline lavas (Gorring and Kay, 2001; Espinoza *et al*., 2005; Guivel *et al*., 2006). **C.** εNdt *versus* Zr/TiO_2. ratio for plutons from the southern area. **D.** εNdt *versus* $(^{87}Sr/^{86}Sr)i$ ratio for plutons from the southern area. Data is compared with the isotopic composition of the Glencross Area and Camusú-Aike volcanic fields (D'Orazio *et al*., 2001 and 2005 respectively). In B and D, SPB data is from Hervé *et al.* (2007).

This pluton has isotopic ratios in the range of Paso de Las Llaves pluton suite (εNd_t=+1.3 and $(Sr/Sr)_i$=0.7046) (Table 5; Figs 14C and 13A, B).

5.2.2. Alkaline plutons in the Meseta del Lago Buenos Aires

The Mifeldi pluton samples have intermediate SiO_2 contents between Pico Rojo (around 60 wt%) and Cerro Lápiz (above 65 wt% in SiO_2) (Espinoza *et al.*, 2008; this work) and they are all alkaline (Figs. 10B and 11A, B). One sample from Cerro Lápiz has normative corundum.

The alkaline granite from Cerro Lápiz neck has the most radiogenic values, with $\varepsilon Nd_t<0$ and $(Sr/Sr)_i>0.7055$, while the other alkaline plutons have isotopic ratios around the bulk Earth intersection (Espinoza *et al.*, 2008; Fig. 14C).

5.3. Southern area plutons

The dataset used consists in original data (Table 4) complemented with data collected by Michael (1983, 1984, 1991) from the Torres del Paine and Monte Balmaceda intrusive complexes, and the Cerro Donoso pluton.

5.3.1. Cerro Donoso Pluton

The pluton has a restricted range of SiO_2 content, between 55 (the quartz diorite) and 66 wt%. Out of

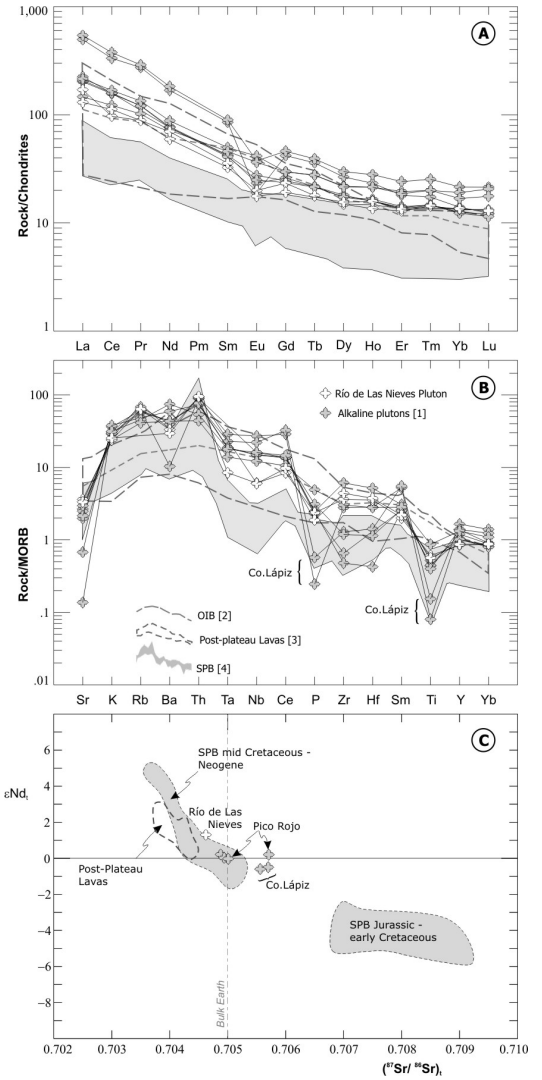

FIG. 14. Trace elements and isotopic composition diagrams for the Pliocene northern area plutons. **A.** REE diagrams normalized to chondrite (Nakamura, 1974). **B.** Spider diagrams normalized to MORB (Pearce, 1983). **C.** εNdt *versus* ($^{87}Sr/^{86}Sr$)i . References: **1.** Espinoza *et al.* (2008); **2.** Sun and McDonough, (1989); **3.** Gorring and Kay (2001); **4.** Hervé *et al.* (2007).

this range are the basaltic and rhyolitic dikes, with 45 and 70 wt%, respectively. The pluton samples are peraluminous. Similarly to SPB, they are mostly sub-alkaline in the TAS diagram and according to Nb/Y ratio (Figs. 10D and 11C), or high K calc-alkaline in the Peccerillo and Taylor (1976) (not shown) and Th-Co diagrams (Fig. 11D). Most samples have normative corundum.

Their REE plots (Fig. 15A) have a steep pattern, with $(La/Yb)_N$=10.41-18.83. They do not have Eu anomalies, with exception of the quartzdiorite sample (07DN6), which has Eu/Eu*=0.78. The HREE show a flat pattern, with $(Dy/Yb)_N$=1.11 and 1.33. The analysed samples have ΣREE=139-164 ppm. Trace elements have high LIL/HFS elements ratios, and their spider diagram shows a very similar pattern to that of SPB (Fig. 15B). Both dike types are characterized by having low REE content, with ΣREE=100-110. The rhyolitic one has a steeper LREE pattern, with $(La/Yb)_N$ up to 24.35, while the basaltic one has an "anomalous" pattern in LILE (noted in its spider diagram, Fig. 15B), probably due to alteration (*s.l.*) effects.

The Nd and Sr isotopic ratios from the pluton are grouped near the bulk Earth intersection, with εNd_t=-0.4 to+0.3 and ($^{87}Sr/^{86}Sr)_i$ =0.7046 to 0.7049 (Fig. 13C, D). The rhyolitic and basaltic dikes have the lowest and highest εNd_t values of the measured samples in the southern area, respectively (Fig. 13C). Even the basaltic dike (sample 07DN2) has an anomalous pattern in LILE (Fig. 15B) and a loss on ignition >4 wt% (Table 4). Finally, there is no anomalous pattern for the HFS elements, so the εNd_t value may reflect the closest isotopic composition to the mantle source of all the suites, with εNd_t (07DN2)=+5.8.

5.3.2. The Paine External Gabbros

According to Michael (1991), these rocks have a 43-56 wt% range of SiO_2 content. They are peraluminous, similar to SPB, and mostly either sub-alkaline in the TAS and Zr/TiO_2-Nb/Y diagrams (Figs. 10D and 11C), or high K calc-alkaline in the Peccerillo and Taylor (1976) and Th-Co diagrams (Fig. 11D).

This unit plots mainly inside the area projected by the Neogene samples from the SPB reflecting arc-signature in the spider diagram pattern (Fig. 15B).

5.3.3. Torres del Paine intrusive complex

In this intrusive complex, bimodality is clearly noted, with a SiO_2 content ranging between 45 and 65 wt% in the Paine Mafic Complex (PMC), and SiO_2>69 wt% in Paine Granite (PG) (Michael, 1984, 1991; Fig. 10C). Based on the alumina criteria both the Paine Granite suite and the Paine Mafic Complex are mainly peraluminous, with an

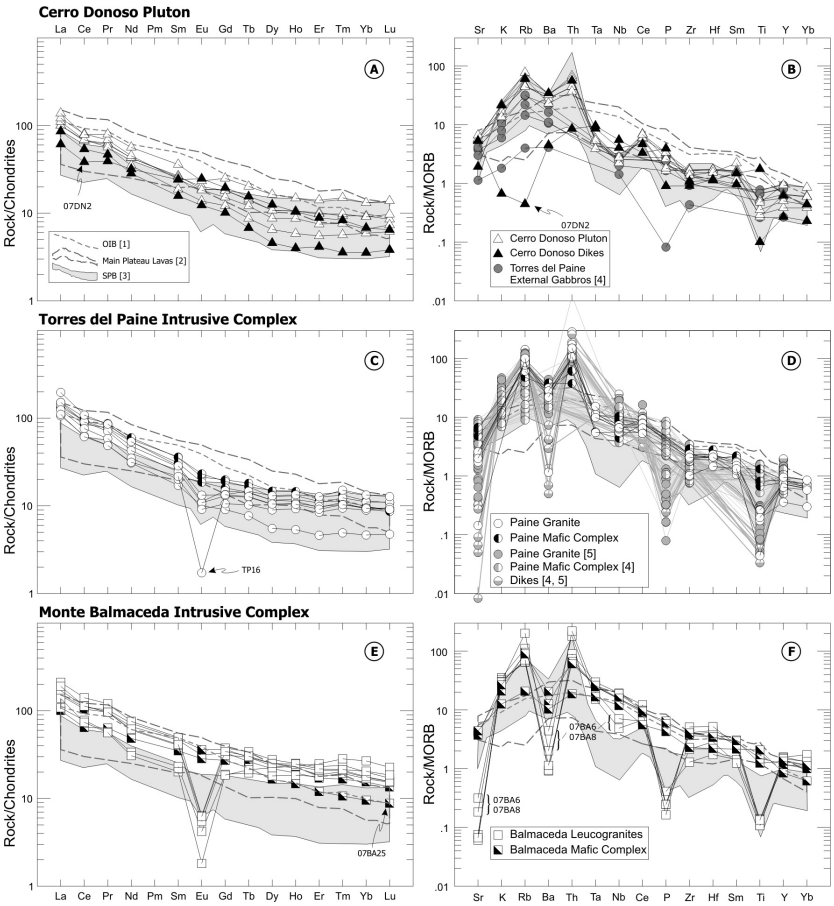

FIG. 15. Trace elements patterns for plutons from the southern area. REE diagrams are normalized to chondrite (Nakamura, 1974), and the spider diagrams to MORB (Pearce, 1983). **A.** REE pattern for samples from Cerro Donoso pluton. **B.** Spider diagrams for rock samples from Cerro Donoso pluton. **C.** REE pattern for samples from Torres del Paine intrusive complex. **D.** Spider diagrams for rock samples from Torres del Paine Intrusive complex. **E.** REE pattern for samples from Monte Balmaceda intrusive complex. **F.** Spider diagrams for rock samples from Monte Balmaceda intrusive complex. **1. OIB:** Ocean Island Basalts average, (Sun and McDonough, 1989); **2.** Pali-Aike volcanic field, Glencross area and Camusú Aike basalts (D'Orazio *et al*., 2000, 2001, 2005); **3. SPB:** Neogene South Patagonian batholith (Hervé *et al.*, 2007); **4.** data from Michael (1991); **5.** data from Michael (1984).

A/CKN ratio (Shand, 1943) ranging between 0.8 and 1.2. Nevertheless, the A/KN ratio from PG is lower than the PMC ratio, with ranges between 0.9 to 1.4 and 1.3 to 2.7 respectively (Michael, 1984, 1991). In this case, the PG suite limits with the metaluminous and peralkaline fields (their A/KN ratio range just above and below 1), and some samples fall within the peralkaline field (data from Michael, 1984, 1991). Additionally, both units plot in the alkaline or high-K calc-alkaline fields in Zr/TiO_2-Nb/Y and Th-Co diagrams, respectively (Fig. 11C, D). One-third of the samples have normative corundum, and 3 of 32 have normative aegerine.

Both units, the Paine Granites (PG) and the Paine Mafic Complex (PMC), have steep and flat patterns in LREE and HREE, respectively (Fig. 15C). Even in this case, the PG can be differentiated by more pronounced Eu negative anomalies, with Eu/Eu*=0.8 to 0.5 for PG, but up to 0.1 for the most silicic sample of this suite *versus* 0.9 to 0.8 for PMC. Instead, PMC is richer in total REE than PG, with ΣREE=187-223 the former and ΣREE=126-187 the later. In the spider diagram, the new data has been plotted together with data from Michael (1984, 1991) (Fig. 15D), showing wide range of values in most elements. In spite of that, there are remarkable features, for example, PG

samples show strong negative anomalies in Sr, Ba, Ti and P and neither of the facies follows arc (SPB), nor back-arc rock patterns.

The εNd_t values for the Paine Mafic Complex (PMC) are>0 (+0.9 to +2.6), while the felsic ones are <0 (-0.2 to-1.1) (Fig. 13C). The PMC displays $(^{87}Sr/^{86}Sr)_i$ <0.7045 while this value is higher in Paine Granite (Fig. 13D).

5.3.4. Monte Balmaceda intrusive complex

Bimodal magmatism is evidenced by the Balmaceda Mafic Complex (BMC), SiO_2 content ranges between 46 and 54 wt%, while the Balmaceda Leucogranites (BLG) contain between 71 and 79 wt% (Fig. 10C). Additionally, the BMC has higher A/KN ratios (>1.3), than BLG (<1.3, even <1). Both units plot in the alkaline (Zr/TiO_2-Nb/Y and TAS diagrams) (Figs. 10C and 11C) or high-K calc-alkaline fields (Th-Co) (Fig. 11D). Most of the analysed BMC samples have normative nepheline, whereas one BLG sample has normative acmite (aegerine), which is in accordance with the modal mineralogy description (Section 4.9).

The Balmaceda Leucogranites (BLG) are characterized by REE pattern having slight concave-upward shapes (Fig. 15E) and a strong negative Eu anomaly (Eu/Eu*=0.2-0.09), while BMC has flat HREE pattern and lacks Eu anomaly. Only the alkaline gabbro from the BMC (07BA25) has a slight steep pattern in HREE (Fig. 15E). In the spider diagram (Fig. 15F), the mafic facies have high LIL/HFS elements ratios, while the felsic ones have negative anomalies in Sr and Ba, the same feature displayed by the evolved granites and aplites from Torres del Paine Intrusive complex suite sampled by Michael (1984) (Fig. 15D). The BLG also exhibit negative anomalies in P and Ti, as well as an absence of Nb-Ta anomalies, except from the northern slope outcrop, where they show a subtle negative anomaly (07BA6,8). Otherwise, the very low Sr content (<40 ppm) for BLG is consistent with their low CaO content (<0.19 wt%) and with their pronounced negative Eu anomaly, and, in turn, these features are in accordance with the scarce plagioclase content in these facies, excluding an important weathering and/or hydrothermal alteration effect in their trace element measurement.

The εNd_t values for the Balmaceda Mafic Complex samples (+5 to +5.1) are higher than those of the felsic ones (+2.1 to +4.6), and have a $(^{87}Sr/^{86}Sr)_i$ isotopic ratio <0.7040 (Fig. 13C, D). The very low Sr concentration (*ca.* 7-38 ppm, Table 4) in the Balmaceda Leucogranites samples implies that they would be susceptible to contamination during analytical procedures, which would result into anomalous high $(^{87}Sr/^{86}Sr)_i$ ratios (Table 6). Therefore, Sr isotopic ratio of the Balmaceda Leucogranites is not considered further in this study.

6. Discussion

6.1. Graded calc-alkaline to alkaline "transitional" character of the plutons

Based on the petrography and the geochemistry, we propose a 4 groups subdivision for the plutons alkalinity: alkaline (*sensu stricto*), "intra-plate transitional" calc-alkaline, "arc transitional" calc-alkaline, and calc-alkaline rocks. These groups can be identified in figures 16 and 17, and their characteristics are described below.

6.1.1. Alkaline plutons

The Monte Balmaceda intrusive complex (Fig. 3) and the Pliocene plutons located in Meseta del Lago Buenos Aires (Fig. 2) (Espinoza *et al*., 2008) are included in this group. The presence of hydrated minerals is rare in these plutons. In addition they have strong "intra-plate" features, specifically high REE content (Fig. 15E)-specially LREE-and HFSE contents, a lack of Nb-Ta negative anomaly, strong negative anomalies in Sr, Ba, P, Ti in the felsic rocks and a flat pattern in the spider diagrams for the mafic rocks (Fig. 15F). The only samples studied with modal and normative alkaline minerals (aegerine) are from the Monte Balmaceda suite.

Espinoza *et al*. (2008) propose that the alkaline Pliocene plutons are derived from evolved magmas, differentiated by AFC processes in a shallow magma chamber filled with OIB-like magmas from enriched basaltic melts. Our data support this hypothesis, as shown in figure 17A, where the Pliocene alkali granites plagioclase fractionation is evidenced in Sr/Nd dispersion, and crust assimilation in Nb/La.

6.1.2. "Intra-plate transitional" calc-alkaline plutons

This group includes the Río de Las Nieves and San Lorenzo plutons (Fig. 2) in the northern area, and the Torres del Paine intrusive Complex in the

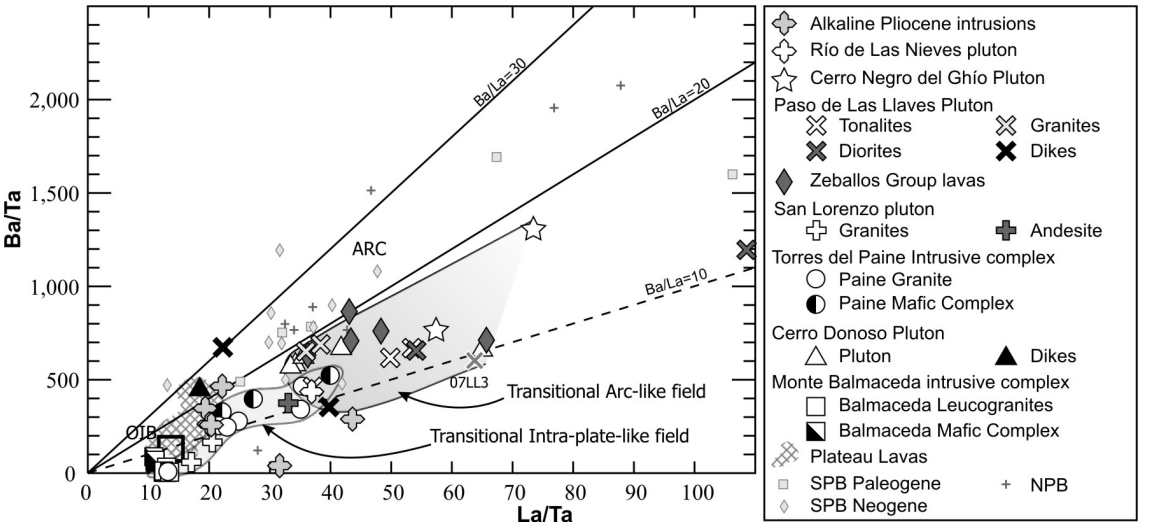

FIG. 16. Ba/Ta *versus* La/Ta diagram, after Kay and Mpodozis (2002) for plutons from the northern and southern areas. Calc-alkaline arc signature is represented by the North and South Patagonian batholith samples (NPB, SPB), most of them with La/Ta >25 and Ba/La >20 (NPB and SPB data from Pankhurst *et al*. (1999) and Hervé *et al.* (2007), respectively). The plateau lavas, and OIB signatures, are well constrained, mostly with La/Ta between 10 and 20. In general terms, the plutonic samples from this study show two intermediate patterns, both with Ba/La <20 (lower than calc-alkaline arc-like) but with La/Ta either close to the arc, or to the intra-plate signatures. The Zeballos Group data is from Espinoza *et al.* (2010); References for the Plateau Lavas data as in figure 14.

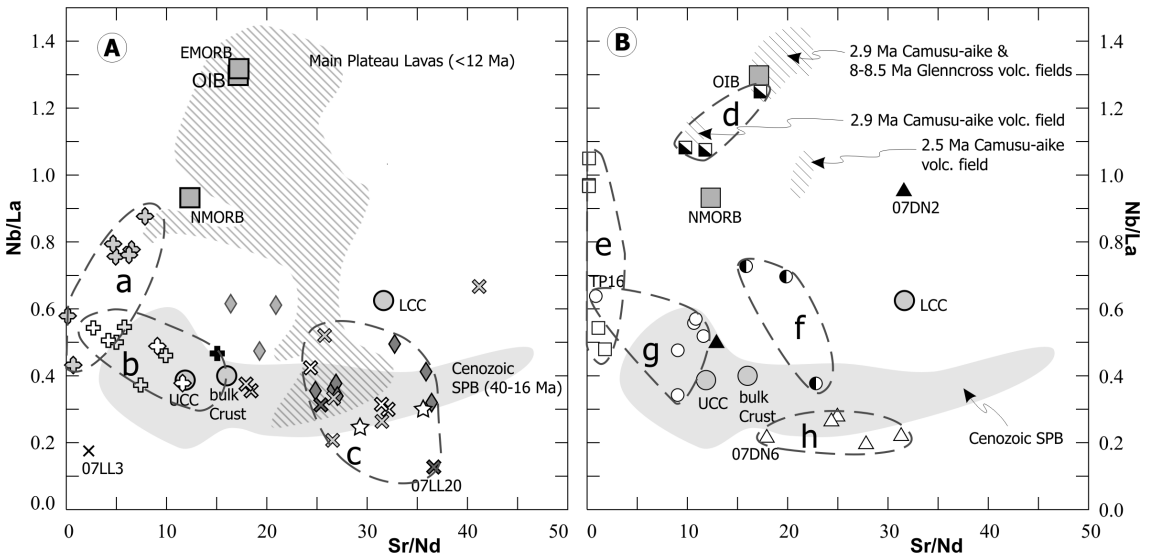

FIG. 17. Sr/Nd *versus* Nb/La diagram for plutons from the northern and southern areas. The Nb/La ratio reflects the Nb-Ta anomaly, while the Sr/Nd ratio the primitive magma evolution with plagioclase fractionation (Hawkesworth and Kemp, 2006). Samples from the northern and southern areas are plotted together with data from Cenozoic rocks from the SPB and alkaline and "transitional" plateau lavas for comparison (references in Fig. 10), as well as OIB, E-MORB, N-MORB (Sun and McDonough, 1989), bulk crust, upper and lower continental crust averages (UCC and LCC respectively) (Rudnick and Gao, 2003). **A.** Northern area, the segmented lines enclose: **a:** the Pliocene alkaline rocks; **b:** the Pliocene and Miocene "intra-plate transitional" calc-alkaline plutons; **c:** the Miocene "arc transitional" calc-alkaline plutons. B. Southern area; **d:** the alkaline gabbros; **e:** alkaline leucogranites; **f:** the Miocene "intra-plate transitional" calc-alkaline mafic rocks; **g:** calc-alkaline granites; **h:** the "arc transitional" calc-alkaline pluton.

southern one (Fig. 3). They have calc-alkaline main characteristics, like modal hornblende and/or biotite, also a slight Nb-Ta negative anomaly (Figs. 12F, 14B and 15F), but their trace element patterns are similar to those of the alkaline group (Figs. 12E, F and 15E, F).

6.1.3. "Arc transitional" calc-alkaline plutons

This group comprises the Paso de Las Llaves and Cerro Negro del Ghío plutons from the northern area (Fig. 2), and the Cerro Donoso pluton from the southern area (Fig. 3). They have distinctive arc features such as hydrated mineral phases, clear Nb-Ta negative anomaly, and trace elements pattern correlated with the South Patagonian batholith (SPB) (Figs. 12B, D and 15B). Notwithstanding, the plutons from this group are subtly more alkaline than SPB, with Na-K content near the Irvine and Baragar (1971) alkaline/sub-alkaline limit (Fig. 10A). Furthermore, they have high content in HFSE (Figs. 12B, D and 15B) that is reflected in the ratio Ba/La<20, which is commonly >20 for arc rocks, including the Cenozoic SPB (Fig. 16).

6.1.4. Calc-alkaline plutons

The only known calc-alkaline pluton with "pristine" arc signature in this "extra-Andean" location in Patagonia is the Fitz-Roy pluton (Michael, 1983; Kosmal and Spikermann, 2002; Ramírez de Arellano, 2011).

Other known intrusive with calc-alkaline signature are the Paine External Gabbros studied by Michael (1991) (Figs. 10D and 11C).

6.2. Origin of the plutonism: conceptual models

The wide "transitional" alkaline character of the plutons and the proposed subdivision described above, together with their isotopic ratios, suggest multiple scenarios for development of magmatism.

6.2.1. Cerro Negro del Ghío and Paso de Las Llaves plutons

Both units have "arc transitional" characteristics (Fig. 16) compatible with arc-magmatism, but also several geochemical evidences of contributions from an enriched mantle magma source (*e.g.*, high HFSE content). As Cerro Negro del Ghío pluton is considered the intrusive equivalent of the Zeballos Lavas Sequence (Espinoza *et al.*, 2010), the magma source model proposed by these authors is considered for the Cerro Negro del Ghío pluton, including calc-alkaline subduction derived components, and an interaction with an enriched component (Espinoza *et al.*, 2010). Based on Hildreth and Moorbath (1988) model, we propose a melting, assimilation, storage and homogenization (MASH) zone in the mantle-crust transition, an open system, compatible with the alkali variations found in this work, and in accordance to evolving tectono-magmatic scenarios. In which alkalinity and incompatible elements (HFSE) content increase in Cerro Negro/Zeballos magmas with enriched sub-continental lithospheric mantle (SCLM) components.

As the rocks from Paso de Las Llaves pluton have a more evolved εNd_t signature than Cerro Negro del Ghío pluton (Table 5), together with subtle lower content in alkali and incompatible elements (La/Ta ratio) (Figs. 10A and 16), closer to SPB, a predominance of subduction related components in the MASH zone is interpreted. Otherwise, the emplacement of this pluton is interpreted to involve 3 different pulses of magma. First, the mafic one produces the pyroxene diorites, then, the tonalites in the coast of the Lago General Carrera area, and finally, the granite in the Río Avilés area (Granito Avilés). Fractional crystallization is evidenced as the main process for differentiation of these three units: the negative correlation of Al_2O_3, CaO, FeO_{tot}, MgO, with the increasing SiO_2 content, observed in the diorites and tonalities, is interpreted as indicative of pyroxene and plagioclase fractionation in the diorite to generate the felsic magmas. Elsewhere, the tonalites and Granito Avilés have negative correlations of Al_2O_3, CaO, FeO_{tot}, MgO, TiO_2 with increasing SiO_2 content. In addition, Granito Avilés has lower content of Sr, P, Ti and larger negative Eu anomaly. All this data is interpreted as plagiocase, apatite and mafic phases (probably pyroxenes+hornblende) early fractionation in the diorite and tonalite before granite crystallization. This interpretation is consistent with the petrographic evidences (Section 4.1).

In the case of Cerro Negro del Ghío pluton, the more enriched magma source evidences are the high alkali, LREE and HFSE contents. Furthermore, the εNd_t values point to mantle sources (+2.4 to +2.9). Therefore, a more fertile mantle source with respect to Paso de Las Llaves pluton is proposed, in which

subduction-derived fluids, and/or magmas, interacted with the enriched SCLM in the proposed MASH zone in the crust-mantle interface to rise alkali, LREE and HFSE contents.

A completely different magma source is suggested for the garnet bearing porphyritic granite, whose isotopic ratios ($^{87}Sr/^{86}Sr$, εNd_t, Table 5) reflect a major crustal component, which may be due to partial melting of the host rocks of the Paso de Las Llaves pluton, *i.e*., either the Tobifera Formation, or the metasedimentary rocks (seen in the xenolith in the border of the pluton) (Fig. 5a).

6.2.2. San Lorenzo and Río de Las Nieves plutons

Both plutons have "intra-plate transitional" geochemical features (Fig. 16). The San Lorenzo pluton is more acidic, closer to the peralkaline field (A/CKN and A/NK ratios just above 1), and isotopic evolved (εNd_t between+0.3 and -1.4) than the Río de Las Nieves pluton (+1.3). Despite this, they share most geochemical features (alkalinity, REE and trace elements patterns, Figs. 10A, B; 11A; 12E, F and 14A, B).

Thus, we interpret a similar magma-genesis for them. Due to the intra-plate geochemical patterns, a MASH zone is proposed in the crust/mantle interface, which may date back to the Paso de Las Llaves plutonism period. This is similar to the model proposed by Welkner (1999) for the San Lorenzo pluton. The higher εNd_t in Río de Las Nieves pluton (+1.3) than in San Lorenzo may implicate more SCLM contribution in this pluton, or alternatively, minor degree of assimilation of the continental crust.

6.2.3. Cerro Donoso Pluton and Paine External Gabbros

Both units are "arc-transitional" calc-alkaline (Fig. 16). The slightly larger content in LREE and alkali of these plutons compared to SPB can be explained by their back-arc location with respect to the Neogene arc (Cerro Donoso pluton is between 45 to 100 km eastward the SPB Neogene plutons, according to Hervé *et al.*, 2007) due to a possible more enriched astenosphere partial melting in this back-arc position, similar to what is proposed for the Cerro Negro del Ghío pluton.

6.2.4. Monte Balmaceda Intrusive Complex

The Balmaceda Mafic Complex geochemical signature, resemble those of OIB for most trace elements, especially HFSE (Fig. 15E, F), but also the LILE/HFSE, LREE/HFSE ratios (Fig. 17), and the Zr/Nb<10 and La/Ta<15 ratios, or also Ba/La <10 (Elliott *et al.*, 1997; Kay and Mpodozis, 2002; Fig. 16). This complex shares many geochemical characteristics with the back-arc Neogene volcanic rocks in south Patagonia (*e.g.,* Figs. 16 and 17B). Otherwise, the isotopic ratio reflects a primitive magma source (εNd_t up to +5). All these features combined suggest a mantle source enriched in incompatible elements for the magmas. Notwithstanding, its high Pb content (up to 51 ppm), as well as its variable high content in Th (3.5 to 13 ppm) and U (1 to 3.5 ppm; Table 4), suggests contribution from slab-derived components and/or crustal contamination (*e.g.,* Elliott *et al.*, 1997).

The Balmaceda Leucogranite (BLG) geochemistry evidences a REE-enriched magma source (Fig. 15E). Their distinctive Sr, P, Eu and especially Ba and Ti negative anomalies (Fig. 15F), are characteristic of intraplate granitoids (Winter, 2001), but these anomalies may also represent strong crystal fractionation of plagiocase (Eu, Sr, minor Ba), amphibole and magnetite (Ti), as these are devoid phases in BLG. Nevertheless, the LILE/HFSE and LREE/HFSE ratios have similar values to those of the OIB like Balmaceda Mafic Complex, with Ba/La <10, La/Ta< 15 and Zr/Nb<10, reflecting intra-plate signatures (Elliott *et al.*, 1997; and Fig. 16). Their isotopic ratios show εNd_t values ranging between +2 and +4.6 (Fig. 13). These data discriminate the samples from different areas, where those from the northern slope of the mount have the lowest εNd_t values. This difference is not recorded in the mafic facies. In any case, the felsic facies with the lowest εNd_t also have high LILE/HFSE and LREE/HFSE ratios, as well as a slight Nb negative anomaly, reflecting subtle subduction components and/or crustal contamination. These isotopic variations may reflect discontinuous emplacement of different batches of felsic magmas as contact relationship suggests strongly that εNd did not have enough time to evolve in the magma after emplacement.

This intrusive complex reflects the emplacement of magmas probably issued from two different reservoirs. Both the OIB-like alkaline gabbro and the leucogranites have subtle subduction and/or crustal contamination components, but their εNd_t (>+4) evidences enriched mantle sources for those magmas. Neither its bulk chemistry nor its petrography suggests further variation by assimilation-fractional crystallization (AFC) processes after emplacement

between the felsic facies. The proposed petrogenetic model for the suite is supported by the strong intra-plate signatures of both facies and it requires three evolutionary stages to accommodate all compositional features: **(1)** Anhydrous melts with alkaline signature, OIB-like trace elements pattern, and high εNd_t produced in fertile mantle, probably the SCLM, and stored in the lower crust. **(2)** Melts produced from (1) stayed in deep crustal levels, where strong *in-situ* crystal fractionation, and/or crustal assimilation produced the highly acidic felsic magmas. As they have primitive isotopic ratios (εNd_t>+4), crystal fractionation is preferred as the main process. **(3)** The injection of new fresh basaltic magmas into the former accumulated magmas may have triggered the upwelling by batches of both, the stored basic magmas and the felsic derived magmas, to get emplaced in shallow levels of the upper crust (<5 Km of the surface). In stage (3) the new magmas with εNd_t *ca.*+2 should evolve due to 2 possible processes: further assimilation of crust rocks (with subduction imprints, not reflected in the rocks with εNd_t=+4) or they are subduction derived. As the εNd_t=+2 rocks have no higher silica or alumina content compared to those with εNd_t=+4 (Tables 4, 5), assimilation should not be the most important process involved.

A pluton with similar petro-mineralogical characteristics but late Cretaceous in age has been described in Del Salto area in an "extra-Andean" position, specifically at Cordillera San Lorenzo (Welkner *et al.*, 2002) (Del Salto pluton in Fig. 2). The similar Ba, Sr and remarkable pronounced Eu negative anomaly, as well as the high Pb content and presence of Na-amphiboles in both intrusives, may be indicative of similar magma sources for the Balmaceda Leucogranites and Del Salto pluton. As a genetic model for the Del Salto pluton, Welkner *et al.* (2002) proposed an extensive interaction between mantle-derived magmas and the crust during the early relaxation stage that followed the mid-Cretaceous Andean crustal thickening and marginal basin closure (Welkner *et al.*, 2002). In this sense, the interaction of SCLM-derived magmas with Jurassic and Paleozoic continental crust is a plausible scenario for both igneous bodies. This interaction may have been favored by an extensional setting. Nevertheless, there is no further evidence of extension in the Monte Balmaceda area, so a period of relaxation, prior to ridge subduction, may be a possible scenario for the localized extensional setting in these periods. This scenario has been suggested in the Meseta del Lago Buenos Aires area (see Fig. 2 for location), where Boutonnet *et al.* (2010) infer an extensional setting prior to the Chile Rise collision coeval with the start of the Meseta del Lago Buenos Aires (*ca.* 47ºS, Fig.2 for location) construction, at 12 Ma.

6.2.5. Torres del Paine Intrusive Complex

This intrusive complex shows an "intra-plate transitional" calc-alkaline chemical signature (Fig. 16), with many geochemical features similar to the San Lorenzo pluton (*e.g.*, Figs.12 and 15). Considering its bimodal character, Michael (1991) suggested a common origin for both mafic and silicic magmas of the suite. This common source for both magmas, was also supported by later geochemical studies by Leuthold *et al.* (2013).

Some of the geochemical characteristics of the Torres del Paine intrusive complex are shared with the Monte Balmaceda intrusive complex, including the bimodal magmatism and the OIB-like signatures for the mafic complexes (*e.g.,* HFSE content, Zr/Nb<10). Nevertheless, subtle arc-like geochemical features are also present, including a Ti content similar to values of the SPB, La/Ta ratio >20 (the La/Ta ratio of Cenozoic rocks from SPB is >25) (Fig. 16), and a slight negative Nb-Ta anomaly (Fig. 15D). These features suggest a geochemically intermediate magma affinity for the Torres del Paine intrusive complex, probably formed in a transitional tectonic setting between arc and back-arc (OIB-like), well reflected in the Ba/La ratio (Fig. 16), which is between 10 and 20 for this intrusive complex, between 10 and 12 for the OIB-like back-arc lavas (D'Orazio *et al.*, 2001), and between 15 and 38 in arc granitoids from the Cenozoic SPB (Hervé *et al*., 2007). Consequently, we propose that the Torres del Paine suite was probably formed by the emplacement of SCLM-derived magmas stored in the lower crust together with magmas generated by the melting of this crust (a MASH zone), similar to the case of the Monte Balmaceda Intrusive Complex mentioned above, with the difference that the stored magmas for the Torres del Paine Complex have been metasomatized by subducted slab-derived components (*e.g.,* Sr, Ba, Th, Ca) and carried by hydrated melts and/or fluids in significantly larger quantities than in Monte Balmaceda Intrusive Complex (if this has any). This process is evidenced either by the higher Ba/La (Fig. 16), Th/Nb and La/Ta (or Nb/La) ratios in Torres

del Paine Intrusive Complex (Figs. 16 and 17B), where the former ratio reflects slab derived fluids (Elliot *et al.*, 1997), and the others reflect slab derived melts (Hawkesworth *et al.*, 1997), or by the occurrence of hydrated mineral phases in the felsic facies.

6.3. Miocene arc migration and "transitional calc-alkaline" magma generation

Based on the new and previous geochemical and isotopic data, we discuss an attempt to explain how the MASH zone at the base of the crust may have been generated in the extra-Andean location according to the characteristics of each pluton, most of them with "transitional" geochemical character.

First, most of the studied plutonic rocks in this work have subtle to strong subduction signatures (*e.g.*, Figs. 12, 14, 15 and 16), which means that they do not derive from magmas formed in a back-arc environment, and consequently the "extra-Andean" plutons denomination is preferred. In this sense, two hypotheses may explain this magmatism: a lateral expansion of the magmatic arc, or the migration of the arc, either case to the east. Arc migration is preferred, as the scarce volume of igneous rocks which crop out in the region, which is not fully consistent with an expansion of the magmatic arc. Furthermore, the known outcrops are at similar distance from the SPB (Fig.1). This arc migration should produce melts from the mantle and/or the crust in diverse amounts according to each region, tectonic feature, and processes involved in the magmatism migration, coherent with the heterogeneous geochemical alkalinity character of the Neogene extra-Andean plutons.

The geochemical diversity found in the studied plutons is put together with their geographic location in figure 18, where a cartoon illustrates the position of the Chile Rise segments before their collision with the trench at *ca.* 16 Ma (Fig. 18A), and three successive stages. A remarkable point is that at *ca.* 14 Ma very

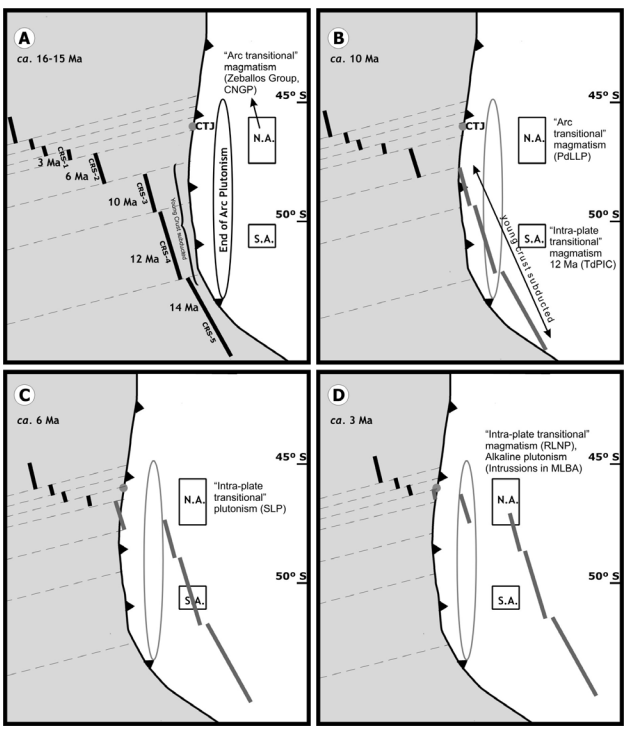

FIG. 18. Sketch of reconstructed Chile Rise Segments (CRS) spreading center locations from Miocene (*ca.* 16 Ma) to Pliocene (*ca.* 3 Ma). The spreading centers beneath the South American Plate (in gray) have been drawn in approximate locations following Cande and Leslie (1986). A more precise reconstruction has been made for the northern area at *ca.* 6 Ma in figure 20. **CNGP:** Cerro Negro del Ghío Puton; **SLP:** San Lorenzo pluton; **PdLLP:** Paso de Las Llaves pluton; **TdPIC:** Torres del Paine intrusive complex; **CTJ:** Chile Triple Junction. Cartoons after Cande and Leslie (1986), Lagabrielle *et al*. (2004) and Breitsprecher and Thorkelson (2009).

young oceanic crust started to subduct beneath almost all the south Patagonian western margin (>700 km), which is linked to three long segments of the Chile Rise. The last of these segments arrived to the trench at *ca.* 10 Ma (Fig. 18B) (Cande and Leslie, 1986). In its foreland region the southern area plutons of this work are located (Fig. 18). Meanwhile in the northern area, the Chile Rise subducted in short segments (around 1/3 compared to the segments in the south) since *ca.* 6 Ma (Fig. 18C). They had much more separation between them by fault zones than those of the south (Fig.18). Having this in mind, we propose that even if the arc migration to the east should have occurred more or less simultaneously in all southern Patagonia, the differences in the tectonic configurations between the northern and southern areas contributed to the strong differences in the geochemistry of the studied plutons. In the northern area magmatism is "arc-transitional" calc-alkaline (slightly more alkaline than the SPB) between the period comprised by the magmatism that generated the Zeballos Group Lavas, the Cerro Negro del Ghío and Paso de Las Llaves plutons (between *ca*. 16 and 8 Ma), while alkaline and "intra-plate transitional" calc-alkaline plutonism took place in the southern area (Monte Balmaceda and Torres del Paine intrusive complexes, respectively).

Arc migration itself should control the characteristic of magmatism. Two hypotheses have been proposed to explain arc-plutonism migration, Sánchez *et al.* (2008) argued for a migration of the arc in mid-Miocene times because the magmatic arc ceases its plutonism just before the Chile Rise segments collided with the trench (at *ca.* 16 Ma) and in this moment the Miocene foreland plutonism started. These authors proposed a slab flattening as a possible mechanism for this arc migration, similar to Gorring *et al.* (1997), and Kay *et al.* (2006) for the Miocene magmatism in the Neuquén Region, Argentina, at 36º S. Later, Espinoza *et al.* (2010) also put forward arc migration for the Cerro Plomo/Zeballos lavas (Northern Area). Alternatively, Ramírez de Arellano *et al.* (2012a) proposed the arc migration mechanism to explain the calc-alkaline (*sensu stricto*) character of the Chalten (Fitz-Roy) plutonic complex, located between the Northern and Southern areas of this work (Fig. 1). These authors argued for subduction erosion as the main process for arc migration, discarding slab flattening because of the need to change the subduction angle from 44 to 29º to fix the magmatism locations; instead, a change in the angle from 34 to 29º with 50 km of subduction erosion is the hypothesis preferred by these authors. However, the geochemical heterogeneity for the plutons compels us not to considerate only one hypothesis. So if we take subduction erosion as the main factor in all south Patagonia, all the plutons should be calc-alkaline *sensu stricto.* Nevertheless, as seen in Section 6.1, it is not the case for most of the plutons.

Even if we suppose that arc migration was a simultaneous process in all south Patagonia, we have to take into account that in the southern area a longer, younger and hotter slab than that in the northern area was subducted at the same time (*ca*. 16-15 Ma; Fig. 18), factors which may have helped to increase the partial melting of the SCLM, and therefore, to produce the high εNd_t alkaline -OIB like- magmatism. Slab flattening process has been related to strong tectonic coupling, and therefore to upper crust deformation (*e.g.,* Kay and Mpodozis, 2002). The timing of deformation in south Patagonia is poorly constrained (Suárez *et al.*, 2000). Fosdick *et al.* (2011) show that thrust faults were active at *ca.* 51º S between 22 and 18 Ma, and propagated eastward after 18 Ma (Fig. 19). This contractional event can be linked to a fast convergence rate period which started at 25 Ma (Pardo Casas and Molnar, 1987) and/or to buoyancy of the subducted plate. At 16.5 Ma a climate change in the foreland region is recorded at *ca.* 49º S. This change is related to a 1 km uplift of the Andean range, and to a cease in sedimentary deposition at 14 Ma (Blisniuk *et al.*, 2005). Both events pre-date the Chile rise subduction south of 49º S. Thus, this strong tectonic coupling previous to the emplacement of the alkaline magmas in the southern area may have been linked to the buoyancy of the hot and young oceanic crust subduction (Suárez *et al.,* 2000; Fig. 19), and after the strong coupling, tectonic relaxation may have triggered the Monte Balmaceda alkaline magmatism as in Del Salto pluton proposed model (Welkner *et al.*, 2002). This could explain the extra-Andean alkaline and "intra-plate transitional" calc-alkaline plutonism (Monte Balmaceda and Torres del Paine intrusive complexes, respectively).

The proposed flat slab model has a variable dipping angle (Fig. 19), instead of a constant one (Ramírez de Arellano *et al.*, 2012a), as observed in the present day Chilean flat subduction zone (*e.g.,* Kay and Mpodozis, 2002; Ramos *et al.*, 2002; Deshayes

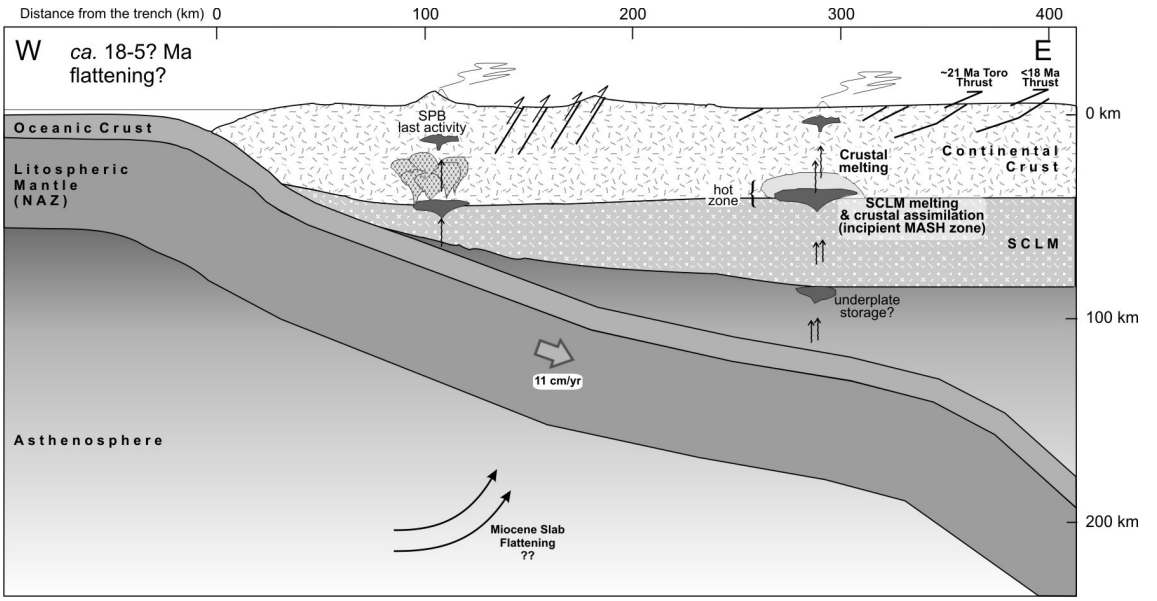

FIG. 19. Schematic W-E section at *ca.* 51ºS, illustrating a possible flat slab subduction scenario prior to the Chile Rise collision at *ca.* 18-16 Ma, for the alkaline magma generation of the Monte Balmaceda intrusive complex. Thrusting in the foreland region, pre- and post-dating the 18 Ma, is shown (from Fosdick *et al.*, 2011). Subducted slab geometry is inspired in the present flat slab subduction zone at 27-33º S in South America (*e.g.*, Kay and Mpodozis, 2002; Deshayes *et al.*, 2008). The "Hot Zone" is following Annen *et al.* (2006). **SPB:** South Patagonian batholith; **SCLM:** Sub-Continental Lithospheric Mantle; **NAZ:** Nazca plate; **11cm/yr:** average convergence rate between Nazca and South American plates, from Pardo-Casas and Molnar (1987), Somoza (1998) and Breitsprecher and Thorkelson (2009) data.

et al., 2008). As Miocene alkaline (*s.s.*) rocks are not widely known in south Patagonia, this relaxation stage should not produce an important volume of magma, so it might have been a local phenomenon.

Although mid-Miocene plutons are found in both the northern and southern areas, in the northern area they have more pristine arc signatures-"arc transitional" calc-alkaline (Fig. 16)-; therefore, a different scenario for magmatism, and hence, for magmatic arc migration process, should occur in this region. Contractional tectonism would have occurred sometime between 29 and 15 Ma (Suárez *et al.*, 2000). This again can be linked to fast convergence rates between 25 to 16 Ma (Pardo-Casas and Molnar, 1987; Somoza, 1998) coeval with arc-migration: Neogene plutonism in arc location (SPB) is 25-15 Ma (Hervé *et al.*, 2007), and begins in extra-Andean location with Cerro Negro del Ghío pluton at *ca.* 15 Ma. Thus, at the end of this period, arc magmatism took place in an extra-Andean location and lasted until, at least, 9 Ma (Paso de Las Llaves intrusive suite). If here the arc shift was linked to buoyancy of the subducted plate, there was no tectonic relaxation like in the southern area, possibly due to the arrival of another Chile Rise short segment at the same latitude, which was coeval with the subduction of young slab (Fig. 18 and 20). Alternatively, subduction erosion may not be dismissed as a factor contributing, together with slab flattening, to shift the arc location and to produce the "arc transitional" calc-alkaline plutons from *ca.* 15 to 9 Ma (Fig. 18) in this area.

A more complex tectonic scenario occurred after *ca.* 10 Ma in the northern area with the oblique subduction of the Chile Rise (77-82º in Breitspecher and Thorkelson, 2009), where the Chile Rise Segment (CRS)-3 (Fig.18) may have developed a slab window, opening north and eastward. Therefore, after 4 Ma of development (at *ca.* 6 Ma), this slab window (or at least the north-eastern corner of it) must have been in back-arc position at the same latitude than CRS-2 (Fig. 20). In this region the "transitional arc" calc-alkaline magmatism evolved to a "transitional intra-plate" magmatism (the San Lorenzo pluton), in which subduction components should had been stored in a

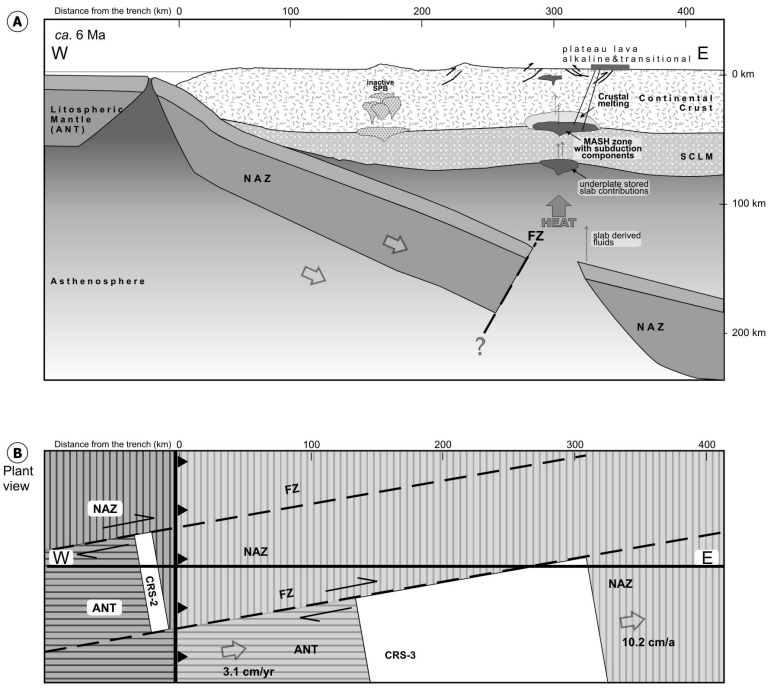

FIG. 20. Schematic W-E section at ~47º30'S., showing a possible subduction setting at *ca*. 6 Ma. It is assumed that the Chile Rise segments (CRS) generated a slab window (in white in plant view) due to the differences in the convergence rates between the Nazca/South American plates and the Antarctic/South American plates, considering rates of 10.2 cm/a and 3.1 cm/a, respectively (averages values from Cande and Leslie (1986), Pardo-Casas and Molnar (1987), Somoza (1998) and Breitspecher and Thorkelson (2009)). Besides, the distances of the edges of this window to the trench has been calculated considering the angle of subduction, the obliquity angle of the slabs convergence (from the same authors) and considering 4 Ma after the CRS-3 started its subduction (Cande and Leslie, 1986). In this model, the wedge of the slab window grows north and eastward. The subducted slabs may contribute fluids to be stored in the astenosphere-sub-continental Lithospheric Mantle (SCLM) interface; and the opening of the window may allow to generate a thermal anomaly, which, together with the addition of fluids, may in turn generate a "Hot Zone" triggering underplate and crust melting. This scenario could occur again at *ca.* 3 Ma, with the opening of a slab window with the CRS-2. The upper crust structures are simplified from Ramos and Kay (1992) and Lagabrielle *et al*. (2004). **NAZ:** Nazca Plate; **FZ:** Fault Zone; **SPB:** South Patagonian batholith.

MASH zone. Then, lower crust plus SCLM melting should have been triggered by heat influx from the slab window development beneath the South American plate (Fig. 20).

At *ca.* 3 Ma, northward, the tectonic configuration must have been very similar to the one explained at 6 Ma, but with CRS-2 at the foreland position, and CRS-1 in the trench. Here, magmatism resulted in the "transitional intra-plate" calc-alkaline Río de Las Nieves pluton. Eastward, there was bimodal alkaline magmatism expressed into the basaltic Meseta del Lago Buenos Aires plateau lavas and the felsic intrusive bodies (Espinoza *et al*., 2008). These authors argued for strong intraplate AFC processes from OIB melts without influence of the subducted slab. Indeed, the melting process they suggested is by decompression due to astenospheric window development, which is fully consistent with our proposed conceptual model at regional scale.

7. Concluding remarks

The new data presented allow us to conclude:

1. The geochemistry of the plutons in the "extra-Andean" region shows a wide range in alkalinity. The only *sensu stricto* alkaline pluton is the Monte Balmaceda intrusive complex, reflecting intra-plate signatures. The rest of the studied plutons have subduction derived components and "transitional" geochemical features between intra-plate and magmatic arc signatures.

2. The "arc transitional" calc-alkaline plutons are the Paso de Las Llaves and Cerro Negro del Ghío plutons in the northern area, and the Cerro Donoso pluton in the southern area. While the "intra-plate transitional" calc-alkaline plutons are the San Lorenzo and Río de Las Nieves plutons in the northern area, and the Torres del Paine intrusive complex in the southern area.
3. The intra-plate signatures are interpreted as reflecting lower continental crust and/or sub-continental lithospheric mantle melts contributing in different proportion to the magmas, according to the geochemical features of each pluton.
4. The common geochemical characteristics in the studied extra-Andean plutons are:
   - High Pb content: over 6 ppm, up to 51 ppm (Tables 3 and 4).
   - High LREE content.
   - Steep LREE and flat HREE pattern.
   - Isotopic ratios with $(^{87}Sr/^{86}Sr)_i<0.705$ and $\varepsilon Nd_t>-1.4$, mostly over 0.
5. An eastward migration of the magmatic arc previous to the Chile Rise arrival to the continent is consistent with the "transitional" geochemistry of the plutons, and the tectonic configuration differences between the northern and southern areas contribute to the particular magmatic evolution of each area.
6. Two ways of magma evolution can be noted: from alkaline to "intraplate-transitional" calc-alkaline (Miocene, southern area) and from "arc transitional" to "intraplate-transitional" calc-alkaline to alkaline (Mio-Pliocene, northern area).

Acknowledgements

This work was possible thanks to "Becas de Doctorado" Conicyt (A. Sánchez), and to ECOS/Conicyt C05U02 grant. Field assistance of M. Gerbault (IRD), N. Croissant (U. de Chile), B. Scalabrino (U. Montpellier) is very appreciated. FONDECYT projects 1010413 and 1095099 financed the geochemical analyses conducted at U. de Chile. We also thank Conaf staff for field support and permission to study in protected areas. Estancia Sol de Mayo owner allowed us to work in his property. Río Arriba and 21 de Mayo enterprises also cooperated for a successful field work in these inhospitable regions. Constructive reviews by A. Echaurren, C. Ramírez de Arellano and AG editor contributed to the improvement of this manuscript. Last but not least, we appreciate "El Ermitaño" for his guidance in the difficult ways of Monte Balmaceda.

References

Allen, R.B. 1982. Geología de la Cordillera Sarmiento, Andes Patagónicos, entre los 51º00' y 52º15' Lat S, Magallanes, Chile. Servicio Nacional de Geología y Minería, Boletín 38: 46 p. Santiago.

Altenberger, U.; Oberhaensli, R.; Putlitz, B.; Wemmer, K. 2003. Tectonic controls of the Cenozoic magmatism at the Torres del Paine, southern Andes (Chile, 51°10'S). Revista Geológica de Chile 30 (1): 65-81. doi: 10.5027/andgeoV30n1-a05.

Anma, R.; Armstrong, R.; Orihashi, Y.; Ike, S.; Shin, K.; Kon, Y.; Komiya, T.; Ota, T.; Kagashima, S.; Shibuya, T.; Yamamoto, S.; Veloso, E.; Fanning, C.M.; Hervé, F. 2009. Are the Taitao granites formed due to subduction of the Chile ridge? Lithos 113: 246-258.

Annen, C.; Blundy, J.D.; Sparks, R.S. 2006. The Genesis of Intermediate and Silicic Magmas in Deep Crustal Hot Zones. Journal of Petrology 47: 505-539.

Aries, S.; Valladon, M.; Polvé, M.; Dupré, B. 2000. A routine method for oxide and hydroxide interference corrections in ICP-MS chemical analyses of environmental and geological samples. Geostandards Newsletter 24: 19-31.

Baker, P.; Rea, N.; Skármeta, J.; Caminos, R.; Rex, D. 1981. Igneous history of the Andean Cordillera and Patagonian Plateau around latitude 46° S. Philosophical Transactions of the Royal Society London A303: 105-149.

Biddle, K.; Uliana, M.; Mitchum, R.; Fitzgerald, M. 1986. The stratrigraphic and structural evolution of the central and eastern Magallanes Basin, southern South America. *In* Foreland Basins (Allen, P.A.; Homewood, P.; editors). International Association of Sedimentologists, Special publication 8: 41-61. Oxford.

Blisniuk, P.; Stern, L.; Chamberlain, C.; Idleman, B.; Zeitler, P. 2005. Climatic and ecologic changes during Miocene surface upliflt in the southern Patagonian Andes. Earth and Planetary Science Letters 230: 125-142.

Boutonnet, E.; Arnaud, N.; Guivel, C.; Lagabrielle, Y.; Scalabrino, B.; Espinoza, F. 2010. Subduction of the South Chile active spreading ridge: A 17 Ma to 3 Ma magmatic record in central Patagonia (western edge of Meseta del Lago Buenos Aires, Argentina). Journal of Volcanology and Geothermal Research 189: 319-339.

Breitsprecher, K.; Thorkelson, D. 2009. Neogene kinematic history of Nazca-Antarctic-Phoenix slab windows beneath Patagonia and the Antarctic Peninsula. Tectonophysics 464: 10-20.

Brown, L.; Singer, B.S.; Gorring, M. 2004. Paleomagnetism and $^{40}Ar/^{39}Ar$ chronology of lavas from Meseta del Lago Buenos Aires, Patagonia. Geochemistry,

Geophysical, Geosystem 5 (1) Q01H04: 21 p. doi: 10.1029/2003GC000526.

Bruce, R.; Nelson, E.; Weaver, S.; Lux, D. 1991. Temporal and spatial variations in the southern Patagonian batholith; constraints on magmatic arc development. *In* Andean Magmatism and its Tectonic Setting (Harmon, R.S.; Rapela, C.W.; editors). Geological Society of America, Special Papers 265: 1-12.

Bruhn, R.; Stern, C.; de Wit, M. 1978. Field and geochemical data bearing on the development of a Mesozoic volcano-tectonic rift zone and back-arc basin in southernmost South America. Earth and Planetary Science Letters 41: 32-46.

Cande, S.; Leslie, R. 1986. Late Cenozoic tectonics of the Southern Chile Trench. Journal of Geophysical Research 3: 471-496.

Calderón, M.; Fildani, A.; Hervé, F.; Fanning, C.M.; Weislogel, A.; Cordani, U. 2007a. Late Jurassic bimodal magmatism in the northern sea-floor remnant of the Rocas Verdes basin, southern Patagonian Andes. Journal of the Geological Society 164: 1011-1022.

Calderón, M.; Hervé, F.; Massonne, H.-J.; Tassinari, C.G.; Pankhurst, R.J.; Godoy, E.; Theye, T. 2007b. Petrogenesis of the Puerto Edén Igneous and Metamorphic Complex, Magallanes, Chile: Late Jurassic syn-deformational anatexis of metapelites and granitoid magma genesis. Lithos 93: 17-38.

Charrier, R.; Linares, E.; Niemeyer, H.; Skármeta, J. 1979. K-Ar ages of basalt flows of the Meseta Buenos Aires in southern Chile and their relation to the southeast Pacific triple junction. Geology 7: 436-439.

D'Orazio, M.; Agostini, S.; Mazzarini, F.; Innocenti, F.; Manetti, P.; Haller, M.; Lahsen, A. 2000. The Pali Aike Volcanic Field, Patagonia: slab-window magmatism near the tip of South America. Tectonophysics 321: 407-427.

D'Orazio, M.; Agostini, S.; Innocenti, F.; Haller, M.J.; Manetti, P.; Mazzarini, F. 2001. Slab window-related magmatism from southernmost South America: the Late Miocene mafic volcanics from the Estancia Glencross Area; ~52° S, Argentina-Chile. Lithos 57: 67-89.

D'Orazio, M.; Innocenti, F.; Manetti, P.; Haller, M. 2004. Cenozoic back-arc magmatism of the southern extra-Andean Patagonia (44°30'-52° S): A review of geochemical data and geodynamic interpretations. Revista de la Asociación Geológica Argentina 59: 525-538.

D'Orazio, M.; Innocenti, F.; Manetti, P.; Haller, M.; Di Vincenzo, G.; Tonarini, S. 2005. The Late Pliocene mafic lavas from the Camusú Aike volcanic field (~50° S, Argentina): Evidences for a geochemical variability in slab window magmatism. Journal of South American Earth Sciences 18: 107-124.

Dalziel, I.W.; de Wit, M.; Palmer, K. 1974. Fossil marginal basin in the southern Andes. Nature 250: 291-294.

Deshayes, P.; Monfret, T.; Pardo, M.; Vera, E. 2008. Three-dimensional P- and S-wave seismic attenuation models in central Chile-western Argentina (30°-34° S) from local recorded earthquakes. *In* International Symposium on Andean Geodynamics, No. 7, Extended Abstracts: 184-187. Nice.

Elliott, T.; Plank, T.; Zindler, A.; White, W.; Bourdon, B. 1997. Element transport from slab to volcanic front at the Mariana arc. Journal of Geophysical Research 102: 14991-15019.

Espinoza, F.; Morata, D.; Pelleter, E.; Maury, R.C.; Suárez, M.; Lagabrielle, Y.; Polvé, M.; Bellon, H.; Cotten, J.; De la Cruz, R.; Guivel, C. 2005. Petrogenesis of the Eocene and Mio-Pliocene alkaline basaltic magmatism in Meseta Chile Chico, Southern Patagonia, Chile: evidence for the participation of two slab windows. Lithos 82: 315-343.

Espinoza, F.; Morata, D.; Polvé, M.; Lagabrielle, Y.; Maury, R.C.; Guivel, C.; Cotton, J.; Bellon, H.; Suárez, M. 2008. Bimodal back-arc alkaline magmatism after ridge subduction: Pliocene felsic rocks from Central Patagonia (47° S). Lithos 101: 191-217.

Espinoza, F.; Morata, D.; Polve, M.; Lagabrielle, Y.; Maury, R.; de la Rupelle, A.; Guivel, C.; Cotten, J.; Bellon, H.; Suárez, M. 2010. Middle Miocene calc-alkaline volcanism in Central Patagonia (47°·S): petrogenesis and implications for slab dynamics. Andean Geology 37: 300-328.

Fanning, C.M.; Hervé, F.; Pankhurst, R.J.; Calderón, M.; Yaxley, G.; Holden, P. 2009. Multi-dimensional Zircon Tracking: A Case Study Using The 150 My Evolution Of The South Patagonian Batholith. *In* Congreso Geológico Chileno, No. 12, Electronic actas S12_005: 4 p. Santiago.

Faúndez, V.; Hervé, F.; Lacassie, J.P. 2002. Provenance and depositional setting of pre-Late Jurassic turbidite complexes in Patagonia, Chile. New Zealand Journal of Geology and Geophysics 45: 411-425.

Feraud, G.; Alric, A.; Fornari, M.; Bertrand, H.; Haller, M. 1999. Ar/Ar dating of the Jurassic volcanic province of Patagonia: migrating magmatism related to Gondwana break-up and subduction. Earth and Planetary Science Letters 172: 83-96.

Fildani, A.; Cope, T.; Graham, S.; Wooden, J. 2003. Initiation of the Magallanes foreland basin: timing of

the southernmost Patagonian Andes orogeny revised by detrital zircon provenance analysis. Geology 31: 1081-1084.

Fosdick, J.; Romans, B.; Fildani, A.; Bernhardt, A.; Calderón, M.; Graham, S. 2011. Kinematic evolution of the Patagonian retroarc fold-and-thrust belt and Magallanes foreland basin, Chile and Argentina, 51°30'S. Geological Society of America Bulletin 123: 1679-1698.

Giacosa, R.; Franchi, M. 2001. Hojas Geológicas 4772-III y 4772-IV, Lago Belgrano y Lago Posadas. Provincia de Santa Cruz. Servicio Geológico Minero Argentino, Boletín 256: 68 p. Buenos Aires.

Gorring, M.; Kay, S. 2001. Mantle processes and sources of Neogene slab window magmas from Southern Patagonia, Argentina. Journal of Petrology 42: 1067-1094.

Gorring, M.; Kay, S.; Zeitler, P.; Ramos, V.; Rubiolo, D.; Fernández, M.; Panza, J. 1997. Neogene Patagonian plateau lavas; continental magmas associated with ridge collision at the Chile triple junction. Tectonics 16: 1-17.

Gorring, M.; Singer, B.; Gowers, J.; Kay, S. 2003. Plio-pleistocene basalts from the Meseta del Lago Buenos Aires, Argentina: evidence for asthenosphere-lithosphere interactions during slab window magmatism. Chemical Geology 193: 215-235.

Guivel, C.; Lagabrielle, Y.; Bourgois, J.; Maury, R.C.; Fourcade, S.; Martin, H.; Arnaud, N. 1999. New geochemical constraints for the origin of ridge-subduction-related plutonic and volcanic suites from the Chile triple junction (Taitao peninsula and Site 862, LEG ODP141 on the Taitao ridge). Tectonophysics 311: 83-111.

Guivel, C.; Morata, D.; Pelleter, E.; Espinoza, F.; Maury, R.; Lagabrielle, Y.; Polve, M.; Bellon, H.; Cotten, J.; Benoit, M.; Suárez, M.; De la Cruz, R. 2006. Miocene to Late Quaternary Patagonian basalts (46-78° S): Geochronometric and geochemical evidence for slab tearing due to active spreading ridge subduction. Journal of Volcanology and Geothermal Research 149: 346-370.

Halpern, M. 1973. Regional Geochronology of Chile south of 50° S latitude. Geological Society of America Bulletin 84: 2407-2422.

Hastie, A.; Kerr, A.; Pearce, J.A.; Mitchell, S. 2007. Classification of altered volcanic island arc rocks using immobile trace elements: Development of the Th-Co discrimination diagram. Journal of Petrology 48: 2341-2357.

Hawkesworth, C.J.; Kemp, A. 2006. The differentiation and rates of generation of the continental crust. Chemical Geology 226: 134-143.

Hawkesworth, C.J.; Turner, S.; Peate, D.; McDermott, F.; van Calsteren, P. 1997. Elemental U and Th variations in island arc rocks: implications for U-series isotopes. Chemical Geology 139: 207-221.

Hervé, F.; Fanning, C.M.; Pankhurst, R.J. 2003. Detrital zircon age patterns and provenance of the metamorphic complexes of southern Chile. Journal of South American Earth Sciences 16: 107-123.

Hervé, F.; Pankhurst, R.J.; Fanning, C.M.; Calderón, M.; Yaxley, G. 2007. The South Patagonian batholith: 150 my of granite magmatism on a plate margin. Lithos 97: 373-394.

Hildreth, W.; Moorbath, S. 1988. Crustal contributions to arc magmatism in the Andes of Central Chile. Contributions to Mineralogy and Petrology 98: 455-489.

Irvine, T.; Baragar, W. 1971. A guide to the chemical classification of the common volcanic rocks. Canadian Journal of Earth Sciences 8: 523-548.

Kaeding, M.; Forsythe, R.; Nelson, E. 1990. Geochemistry of the Taitao ophiolite and near-trench intrusions from the Chile margin triple junction. Journal of South American Earth Sciences 3: 161-177.

Kay, S.M.; Mpodozis, C. 2002. Magmatism as a probe to the Neogene shallowing of the Nazca plate beneath the modern Chilean flatslab. Journal of South American Earth Sciences 15: 39-58.

Kay, S.; Mancilla, O.; Copeland, P. 2006. Evolution of the late Miocene Chachahuén volcanic complex at 37°S over a transient shallow subduction zone under the Neuquén Andes. Geological Society of America, Special Papers 407: 215-246.

Kosmal, A.; Spikermann, J. 2002. Caracterización del granito Fitz Roy, Provincia de Santa Cruz, Argentina. Revista del Museo Argentino de Ciencias Naturales 4: 145-157.

Lagabrielle, Y.; Suárez, M.; Rossello, E.; Heráil, G.; Martinod, J.; Régnier, M.; De La Cruz, R. 2004. Neogene to Quaternary tectonic evolution of the Patagonian Andes at the latitude of the Chile Triple Junction. Tectonophysics 385: 211-241.

Lagabrielle, Y.; Suárez, M.; Malavieille, J.; Morata, D.; Espinoza, F.; Maury, R.C.; Scalabrino, B.; Barbero, L.; De la Cruz, R.; Rosselló, E.; Bellon, H. 2007. Pliocene extensional tectonics in Eastern Central Patagonian Cordillera: geochronological constraints and new field evidence. Terra Nova 19: 413-424.

Leuthold, J.; Muntener, O.; Baumgartner, L.; Putlitz, B.; Ovtcharova, M.; Schaltegger, U. 2012. Time resolved

construction of a bimodal laccolith (Torres del Paine, Patagonia). Earth and Planetary Science Letters 325-326: 85-92.

Leuthold, J.; Muntener, O.; Baumgartner, L.; Putlitz, B.; Chiaradia, M. 2013. A detailed geochemical study of a shallow, arc-related laccolith: the Torres del Paine mafic complex, Patagonia. Journal of Petrology 54: 273-303.

Macellari, C.; Barrio, C.; Manassero, M. 1989. Upper Cretaceous to Paleocene depositional sequences and sandstone petrography of southwestern Patagonia (Argentina and Chile). Journal of South American Earth Sciences 2: 223-239.

Michael, P.J. 1983. Emplacement and differentiation of Miocene plutons in the foothills of the southernmost Andes. Ph.D. Thesis (Unpublished), Columbia University: 367 p.

Michael, P.J. 1984. Chemical differentiation of the Cordillera Paine granite (southern Chile) by *in situ* fractional crystallization. Contributions to Mineralogy and Petrology 87: 179-195.

Michael, P.J. 1991. Intrusion of basaltic magma into a crystallizing granitic magma chamber: The Cordillera del Paine pluton in southern Chile. Contribution to Mineralogy and Petrology 108: 396-418.

Michel, J.; Baumgartner, L.; Putlitz, B.; Schaltegger, U.; Ovtchaarova, M. 2008. Incremental growth of the Patagonian Torres del Paine laccolith over 90 k.y. Geology 36: 459-462.

Morata, D.; Barbero, L.; Suárez, M.; De La Cruz, R. 2002. Early Pliocene magmatism and high exhumation rates in the Patagonian Cordillera (46°40'S) K-Ar and fission track data. *In* International Symposium on Andean Geodynamics, No. 5, Abstracts: 433-436. Toulouse.

Muñoz, J. 1981. Geología y petrología de las rocas ígneas e inclusiones ultramáficas del sector SW de Meseta Las Vizcachas, Última Esperanza, Magallanes, XII Región, Chile. Ms. Thesis (Unpublished), Universidad de Chile: 186 p.

Muñoz, J. 1982. Basaltos alcalinos y toleíticos del cenozoico superior en meta Las Vizcachas, Magallanesm Chile. *In* Congreso Geológico Chileno, No.3, Actas: D136-D153.

Nakamura, N. 1974. Determination of REE, Ba, Fe, Mg, Na and K in carbonaceous and ordinary chondrites. Geochimica et Cosmochimmica Acta 38: 757-775.

Nullo, F.; Proserpio, C.; Ramos, V. 1978. Estratigrafía y tectónica de la vertiente este del hielo continental patagónico, Argentina-Chile. *In* Congreso Geológico Argentino, No. 7, Actas 1: 455-470. Neuquén.

Pankhurst, R.; Weaver, S.; Hervé, F.; Larrondo, P. 1999. Mesozoic-Cenozoic evolution of the North Patagonian Batholith in Aysén, southern Chile. Journal of the Geological Society 156: 673-694.

Pankhurst, R.; Riley, T.; Fanning, M.C.; Kelley, S. 2000. Episodic silicic volcanism in Patagonia and the Antarctic peninsula: chronology of magmatism associated with the breakup of Gondwana. Journal of Petrology 41: 605-625.

Pardo-Casas, F.; Molnar, P. 1987. Relative motion of the Nazca (Farallon) and South American plates since Late Cretaceous time. Tectonics 6: 233-248.

Pearce, J.A. 1983. Role of sub-continental lithosphere in magma genesis at active continental margins. *In* Continental Basalts and Mantle Xenoliths (Hawkesworth, C.J.; Nurry, M.J.; editors). Shiva Publishing: 230-249. Nantwich.

Pearce, J.A.; Cann, J. 1973. Tectonic setting of basic volcanic rocks determined using trace element analyses. Earth and Planetary Science Letters 19: 290-300.

Peccerillo A.; Taylor S. 1976. Geochemistry of eocene calcalkaline volcanic rocks from Kastamonu area, northern Turkey. Contributions to Mineralogy and Petrology 56: 221-246.

Petford, N.; Turner, P. 1996. Reconnaissance $^{40}Ar/^{39}Ar$ age and palaeomagnetic study of igneous rocks around Coyhaique, S. Chile (45º30'-47ºS). *In* International Symposium on Andean Geodynamics, No. 3: 629-632. St. Malo.

Ramírez de Arellano, C. 2011. Petrology and chemistry of the Chaltén Plutonic Complex and implications on the magmatic and tectonic evolution of the Southernmost Andes (Patagonia) during the Miocene. Ph.D. Thesis (Unpublished), Université de Lausanne: 147 p.

Ramírez de Arellano, C.; Putlitz, B.; Müntener, O. 2008. Magmatic history of the Fitz Roy Plutonic Complex, Southern Patagonia (Argentina). *In* International Symposium on Andean Geodynamics, No. 7, Extended Abstract: 421-422. Nice.

Ramírez de Arellano, C.; Putlitz, B.; Müntener, O.; Ovtcharova, M. 2012a. High precision U/Pb zircon dating of the Chaltén Plutonic Complex (Cerro Fitz Roy, Patagonia) and its relationship to arc migration in the southernmost Andes. Tectonics 31: 18 p. doi: 10.1029/2011TC003048

Ramírez de Arellano, C.; Putlitz, B.; Müntener, O. 2012b. The transition to alkaline magmatism in Patagonia during the Miocene, a new petrogenetic interpretation.

In Congreso Geológico Chileno, No.13, Actas electrónicas: 3 p. Anfofagasta.

Ramos, V. 2002. El magmatismo neógeno de la Cordillera Patagónica. *In* Geología y recursos naturales de Santa Cruz (Haller, M.J.; editor). Congreso Geológico Argentino, No. 15, Relatorio I (13): 187-200. Buenos Aires.

Ramos, V.; Kay, S. 1992. Southern Patagonian plateau basalts and deformation: backarc testimony of ridge collision. Tectonophysics 205: 261-282.

Ramos, V.; Cristallini, E.; Pérez, D. 2002. The Pampean flat-slab of the Central Andes. Journal of South American Earth Sciences 15: 59-78.

Ramos, V.; Kay, S.; Singer, B. 2004. Las adakitas de la Cordillera Patagónica: Nuevas evidencias geoquímicas y geocronológicas. Revista de la Asociación Geológica Argentina 59: 693-706.

Rudnick, R.L.; Gao, S. 2003. Composition of the continental crust. *In* Treatise on Geochemistry 3, The Crust (Holland, H.D.; Turekian, K.K.; editors). Elsevier: 1-64. Amsterdam.

Sánchez, A.; de Saint-Blanquat, M.; Hervé, F.; Pankhurst, R.J.; Fanning, C.M. 2006. A Shrimp U-Pb zircon late Miocene crystallization age for the Torres del Paine Pluton, Chile. *In* South American Symposium on Isotope Geology, No. 5, Short papers: 196-199. Punta del Este.

Sánchez, A.; Hervé, F.; de Saint-Blanquat, M. 2008. Relations between plutonism in the back-arc region in southern Patagonia and Chile Rise subduction: A geochronological review. *In* International Symposium on Andean Geodynamics, No. 7, Extended Abstracts: 485-488. Nice.

Sánchez, A.; Saint Blanqat, M.; Polvé, M.; Hervé, F. 2009. Different plutonic events in extra-andine southern Patagonia, Chile. *In* Congreso Geológico Chileno, No.12, Actas electrónicas S8_026: 4 p. Santiago.

Scalabrino, B.; Lagabrielle, Y.; Malavieille, J.; Domínguez, S.; Melnick, D.; Espinoza, F.; Suárez, M.; Rossello, E.A. 2010. A morphotectonic analysis of Central Patagonian Cordillera. Negative inversion of the Andean belt over a buried spreading center? Tectonics 29: 27 p. doi: 10.1029/2009TC002453.

Sernageomin. 2002. Mapa Geológico de Chile. Servicio Nacional de Geología y Minería, Carta Geológica de Chile, Serie Geología Básica 75: 1 mapa en 3 hojas, escala 1:1.000.000. Santiago.

Shand, S.J. 1943. Eruptive Rocks. Their Genesis, Composition, Classification, and their Relation to Ore Deposits, with a chapter on Meteorites (revised second edition). Hafner Publishing Co.: 444 p. New York.

Soffia, J. 1988. Interpretación estructural del sector Laguna Amarga, Parque Nacional Torres del Paine. Región de Última Esperanza, Magallanes-Chile. *In* Congreso Geológico Chileno, No. 5, Actas, tomo 1: A157-A172. Santiago.

Somoza, R. 1998. Updated Nazca (Farallon)-South America relative motions during the last 40 My: Implications for mountain building in the central Andean region. Journal of South American Earth Sciences 11: 211-215.

Stern, C.; Kilian, R. 1996. Role of the subducted slab, mantle wedge and continental crust in the generation of adakites from the Andean Austral Volcanic Zone. Contributions to Mineralogy and Petrology 123: 263-281.

Stern, C.; de Wit, M. 2003. Rocas Verdes ophiolites, southernmost South America: remnants of progressive stages of development on oceanic-type crust in a continental margin back-arc basin. *In* Ophiolites in Earth History (Dilek, Y.; Robinson, P.T.; editors). Geological Society of London, Special Publications 218: 1-19.

Stern, C.; Futa, K.; Muehlenbachs, K. 1984. Isotope and trace element data for orogenic andersites in the Austral Andes. *In* Andean magmatism: chemical and isotopic constraints (Harmon, R.; Barreirro, B.; editors). Shiva Press: 31-46. Cheshire.

Stern, C.; Zartman, F.; Futa, K.; Zartman, R.; Peng, Z.; Kyser, T. 1990. Trace element and Sr, Nd, Pb, and O isotopic composition of Pliocene and Quaternary alkali basalts of the Patagonian Plateau lavas of southernmost South America. Contributions to Mineralogy and Petrology 104: 294-308.

Stewart, J.; Cruzat, A.; Page, B.; Suárez, M.; Stambuk, V. 1971. Estudio geológico económico de la Cordillera Patagónica entre los paralelos 51º00 y 53º30 Lat. S, provincia de Magallanes (Inédito). Instituto de Investigación Geológica: 174 p. Santiago.

Suárez, M.; De la Cruz, R. 2000. Tectonics in the eastern central Patagonian Cordillera (45°30'-47°30'S). Journal of the Geological Society 157: 995-1001.

Suárez, M.; De la Cruz, R. 2001. Jurassic to Miocene K-Ar dates from eastern central Patagonian Cordillera plutons, Chile (45°-48° S). Geological Magazine 138: 53-66.

Suárez, M.; De la Cruz, R.; Bell, C. 2000. Timing and origin of deformation along the Patagonian fold and thrust belt. Geological Magazine 137: 345-353.

Sun, S.; McDonough, W. 1989. Chemical and isotopic systematics of oceanic basalts: implications for mantle

composition and processes. *In* Magmatism in the Ocean Basins (Saunders, A.D.; Norry, M.J.; editors). Geological Society of London, Special Publications 42: 313-345.

Vargas, G.; Hervé, F. 1995. Emplazamiento hipabisal mioceno tardío del stock de Paso de Las Llaves en la región de tras arco, Aysen. Comunicaciones 46: 3-15.

Weaver, S.; Bruce, R.; Nelson, E.; Brueckner, H.; LeHuray, A. 1990. The Patagonian Batholith at 48°S latitude, Chile: geochemical and isotopic variations. *In* Plutonism from Alaska to Antarctica (Kay, S.; Rapela, C.; editors). Geological Society of America, Special Paper 241: 33-50.

Welkner, D. 1999. Geología del área del cerro San Lorenzo: Cordillera Patagónica Oriental, XI Región de Aysén, Chile (47°25'-47°50'S). Memoria de Título (Inédito), Universidad de Chile, Departamento de Geología: 151 p.

Welkner, D. 2000. Geocronología de los plutones del área del cerro San Lorenzo, XI Región de Aysén. *In* Congreso Geológico Chileno, No. 9, Actas 2: 269-273. Puerto Varas.

Welkner, D.; Godoy, E.; Bernhardt, H-J. 2002. Peralkaline rocks in the Late Cretaceous Del Salto Pluton, Eastern Patagonian Andes, Aisén, Chile (47°35'S). Revista Geológica de Chile 29: 3-15.

Wilson, T. 1991. Transition from a back-arc to foreland basin development in the southernmost Andes: Stratigraphic record from the Ultima Esperanza District, Chile. Geological Society of America Bulletin 103: 98-111.

Winchester, J.; Floyd, P. 1977. Geochemical discrimination of different magma series and their differentiation products using immobile elements. Chemical Geology 20: 325-343.

Winter, J. 2001. An Introduction to Igneous and Metamorphic Petrology. Prentice Hall: 699 p. New Jersey.

Zen, E. 1988. Phase relations of peraluminous granitic rocks and their petrogenetic implications. Annual Review of Earth and Planetary Sciences 16: 21-51.

Manuscript received: January 26, 2018; revised/accepted: March 30, 2021; available online: May 31, 2021.